Přílohy

Appl Microbiol Biotechnol (2016) 100:9809–9819
DOI 10.1007/s00253-016-7901-1

MINI-REVIEW

Ecotoxicity and environmental safety related to nano-scale zerovalent iron remediation applications

Jaroslav Semerád[1,2] · **Tomáš Cajthaml**[1,2]

Received: 5 June 2016 / Revised: 22 September 2016 / Accepted: 27 September 2016 / Published online: 11 October 2016

Abstract This mini-review summarizes the current information that has been published on the various effects of nano-scale zerovalent iron (nZVI) on microbial biota, with an emphasis on reports that highlight the positive aspects of its application or its stimulatory effects on microbiota. By nature, nZVI is a highly reactive substance; thus, the possibility of nZVI being toxic is commonly suspected. Accordingly, the cytotoxicity of nZVI and the toxicity of nZVI-related products have been detected by laboratory tests and documented in the literature. However, there are numerous other published studies on its useful nature, which are usually skipped in reviews that deal only with the phenomenon of toxicity. Therefore, the objective of this article is to review both recent publications reporting the toxic effects of nZVI on microbiota and studies documenting the positive effects of nZVI on various environmental remediation processes. Although cytotoxicity is an issue of general importance and relevance, nZVI can reduce the overall toxicity of a contaminated site, which ultimately results in the creation of better living conditions for the autochthonous microflora. Moreover, nZVI changes the properties of the site in a manner such that it can also be used as a tool in a tailor-made approach to support a specific microbial community for the decontamination of a particular polluted site.

Keywords Nano-scale zerovalent iron · In situ remediation · Stimulation · Toxicity · Oxidative stress

✉ Tomáš Cajthaml
cajthaml@biomed.cas.cz

[1] Institute for Environmental Studies, Faculty of Science, Charles University, Benátská 2, 128 01 Prague 2, Czech Republic

[2] Institute of Microbiology, v.v.i., Czech Academy of Sciences, Vídeňská 1083, 142 20 Prague 4, Czech Republic

Introduction

Nano-materials started attracting research attention in recent decades due to their unique chemical properties to which their enhanced chemical reactivities could be attributed, which also made these nano-scale materials increasingly useful for various applications, including remediation technologies. However, one of the main reasons that prompted their adoption for remediation was the availability of a very limited number of successful and effective remediation technologies for recalcitrant harmful compounds, including persistent organic pollutants and toxic metals. In this context, nano-scale zerovalent iron (nZVI) represents a prospective chemical agent with applicability toward the aquatic phase, including groundwater, and its effectivity against various types of pollutants, including chlorinated compounds, pesticides, and heavy metals, has been proven and documented in numerous publications (Barrera-Diaz et al. 2012; Gomes et al. 2013; Morrison et al. 2002). The typical mechanisms that are known to be involved in the transformation of the pollutants by nZVI are reduction, reductive dechlorination, adsorption or the formation of insoluble iron oxides, with the inclusion of toxic metals (Mitrano et al. 2015).

The oxidation of nZVI occurs naturally, under both aerobic and anaerobic conditions, and the oxidizing agent, i.e., the "counterpart" for this redox system, could be either water, oxygen, or the targeted pollutant. Through this process, the whole nanoparticle, the majority of which is composed of Fe(0), is gradually oxidized to soluble Fe^{2+} and Fe^{3+} ions. Thereafter (or at the end of the process), the injected nZVI could be detected as a partially or fully oxidized structure that is generally composed of a Fe(0) core and an iron oxide shell.

The formation of the iron oxide species depends primarily on the rate of redox reactions in the environment. For example, whereas lepidocrocites and goethites are primarily formed

under oxic conditions, the depletion of oxygen or the prevalence of an anoxic condition leads to the precipitation of iron hydroxide like material known as "green rust." Subsequently, this iron hydroxide is further oxidized to produce magnetite, the final product of oxidation (Kumar et al. 2014).

It is noteworthy that cytotoxic ions are released during the initial phase of nZVI oxidation but that these ions are subsequently oxidized into insoluble oxides and hydroperoxides of iron on the surface of the nanoparticles. The Fe^{2+} ions thus produced further participate in the generation of reactive oxygen species (ROS). In the living cells, ferrous ions react with H_2O_2 (produced in mitochondria) to generate ROS via Fenton chemistry (Sevcu et al. 2011). Therefore, it could be surmised that the highly reductive Fe (0), together with radicals from aqueous reactions, and its interaction with the ions present or produced in the aquatic phase and the Fenton reactions could comprise the two main mechanisms of a toxic effect of nZVI (Lefevre et al. 2016; Jang et al. 2014). The set of possible chemical reactions involved the in production of reactive oxygen species and other related compounds are visualized in Fig. 1.

Due to the manner in which nZVI is applied to the environment, the resident microorganisms represent the main exposed biota and are therefore optimally suited as an organismal model for monitoring the adverse effects of nZVI. An overview of the route of nZVI and its fate in the environment, exposure and the main toxic properties are shown in Fig. 2.

Over the past several years, many authors have demonstrated that nZVI can affect microbial species and could potentially induce adverse/toxic effect(s). In this mini-review, we summarize the recently published knowledge regarding the interactions of nZVI with microorganisms, with special attention to newly published articles that deal with using nZVI in bioremediation techniques. The aim of this article is not only to review the recent publications expressing possible concern about the ecotoxicity of nZVI but also to specifically review other recent studies indicating the positive/stimulating effects of nZVI on the ecotoxicity of contaminated sites due to its remediation potential.

$$Fe^0 + 2H_2O \rightarrow Fe^{2+} + H_2 + 2OH^-$$
$$2Fe^0 + 2H_2O + O_2 \rightarrow 2Fe^{2+} + 4OH^-$$
$$4Fe^{2+} + 4H^+ + O_2 \rightarrow 4Fe^{3+} + 4H_2O$$
$$Fe^0 + O_2 + 2H^+ \rightarrow Fe^{2+} + H_2O_2$$
$$Fe^0 + H_2O_2 \rightarrow Fe^{2+} + 2OH^-$$
$$Fe^{2+} + H_2O_2 \rightarrow Fe^{3+} + OH\bullet + OH^-$$
$$Fe^{3+} + H_2O_2 \rightarrow Fe^{2+} + OOH^- + H^+ \rightarrow Fe^{2+} + 2H^+ + 2O_2^-$$
$$Fe^{2+} + H_2O_2 \rightarrow FeO_2^+ + H_2O$$

Fig. 1 Typical nZVI reactions and reactions related to nZVI oxidation products (Sevcu et al. 2011; Auffan et al. 2008; El-Temsah and Joner 2013)

Cytotoxicity and oxidative stress to microorganisms—negative effects

There are many published articles that consider toxicity to bacterial cultures, and they have been reviewed in detail (see Lefevre et al. 2016; Jang et al. 2014 and references therein). The other studies considered in this mini-review are summarized in Table 1. Many authors have monitored basic parameters, such as cell viability and integrity, in more recent articles, but only a few studies have focused on biochemical and molecular biological parameters, such as the expression of specific genes (e.g., *gyrA*, *katB*, *nirS*, and *narG* by Fajardo et al. 2013). One of the main problems with studies in this field is that many or most of them are performed at concentrations that are extremely high and occasionally even higher than those used for remediation applications (approximately 2 g/L in the injected suspension; Němeček et al. 2014). It is noteworthy that a concentration of nZVI in the range of unit grams per liter can only be found in the injection boreholes; due to the limited mobility and gradual consumption of nZVI, the surrounding environment is exposed to concentrations that are lower by at least an order of magnitude. Laboratory experiments with a single bacterial culture can serve as a test for comparing various nano-materials, e.g., surface-modified nZVI derivatives; however, its implication in the context of real environmental conditions is limited. Moreover, even these single-strain tests should focus on more specific parameters and responses related to oxidative stress, which is the main cause of nZVI-associated cytotoxicity.

In this light, a new and interesting study was published by Ortega-Calvo et al. (2016), who observed behavioral differences in *Pseudomonas putida* G7 as a response to exposure to nZVI at environmentally relevant concentrations (1–10 μg/L). It is possible that such an approach could be utilized as a new test for evaluating stress related to low concentrations of nZVI and similar materials. The importance of the effect of the nZVI concentration was well demonstrated by Jiang et al. (2015), who investigated the effect of nZVI on the growth of *Paracoccus* sp. strain bio-denitrification under aerobic conditions. In addition to other parameters, they found that a low concentration of nZVI (50 mg/L) could promote the growth of cells and the biodegradation of nitrate, which led the authors to conclude that Fe(II) served as an electron donor for the reduction of nitrate in this situation. A much higher nZVI concentration (1000 mg/L) causes toxicity toward the studied strain, and the excess of Fe(II) starts to participate in the elevation of oxidative stress.

Dong et al. (2016) studied the effect of coating the surface of nZVI (500 mg/L) with carboxymethylcellulose and its effect on the cytotoxicity of nZVI toward *Escherichia coli*. The authors found that the observed levels of toxicity decreased

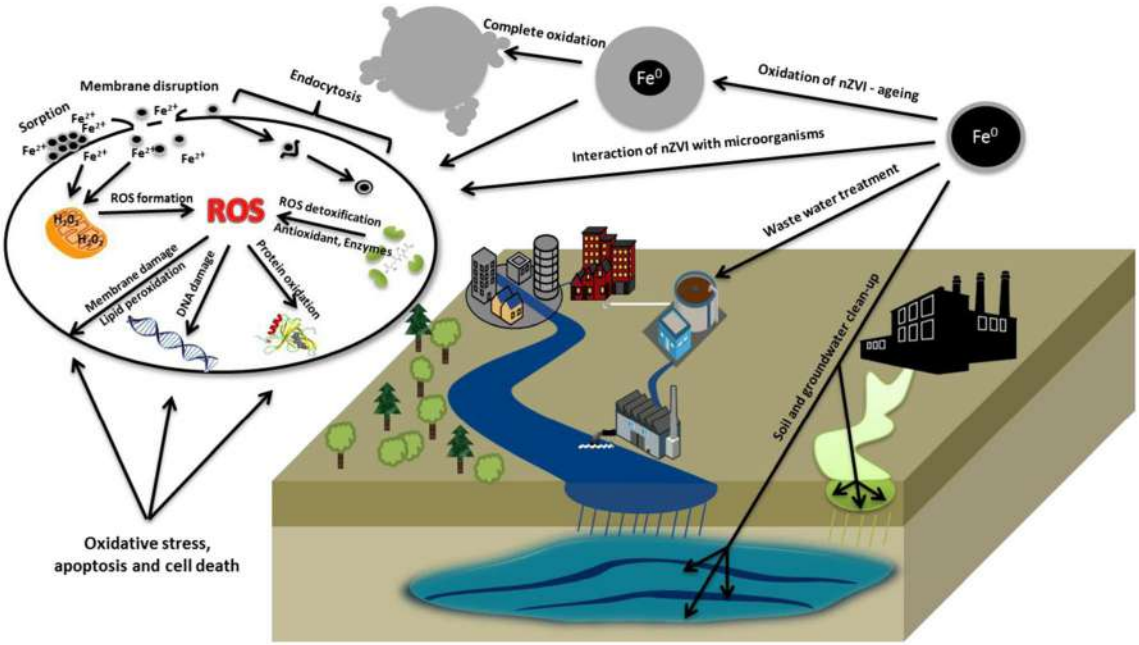

Fig. 2 Typical nZVI applications, fates, and toxicity effects on microbiota

with an increased organic coating, despite the bacterial strain becoming increasingly exposed to nZVI, because the organic coating helps the nano-material disperse better.

Chaithawiwat et al. (2016) tested oxidative stress concomitantly on the *E. coli* BW25113 strain and its mutants possessing knock-outs of genes that are related to the natural protection of cells against oxidative stress. Mutants lacking the *rpoS* gene and genes encoding cytosolic superoxide dismutases (*sodA* and *sodB*) were found to be more susceptible to nZVI exposure. The authors proved that nZVI induces oxidative stress inside the cells via superoxide generation and stated that inside the cell membrane, superoxide dismutase contributes more to the protection of cells against nZVI and nZVI-related toxicity than catalase does.

Another piece of evidence, related to the involvement of oxidative stress in the cytotoxicity of nZVI and its related products, was provided by Chen et al. (2013). The authors investigated the influence of nZVI (0.56 g/L), Fe^{2+} (0.01 M) and Fe^{3+} (0.01 M) on two G+ (*Bacillus subtilis* and *Staphylococcus aureus*) and two G− bacteria (*Pseudomonas fluorescens*, *E. coli*). The bacterial inactivation was determined by the use of an agar plate CFU counting method, and it revealed that Fe^{2+} and Fe^{3+} had stronger inactivating effects on all tested bacteria compared to nZVI itself. The results also revealed that culturing and viability tests showed stronger inactivating effects of Fe^{2+} on G− bacteria, whereas the effect of Fe^{3+} was more pronounced on G+ species. The authors also monitored the intracellular levels of ROS and found that at lower nZVI and corresponding Fe^{2+} and Fe^{3+} levels, bacteria might regulate the iron content; however, at higher levels, the ROS scavenging is also triggered. Although the abovementioned studies also represent laboratory tests with an isolated and cultivable bacteria, taken together, these results suggest that the phenomenon of toxicity should be borne in mind and call for an approach to utilize a methodological scan to develop a standardized set of tests to measure the toxicity of various types of nZVI and possibly other nanomaterials. In this way, it is also possible to interpret the results published by Ravikumar et al. (2016), who tested biologically and chemically synthesized nZVI materials using five bacterial isolates from a Cr(VI)-contaminated site. A decrease in the cell viability and subsequent damage to the cell membrane were observed in bacterial isolates after 24 h of exposure. The bio-uptake of nZVI by the bacterial cells probably led to the release of Fe^{2+} ions and the generation of ROS. In a recently published work, Rónavári et al. (2016) tested several types of bare nZVI on an anaerobic community under laboratory conditions and detected certain differences in the community profiles; however, the diversity of the samples was analyzed using only the denaturing gradient gel electrophoresis (DGGE) method. Using qPCR, the authors quantified several specific genes representing *Dehalococcoides*, sulfate-reducing bacteria, methanogenes, and genes related to chlororespiration activity (*vcrA*, *tceA*). Although the data were based only on duplicates, they indicated both positive and negative shifts in the community during the incubation. In this case, it is necessary to keep in mind that the application of nZVI not only causes oxidative stress but also reacts with the components of the cultivation medium used for the culture. Another lab-scale, batch experiment, focusing on the effects of nZVI and micro-scale zerovalent iron (mZVI), was published by Velimirovic et al. 2015. These authors detected

Table 1 Summary of recent publications documenting positive or negative interaction of nZVI with microbial biota with descriptions of the effects and methods used

Monitored organism	nZVI characteristics	Time of exposure	nZVI concentration	Effects (− negative; + positive)	Pollutant	Analytical method used	Reference
Bacillus cereus ATCC 14579	Commercial nZVI Nanofer 25 S from NANO IRON, Ltd.	Up to 48 h	5000 mg/L	− sporulation and upregulation of stress response genes	–	RT-qPCR, Proteomic analysis, TEM, CFU cell counting	(Fajardo et al. 2013)
Pseudomonas putida G7	Commercial nZVI Nanofer STAR from NANO IRON, Ltd.	24 h	0.1 mg/L 0.01 mg/L	− significant mortality − tactile response to stress, altered swimming behavior	–	CFU cell counting , Chemical-in-pond method, monitoring of swimming behavior	(Ortega-Calvo et al. 2016)
Paroccocus spp. isolated from sludge	Customized nZVI particles synthesized using $NaBH_4$ and $FeCl_3$	Up to 50 h	1000 mg/L 50–500 mg/L	− inhibition of biological reduction of nitrate + promotion of growth and biodegradation of nitrate	Nitrate	SEM, EDS, OD_{600}	(Jiang et al. 2015)
Escherichia coli ATCC 25922	Commercial nZVI Nanofer 25 from NANO IRON, Ltd., CMC-modified nZVI	18 h	100–500 mg/L	− decreased cell viability	–	CFU cell counting, TEM	(Dong et al. 2016)
Escherichia coli BW25113, JW3879-1, JW1648-1, JW1638-1, JW3914-1, JW1721-1, JW5437-1	Commercial nZVI from Toda Co.	Up to 60 h	500 and 1000 mg/L	− generation of oxidative stress resulting in decreased cell viability	–	CFU cell counting , qPCR	(Chaithawiwat et al. 2016)
Bacillus subtilis var. *niger* ATCC 9372, *Staphylococcus aureus* CDC JS06081-SP, *Escherichia coli* ATCC 15597, *Pseudomonas fluorescens* ATCC 13525	Customized nZVI synthesized using $Fe(NO_3)_3$ and $NaBH_4$ and, Fe^{2+} and Fe^{3+} solutions	Up to 24 h	560 mg/L	− Fe^{2+} and Fe^{3+} had stronger inactivating effect than nZVI on all tested bacteria − Fe^{2+} preferentially inactivates G− bacteria , while Fe^{3+} is more potent toward G+ species	–	CFU cell counting, Quantification of ROS (DCFH-DA assay), Cell viability assay	(Chen et al. 2013)
5 bacterial isolates from lake water sediment	Customized nZVI biologically/chemically synthesized using ($FeSO_4$, $NaBH_4$, fresh neem leaves)	Up to 24 h	1000 mg/L	− decrease in cell viability, increased ROS generation, higher membrane permeability/membrane damage after 24 h	Cr(VI)	Quantification of ROS (DCFH-DA assay), CFU cell counting, lactate dehydrogenase assay, bio-uptake measurement	(Ravikumar et al. 2016)
Dehaloccocoides spp. consortium	Two types of customized nZVI prepared from $FeCl_3$ and $Na_2S_2O_4$ or $NaBH_4$	Up to 20 days	100 mg/L	− decreased 16 S rDNA in *Dehalococcoides* sp. and dehalogenase gene containing bacteria depending on nZVI precursors and its reducing agents	TCE, cDCE, VC	qPCR, DGGE, CFU cell counting	(Ronavari et al. 2016)
CAH-degrading bacterial consortium isolated from contaminated site	Commercial nZVI Nanofer 25 S from NANO IRON, Ltd. and mZVI	Up to 16 weeks	50 mg/L for nZVI and 15,000 mg/L for mZVI	− decreased ATP production in CAH-degrading consortium	TCE	ATP assay	(Velimirovic et al. 2015)
Bacillus fusiformis isolated from activated sludge	Customized bimetallic nZVI synthesized using $FeCl_3$ and $NaBH_4$	Up to 12 h	100 mg/L	+ no negative effect, enhanced bacterial growth and biodegradation of phenol at various pH values in the presence of nZVI and Ni/Fe	Phenol	SEM, OD_{600}	(Kuang et al. 2013)
Microbial community from waste activated sludge	Commercial nZVI from Aladdin Industrial Corporation	Up to 6 days	5000 mg/L	+ increases in several populations of fermentative bacteria + increases in ATP production + Increases in enzyme activity	–	454 high-throughput pyrosequencing analysis, ATP assay, key enzyme activity assays	(Luo et al. 2014)
Microbial community of sludge	Commercial nZVI and Fe_3O_4 from Aladdin Industrial Corporation	Up to 12 days	5000 mg/L	+ increased methanogenesis, nZVI supported anaerobic digestion	–	Monitoring of methanogenesis	(Suanon et al. 2016a)
Microbial community of sewage sludge	Customized nZVI synthesized using $NaBH_4$ and $FeCl_3$	Up to 30 days	1000 mg/kg	+ increased methanogenesis and increase in the removal of chlorinated pharmaceuticals and personal care products	Pharmaceutical and personal care products	Monitoring of methanogenesis	(Suanon et al. 2016b)

Table 1 (continued)

Monitored organism	nZVI characteristics	Time of exposure	nZVI concentration	Effects (− negative; + positive)	Pollutant	Analytical method used	Reference
Microbial community of anaerobic granular sludge	Commercial nZVI from Sigma Aldrich	Up to 30 days	≤500 mg/g	+ increased methanogenesis and biomass at lower concentration (10 mg/g)	–	Enzymatic activity, DIET, FISH, FQ-PCR	(Wang et al. 2016)
Acinetobacter baylyi ADP1_recA_ lux biosensor	Customized nZVI synthesized from iron nitrate and urea	Up to 12 h	≤5000 mg/L	+ decreased total toxicity of effluent resulted in enhanced biodegradation of recalcitrant pollutants in the wastewater	Metal working fluids	Chromosome-based bioluminescence reporter expression assay, OD_{600}	(Jagadevan et al. 2012)
Escherichia coli DH5α	Customized bimetallic nZVI (nFe–Pd) prepared by the reduction of $FeSO_4$ by $NaBH_4$	48 h	1000 mg/L	+ decreased total toxicity (ROS, GPx, dead cells) of the treated PCB solution − nFe–Pd nanoparticles induced oxidative stress in pure bacterial culture	(PCB) Aroclor 1248	GPx activity assay, Quantification of ROS, PI staining	(Le et al. 2015)
Desmodesmus subspicatus, *Dunaliella salina*, *Parachlorella kessleri*, *Raphidocelis subcapitata*, *Nannochloropsis limnetica*, *Trachydiscus minutus*, *Arthrospira maxima*	Commercial nZVI Nanofer 25 and 25 S from NANO IRON, Ltd.	216 h	5.1 mg/L	+ increased algal growth, enhanced lipid accumulation	–	Analysis of lipids and fatty acids	(Pádrová et al. 2015)
Candida sp. DBM2163, *Kluyveromyces polysporus* DBM2171 (CCY 30-5-10), *Rhodotorula glutinis* CCY 20-2-20, *Saccharomyces cerevisiae* DBM 2115, *Torulaspora delbrueckii* DBM 39, *Trichosporon cutaneum* CCY 30-5-10 and *Yarrowia lipolytica* CCY 29-26-36	Comercial nZVI Nanofer 25 from NANO IRON, Ltd.	Up to 72 h	9–13 mg/L	+ enhanced lipid accumulation in yeasts	–	Analysis of lipids and fatty acids	(Pádrová et al. 2016)
Rowland series silt loam soil population	Commercial nZVI from Golder Associates Inc.	Up to 14 days	10 mg/g	+ no negative effect on the population of microorganisms	–	Ammonia -oxidation potential, dehydrogenase and FDH activity assay	(Cullen et al. 2011)
Dehalococcoides sp. strain CBDB1	Commercial nZVI from DK Nano technology	Up to 30 days	≤250 mg/L	+/− bacterial strain resistant to negative effects of nZVI	Polybrominated diphenyl ethers	Bacterial count with SYBR green	(Xu et al. 2014)
Pseudomonas stutzeri KS0013	Commercial nZVI from Sigma Aldrich	Up to 24 h	≤2000 mg/L	− inhibitory effect of nZVI at concentrations >500 mg/L + removal efficiency improvement at lower concentrations (<500 mg/L)	Polybrominated diphenyl ethers	OD_{600}	(Huang et al. 2016)
Bacillus fusiformis isolated from activated sludge	Commercial nZVI from Hongwu Nano Material Co., Ltd.	Up to 96 h	500 mg/L	+ no negative effect observed	Naphthalene	OD_{600}	(Yu et al. 2015)
Population of microorganisms collected from remediated site	Commercial nZVI Nanofer 25 from NANO IRON, Ltd.	Up to 217 days	2000 mg/L	+ stimulation of growth of G+ bacteria, no effect on G−, positive effect on the autochthonous microflora, no effect of nZVI on total toxicity	Cr (VI)	PLFA, Inhibition of bioluminescence test, Cultivation of indigenous bacteria (based on ISO 8692,1989)	(Němeček et al. 2014)
Population of microorganisms collected from remediated site	Commercial nZVI Nanofer 25 from NANO IRON, Ltd.	20 months	2000 mg/L	+ observed biomass growth after injection of whey, generally positive impact on autochthonous microflora	Cr(VI)	PLFA, Cultivation tests (ISO 8199,2005), qPCR, 454 pyrosequencing	(Němeček et al. 2015)
Population of microorganisms collected from remediated site	Commercial nZVI Nanofer STAR and Nanofer 25S from NANO IRON, Ltd.	13 months	2-step injection, first 1000 mg/L and then 2000 mg/L	+ stimulation of soil G− bacteria after injection of whey, increased number of psychrophilic bacteria and bacterial density	Cr(VI) and TCE	PLFA, Cultivation tests (ISO 8199,2005)	(Němeček et al. 2016)

Table 1 (continued)

Monitored organism	nZVI characteristics	Time of exposure	nZVI concentration	Effects (− negative; + positive)	Pollutant	Analytical method used	Reference
Population of *Dehalococcoides* from remediated site	Customized CMC-nZVI synthesized by borohydride precipitation	21 days	1000 mg/L	+ increase in population of *Dehalococcoides* immediately after injection of nZVI	cVOC	qPCR	(Kocur et al. 2015)
Microbial community of contaminated site	Customized CMC-nZVI synthesized directly on site	Over 2 years	1000 mg/L	+ increase in population of *Dehalococcoinides* and *Dehalogenimonas*	cVOC	qPCR, 16S rRNA pyrosequencing	(Kocur et al. 2016)

negative effects on the bacterial consortia, mainly by measuring the levels of ATP and several other biochemical parameters, such as lactate consumption. The bacterial culture was affected by nZVI at doses as low as 0.05 g/L, and very high doses of 15–30 g/L of mZVI showed an inhibitory effect on the bacterial community, which the authors tested as the worst-case scenario during remediation application. The negative effects of ZVIs (H_2 and absence of lactate consumption) also corresponded to an increase of pH above 7.5, related to the dose-dependent corrosion of ZVI. Other, more recent laboratory and cytotoxicity works related to this subject were reviewed in detail by Lefevre et al. (2016).

Effects on microbial populations and processes

As mentioned above, low concentrations of nZVI can also have considerable positive biotechnological effects on various microorganisms. Pádrová et al. (2015) tested several green algae and cyanobacterial strains and found that a low concentration of nZVI (5.1 mg/L) substantially enhanced lipid accumulation, decreased the content of saturated and monounsaturated fatty acids, with the exception of palmitoleic acid, and increased the content of polyunsaturated fatty acids in the cells of all microorganism employed in the study. The authors suggested that nZVI amendment could contribute to optimizing the economical production of oils from oleaginous microorganisms. Similarly, Pádrová et al. (2016) found that oxidative stress induced by nZVI could improve lipid accumulation in various oleaginous and non-oleaginous yeasts. The highest lipid production was observed at a dose range of 9–13 mg/L of nZVI. The results indicated an increased synthesis of polyunsaturated fatty acids, especially essential linoleic acid, which suggests that nZVI could also be used to improve the nutritional value of biosynthesized unsaturated fatty acids. Another promising strategy would be the support of anaerobic fermentation processes, as shown by Luo et al. (2014). The authors tested the effect of 5 g/L of nZVI on the fermentation (hydrolysis and solubilization) process, and by using 454 pyrosequencing, they observed an increase in the abundance of bacteria responsible for hydrolysis of waste sludge and a general increase in both the microbial activity of anaerobes and the activities of their hydrolytic enzymes. The production of short-chain fatty acids was also stimulated by the addition of nZVI, and the time required for the fermentation of the maximal amount of short-chain fatty acids was shortened.

Suanon et al. (2016a) showed a positive effect of nZVI (0.5 %) on the mesophilic anaerobic digestion of sludge. The authors detected elevated biogas production and an increased immobilization of both artificially added heavy metal representatives and phosphorus in the digestate, which was examined by sequential extraction. In another work, Suanon et al. (2016b) recorded enhanced methane yields,

which reached 25 and 40 % after the application of nZVI and ZVI, respectively, during sludge anaerobic digestion. However, the authors also observed a certain increase in the removal of chlorinated pharmaceuticals and personal care products from the sludge. Similarly, Wang et al. (2016) investigated the effects of four representative nanoparticles, including nZVI, on methane production during the anaerobic digestion of waste activated sludge. The authors found that low nZVI doses (10 mg/kg) increased methane generation by 20 % and that the biomass of bacteria and archea increased to a similar extent.

The typical problems associated with interpreting the effects of nZVI on microbes and their communities were shown by Cullen et al. (2011), who tested nZVI on general (dehydrogenase and hydrolase) and specific (ammonia oxidation potential) activities mediated by a microbial community in uncontaminated soil. The authors showed that 10 mg/g of nZVI suppressed the ammonia oxidation potential, stimulated dehydrogenase activity and had a negligible influence on the activity of hydrolases. However, using microbe-free controls, the authors finally showed that although the inhibitory effects were not caused by nZVI, the stimulation of dehydrogenase activity was brought about by the addition of nZVI. The authors concluded that under the experimental conditions, any negative effect of nZVI on microbes could not be proven. Similar non-negative effects of nZVI (0.1 g/L) on a bacterial strain (*Bacillus fusiformis*) tested during the biodegradation of phenol under aerobic conditions were recorded by Kuang et al. (2013), who tested the influence at various pH levels and observed growth stimulation and higher rates of biodegradation in the presence of nZVI.

However, a typical situation when nZVI is applied in situ to a damaged environment was published in a work by Němeček et al. (2014), which represents one of the few studies to describe the effect of nZVI on microbes in real environmental conditions. The authors successfully remediated a site contaminated by highly toxic hexavalent chromium via reduction and geofixation using an injection of nZVI. The nZVI injection removed Cr(VI) and the total Cr from groundwater, without any substantial effect on its chemical properties, except for a decrease in the redox potential. The system was monitored using classical approaches such as ecotoxicological tests with *Vibrio fischeri* and the cultivation of psychrophilic autochtonous bacteria, neither of which yielded any reasonable results or clear trends. In contrast, phospholipid fatty acid analysis (PLFA), which serves as a direct non-cultivable method for estimating microbial biomass, revealed that the application of nZVI did stimulate the growth of G+ bacteria and principal component analysis indicated a correlation between the number of bacteria and the concentration of Fe following the nZVI application. The results of this study clearly document that despite possible concerns about the ecotoxicity of nZVI, its application improved ecotoxicological conditions and resulted in a positive effect on the autochthonous microflora in the site due to the reduction of highly toxic Cr(VI); further, the corresponding decrease in the redox potential probably facilitated the natural development of the anaerobic community.

Nano-bioremediation

Because nZVI is produced as a material for remediation, it is consequentially logical to study the effect of nZVI on microorganisms during its action, i.e., the process of remediation. Moreover, it is important to investigate whether nZVI can be used sequentially with another bioremediation process due to the possibility that this combination might alter and facilitate the overall bioremediation process because the condition of the contaminated site could change substantially after the application of nZVI. Such a concept was proposed by Jeon et al. (2013). Using more recently published studies, the authors documented the possibilities of a sequential nZVI-bioremediation process on either strongly recalcitrant (e.g., polychlorinated dibenzodioxins, polychlorinated biphenyls, polybrominated diphenylethers) or toxic (antimicrobial) compounds. The idea regarding recalcitrant compounds can be exemplified by brominated flame retardants. This "novel" concept of using bromine for halogenation and replacing chlorine, which was used in the past, ultimately led to the production of compounds that are seemingly less mobile and less toxic. However, the problem associated with their biodegradation in the environment is linked to the fact that they often contain aromatic moieties that are substituted "xenophores" that are somewhat larger than other substituents, which limits the ability of the microbial intracellular transformation processes to access these compounds and causes them to accumulate in the environment (Ezechiáš et al. 2014). The problems arising from the halogenation-induced steric effects could be solved by the use of nZVI, which is well known for its effectiveness in the reductive dehalogenation of various chlorinated organic pollutants that are generally more susceptible to further microbial transformations (Cundy et al. 2008). In contrast, less halogenated derivatives also present certain concerns regarding the possibility of an elevation in its toxicity; therefore, further biodegradation is a desirable process. Another concern is the fact that some of the contaminated sites are often highly toxic to biodegrading microorganisms, and the conditions (e.g., redox potential) prevailing in the contaminated areas do not allow the growth or development of an active microbial population.

Jagadevan et al. (2012) published an article regarding the nZVI treatment of exhausted metal working fluid, which is a very complex and problematic mixture of toxic organic biocides that are added specifically to suppress the biodeterioration of these liquids. The authors applied an

nZVI/peroxide system to oxygenated wastewater, which resulted in the oxidation of the organic compounds. The process led to a substantial reduction in the toxicity and enabled the authors to perform a second biological oxidative step in a bioreactor via bioaugmentation by a bacterial consortium. Yu et al. (2015) used an opposite biodegradation and nZVI/Fenton reaction-based approach to increase the effectiveness of naphthalene degradation. The authors used a bacterial strain, *B. fusiformis*; however, the strain only partially converted the applied pollutant into transformation products, which were further decomposed using a Fenton-like oxidation process.

Another case-specific work describing a combination of nZVI/Pd reductive dechlorination and an aerobic bacterial strain *Burkholderia xenovorans* LB400 was recently published by Le et al. (2015). The authors performed a laboratory study with Aroclor 1248 when dechlorination reached 99, 92, 84, and 28 % of tri-, tetra-, penta-, and hexachlorinated biphenyls, respectively. The applied bacterium degraded the resulting metabolite biphenyl. The process was monitored in terms of the toxicity of the samples using another bacterial species, *E. coli*. A general decrease in the toxicity was recorded, as documented by the lowered activity of glutathione peroxidase and the lowered concentration of ROS.

Reductive dehalogenation using nZVI and ZVI, followed by anaerobic bacterial treatment, was studied by Xu et al. (2014) in a laboratory experiment that demonstrated the suitability of combining nZVI and microbial debromination. The authors investigated the effect of iron material on the *Dehaloccocoides* species, which is capable of utilizing less brominated derivatives of brominated diphenyl ethers, and detected an inhibition of the strain that occurs at an nZVI concentration higher than 0.25 g/L. The authors applied nZVI or micro-ZVI together with the strain and BDE-209, and the results indicated that the application of nZVI resulted in a partial reductive debromination followed by bacterial reductive dehalogenation.

Similar outcomes were published by Huang et al. (2016), who studied the effect of nZVI on the removal of BDE-47 by *Pseudomonas stutzeri*. Concentrations higher than 0.5 g/L of nZVI had an inhibitory effect on the bacterial strain; however, the amounts equal to this value were not toxic, and the authors even detected a slight improvement in the degradation by the bacteria.

Another combination of nZVI with chlorespiring bacteria was published by Koenig et al. (2016). The dechlorination study of 1,2-dichloroethane (DCA) and 1,1,2-trichloroethane (TCA) showed that 1 g/L of nZVi is capable of transforming only TCA, whereas the anaerobic bacterial consortium from a real contaminated site was able to transform both the pollutants to ethane. As mentioned above, the authors tested combinations of various nZVI doses on the bacterial community, and by using the CFU calculation, they found that nZVI concentrations of 0.1 g/L and higher had a negative impact on both the viability of the bacteria and the effectiveness of dechlorination. Doses below this limit could stimulate the activity of the bacterial consortium.

The fact that nZVI can potentially facilitate microbial growth by reducing the toxicity of a contaminated site was examined by Němeček et al. (2015). The authors applied nZVI to a site that was contaminated by Cr(VI). After an initial reduction in toxicity, the partial removal of chromium from the ground water and a drop in redox potential, the authors noted that anaerobic microbiota were present in the environment, with the injection of whey into the ground water. The application of the organic substrate promoted a biotic reduction of Cr(VI), which resulted in a further and long-term decrease in the Cr(VI) content of the groundwater. The effect of biotic reduction was observed even in a monitoring well located 22 m from the substrate injection wells after 10 months. The results indicated a reciprocal effect on both phases: the nZVI that oxidized to Fe(III) during the abiotic phase was reduced back to Fe(II) by microbes and acted as a reducing agent for Cr(VI), even when the microbial density was already low due to the consumption of the substrate. A massive development of the anaerobic biomass was documented by PLFA analysis. Community analysis with pyrosequencing of the 16S ribosomal RNA (rRNA) genes further confirmed the partial recycling of nZVI into the form of Fe(II), and the results showed that the Cr(VI) reduction process was probably mediated not only by Cr(VI)-reducing bacteria but also by the iron- and sulfate-reducing bacteria. Using this approach, the authors showed that the application of nZVI in combination with microbially mediated reduction can be an efficient approach for remediation under the specific conditions prevailing in that site.

In another study, the authors (Němeček et al. 2016) experimented on an even more complex situation in situ using a similar approach. The sequential application of nZVI and whey was used at a site that was highly contaminated with Cr(VI) and chlorinated ethylenes. The authors monitored the process using numerous methods, including physical–chemical analyses and molecular biological approaches, which enabled the characterization of both the pollutants and their transformation products as well as the mechanisms involved in the process. Additionally, in this case, the applied nZVI was very efficient in the removal of Cr(VI); however, its removal efficiency of chlorinated ethylenes was limited. In contrast, the injection of whey immediately resulted in the classical and gradual dechlorination of the main pollutant (i.e., trichloroethylene) to non-chlorinated structures. The resulting community was characterized by the use of Illumina sequencing, and the course of vinylchloride reductive genes (*vcrA* and *bvcA*) was monitored by qPCR that corresponded to the appearance and subsequent decline of vinylchloride. These results, together with Illumina sequencing and specific detection

using PCR, indicated the presence of an active community of chlororespiring *Dehalococcoides* in both the monitoring wells (distant from injection) and the injection wells. Similar to the previous study, the subsequent application of whey assisted the microbial regeneration of spent nZVI by promoting its reduction into Fe(II), which further supported the remediation conditions at the site toward Cr(VI). However, the results also documented that the application of nZVI and its related products (Fe(II), in both the dissolved and solid forms indicated in green rust) did not suppress the chlororespiring community, which is in contradiction to the data published by other authors (Xiu et al. 2009, 2010).

Kocur et al. (2015) investigated whether carboxymethyl cellulose stabilized nZVI effects on chlororespiring bacteria at a field site contaminated with chlorinated ethenes and ethanes. The nZVI injection successfully transformed the studied chlorinated ethanes to less chlorinated representatives, and the authors showed that the abiotic transformation period was followed by a period with increased chlororespiring organism activity. Surprisingly, the abundance of *Dehalococcoides* spp. increased immediately after the injection by an order of magnitude throughout the area that was influenced by nZVI.

In another work, the same group of authors monitored the same site for a substantially longer period of 2 years. Apart from the transformation of the chlorinated pollutants, the authors focused on the response of *Dehalococcoides* to the modified nZVI material, vinyl chloride reductase (*vcrA*) genes and generally to shifts in the microbial community. The study showed that the abundance of dechlorinating genera *Dehalococcoides* and *Dehalogenimonas* increased after nZVI application when carboxymethyl cellulose served as an organic substrate. The process was also followed by the significant removal of chlorinated ethylenes (Kocur et al. 2016).

Conclusion and perspectives

Numerous articles on nZVI have been published over the last decade expressing concern regarding its possible use in remediation. However, many studies have also been published documenting the feasibility of applying this new technology for the decontamination of sites polluted with various organic and inorganic pollutants. There are instances of many chemical substances of anthropogenic origin, which were introduced into the environment in the past and were later found to be toxic toward the biota in specific ways that had not been expected and could not be predicted at the time of its introduction. Therefore, a certain amount of concern regarding the use of a new nano-scale substance is reasonable. However, from this point of view, it is necessary to emphasize that there is still a lack of a suitable, comprehensive, and standardized set of tests for the ecotoxicological evaluation of novel nanomaterials, and further research in this direction is needed. In this regard, the situation related to nZVI is unique because it is predominantly designed for use in highly damaged environments; therefore, the risk associated with its possible harmful effects on the biota is already limited in these sites. nZVI is, by nature, a reactive substance, and its toxic properties are linked to this reactivity and its ability to produce ROS. However, in this case, its toxic effects are physically restricted to the area surrounding its application. It is necessary to bear in mind that nZVI itself is further transformed into non-toxic iron oxides. Moreover, as evident from the studies described herein, nZVI can influence the environmental parameters, thus stimulating the microbiota; such a tailor-made approach was documented by a substantial decrease in redox potential at a site that facilitated the activity of anaerobic microflora that were capable of the "natural" transformation of pollutants. Thus, the potential environmental hazards associated with the application of nZVI should not be overestimated, but most importantly, the message of this mini-review emphasizes the need to conduct further studies on the mechanism of nZVI toxicity/stimulation and remediation under real environmental conditions.

Acknowledgments This work was funded by grant Competence Centre TE01020218 of the Czech Technology Agency Foundation. The research leading to these results has received funding from the Norwegian Financial Mechanism 2009–2014 and the Ministry of Education, Youth and Sports under Project Contract no. MSMT-23681/2015-1.

Compliance with ethical standards This article does not contain any studies with human participants or animals performed by any of the authors.

Conflict of interest The authors declare that they have no conflict of interests.

References

Auffan M, Achouak W, Rose J, Roncato MA, Chanéac C, Waite DT, Maison A, Woicik JC, Wiesner MR, Bottero J-Y (2008) Relation between the redox state of iron-based nanoparticles and their cytotoxicity toward *Escherichia coli*. Environ Sci Technol 42:6730–6735. doi:10.1021/es800086f

Barrera-Diaz CE, Lugo-Lugo V, Bilyeu B (2012) A review of chemical, electrochemical and biological methods for aqueous Cr(VI) reduction. J Hazard Mater 223:1–12. doi:10.1016/j.jhazmat.2012.04.054

Chaithawiwat K, Vangnai A, McEvoy JM, Pruess B, Krajangpan S, Khan E (2016) Role of oxidative stress in inactivation of *Escherichia coli* BW25113 by nanoscale zero-valent iron. Sci Total Environ. doi:10.1016/j.scitotenv.2016.02.191

Chen Q, Li J, Wu Y, Shen F, Yao M (2013) Biological responses of gram-positive and gram-negative bacteria to nZVI (Fe-0), Fe^{2+} and Fe^{3+}. RSC Adv 3:13835–13842. doi:10.1039/c3ra40570b

Cullen LG, Tilston EL, Mitchell GR, Collins CD, Shaw LJ (2011) Assessing the impact of nano- and micro-scale zerovalent iron particles on soil microbial activities: particle reactivity interferes with

assay conditions and interpretation of genuine microbial effects. Chemosphere 82:1675–1682. doi:10.1016/j.chemosphere.2010.11.009

Cundy AB, Hopkinson L, Whitby RLD (2008) Use of iron-based technologies in contaminated land and groundwater remediation: a review. Sci Total Environ 400:42–51. doi:10.1016/j.scitotenv.2008.07.002

Dong H, Xie Y, Zeng G, Tang L, Liang J, He Q, Zhao Y, Wu Y (2016) The dual effects of carboxymethyl cellulose on the colloidal stability and toxicity of nanoscale zero-valent iron. Chemosphere 144:1682–1689. doi:10.1016/j.chemosphere.2015.10.066

El-Temsah YS, Joner EJ (2013) Effects of nano-sized zero-valent iron (nZVI) on DDT degradation in soil and its toxicity to collembola and ostracods. Chemosphere 92:131–137. doi:10.1016/j.chemosphere.2013.02.039

Ezechiáš M, Covino S, Cajthaml T (2014) Ecotoxicity and biodegradability of new brominated flame retardants: a review. Ecotox Environ Safe 110:153–167. doi:10.1016/j.ecoenv.2014.08.030

Fajardo C, Sacca ML, Martinez-Gomariz M, Costa G, Nande M, Martin M (2013) Transcriptional and proteomic stress responses of a soil bacterium *Bacillus cereus* to nanosized zero-valent iron (nZVI) particles. Chemosphere 93:1077–1083. doi:10.1016/j.chemosphere.2013.05.082

Gomes HI, Dias-Ferreira C, Ribeiro AB (2013) Overview of in situ and ex situ remediation technologies for PCB-contaminated soils and sediments and obstacles for full-scale application. Sci Total Environ 445:237–260. doi:10.1016/j.scitotenv.2012.11.098

Huang Z, Chen Y, Hu Y (2016) The role of nanoscale zerovalent iron particles in the biosorption and biodegradation of BDE-47 by *Pseudomonas stutzeri* under aerobic conditions. Int Biodeter Biodeg 112:51–58. doi:10.1016/j.ibiod.2016.04.039

Jagadevan S, Jayamurthy M, Dobson P, Thompson IP (2012) A novel hybrid nano zerovalent iron initiated oxidation—biological degradation approach for remediation of recalcitrant waste metalworking fluids. Water Res 46:2395–2404. doi:10.1016/j.watres.2012.02.006

Jang M-H, Lim M, Hwang YS (2014) Potential environmental implications of nanoscale zero-valent iron particles for environmental remediation. Environ Health Toxicol 29:e2014022. doi:10.5620/eht.e2014022

Jeon J-R, Murugesan K, Nam I-H, Chang Y-S (2013) Coupling microbial catabolic actions with abiotic redox processes: a new recipe for persistent organic pollutant (POP) removal. Biotechnol Adv 31:246–256. doi:10.1016/j.biotechadv.2012.11.002

Jiang C, Xu X, Megharaj M, Naidu R, Chen Z (2015) Inhibition or promotion of biodegradation of nitrate by *Paracoccus* sp. in the presence of nanoscale zero-valent iron. Sci Total Environ 530–531:241–246. doi:10.1016/j.scitotenv.2015.05.044

Kocur CMD, Lomheim L, Boparai HK, Chowdhury AIA, Weber KP, Austrins LM, Edwards EA, Sleep BE, O'Carroll DM (2015) Contributions of abiotic and biotic dechlorination following carboxymethyl cellulose stabilized nanoscale zero valent iron injection. Environ Sci Technol 49:8648–8656. doi:10.1021/acs.est.5b00719

Kocur CMD, Lomheim L, Molenda O, Weber KP, Austrins LM, Sleep BE, Boparai HK, Edwards EA, O'Carroll DM (2016) Long-term field study of microbial community and dechlorinating activity following carboxymethyl cellulose-stabilized nanoscale zero-valent iron injection. Environ Sci Technol 50:7658–7670. doi:10.1021/acs.est.6b01745

Koenig JC, Boparai HK, Lee MJ, O'Carroll DM, Barnes RJ, Manefield MJ (2016) Particles and enzymes: combining nanoscale zero valent iron and organochlorine respiring bacteria for the detoxification of chloroethane mixtures. J Hazard Mater 308:106–112. doi:10.1016/j.jhazmat.2015.12.036

Kuang Y, Zhou Y, Chen Z, Megharaj M, Naidu R (2013) Impact of Fe and Ni/Fe nanoparticles on biodegradation of phenol by the strain *Bacillus fusiformis* (BFN) at various pH values. Bioresource Technol 136:588–594. doi:10.1016/j.biortech.2013.03.018

Kumar N, Auffan M, Gattacceca J, Rose J, Olivi L, Borschneck D, Kvapil P, Jublot M, Kaifas D, Malleret L, Doumenq P, Bottero J-Y (2014) Molecular insights of oxidation process of iron nanoparticles: spectroscopic, magnetic, and microscopic evidence. Environ Sci Technol 48:13888–13894. doi:10.1021/es503154q

Le TT, Nguyen K-H, Jeon J-R, Francis AJ, Chang Y-S (2015) Nano/bio treatment of polychlorinated biphenyls with evaluation of comparative toxicity. J Hazard Mater 287:335–341. doi:10.1016/j.jhazmat.2015.02.001

Lefevre E, Bossa N, Wiesner MR, Gunsch CK (2016) A review of the environmental implications of in situ remediation by nanoscale zero valent iron (nZVI): behavior, transport and impacts on microbial communities. Sci Total Environ. doi:10.1016/j.scitotenv.2016.02.003

Luo J, Feng L, Chen Y, Li X, Chen H, Xiao N, Wang D (2014) Stimulating short-chain fatty acids production from waste activated sludge by nano zero-valent iron. J Biotechnol 187:98–105. doi:10.1016/j.jbiotec.2014.07.444

Mitrano DM, Motellier S, Clavaguera S, Nowack B (2015) Review of nanomaterial aging and transformations through the life cycle of nano-enhanced products. Environ Int 77:132–147. doi:10.1016/j.envint.2015.01.013

Morrison SJ, Metzler DR, Dwyer BP (2002) Removal of As, Mn, Mo, Se, U, V and Zn from groundwater by zero-valent iron in a passive treatment cell: reaction progress modeling. J Contam Hydrol 56:99–116. doi:10.1016/s0169-7722(01)00205-4

Němeček J, Lhotský O, Cajthaml T (2014) Nanoscale zero-valent iron application for in situ reduction of hexavalent chromium and its effects on indigenous microorganism populations. Sci Total Environ 485:739–747. doi:10.1016/j.scitotenv.2013.11.105

Němeček J, Pokorný P, Lacinová L, Černík M, Masopustová Z, Lhotský O, Filipová A, Cajthaml T (2015) Combined abiotic and biotic in-situ reduction of hexavalent chromium in groundwater using nZVI and whey: a remedial pilot test. J Hazard Mater 300:670–679. doi:10.1016/j.jhazmat.2015.07.056

Němeček J, Pokorný P, Lhotský O, Knytl V, Najmanová P, Steinová J, Černík M, Filipová A, Filip J, Cajthaml T (2016) Combined nano-biotechnology for in-situ remediation of mixed contamination of groundwater by hexavalent chromium and chlorinated solvents. Sci Total Environ 563:822–834. doi:10.1016/j.scitotenv.2016.01.019

Ortega-Calvo J-J, Jimenez-Sanchez C, Pratarolo P, Pullin H, Scott TB, Thompson IP (2016) Tactic response of bacteria to zero-valent iron nanoparticles. Environ Pollut 213:438–445. doi:10.1016/j.envpol.2016.01.093

Pádrová K, Čejková A, Cajthaml T, Kolouchová I, Vítová M, Sigler K, Řezanka T (2016) Enhancing the lipid productivity of yeasts with trace concentrations of iron nanoparticles. Folia Microbiol 61:329–335. doi: 10.1007/s12223-015-0442-7

Pádrová K, Lukavský J, Nedbalová L, Čejková A, Cajthaml T, Sigler K, Vítova M, Řezanka T (2015) Trace concentrations of iron nanoparticles cause overproduction of biomass and lipids during cultivation of cyanobacteria and microalgae. J Appl Phycol 27:1443–1451. doi:10.1007/s10811-014-0477-1

Ravikumar KVG, Kumar D, Rajeshwari A, Madhu GM, Mrudula P, Chandrasekaran N, Mukherjee A (2016) A comparative study with biologically and chemically synthesized nZVI: applications in Cr (VI) removal and ecotoxicity assessment using indigenous microorganisms from chromium-contaminated site. Environ Sci Pollut R 23:2613–2627. doi:10.1007/s11356-015-5382-x

Ronavari A, Balázs M, Tolmacsov P, Molnar C, Kiss I, Kukovecz A, Konya Z (2016) Impact of the morphology and reactivity of nanoscale zero-valent iron (NZVI) on dechlorinating bacteria. Water Res 95:165–173. doi:10.1016/j.watres.2016.03.019

Sevcu A, El-Temsah YS, Joner EJ, Cernik M (2011) Oxidative stress induced in microorganisms by zero-valent iron nanoparticles. Microbes Environ 26:271–281. doi:10.1264/jsme2.ME11126

Suanon F, Sun Q, Li M, Cai X, Zhang Y, Yan Y, Yu C-P (2016b) Application of nanoscale zero valent iron and iron powder during sludge anaerobic digestion: impact on methane yield and pharmaceutical and personal care products degradation. J Hazard Mater 321:47–53. doi:10.1016/j.jhazmat.2016.08.076

Suanon F, Sun Q, Mama D, Li J, Dimon B, Yu C-P (2016a) Effect of nanoscale zero-valent iron and magnetite (Fe_3O_4) on the fate of metals during anaerobic digestion of sludge. Water Res 88:897–903. doi: 10.1016/j.watres.2015.11.014

Velimirovic M, Simons Q, Bastiaens L (2015) Use of CAH-degrading bacteria as test-organisms for evaluating the impact of fine zerovalent iron particles on the anaerobic subsurface environment. Chemosphere 134:338–345. doi:10.1016/j.chemosphere.2015.04.068

Wang T, Zhang D, Dai LL, Chen YG, Dai XH (2016) Effects of metal nanoparticles on methane production from waste-activated sludge and microorganism community shift in anaerobic granular sludge. Sci Rep 6:25857. doi:10.1038/srep25857

Xiu Z-M, Gregory KB, Lowry GV, Alvarez PJJ (2010) Effect of bare and coated nanoscale zerovalent iron on *tceA* and *vcrA* gene expression in *Dehalococcoides* spp. Environ Sci Technol 44:7647–7651. doi:10.1021/es101786y

Xiu Z-M, Jin Z-H, Li T-L, Mahendra S, Lowry GV, Alvarez PJJ (2009) Effects of nano-scale zero-valent iron particles on a mixed culture dechlorinating trichloroethylene. Bioresource Technol 101:1141–1146. doi:10.1016/j.biortech.2009.09.057

Xu G, Wang J, Lu M (2014) Complete debromination of decabromodiphenyl ether using the integration of *Dehalococcoides* sp. strain CBDB1 and zero-valent iron. Chemosphere 117:455–461. doi:10.1016/j.chemosphere.2014.07.077

Yu B, Jin X, Kuang Y, Megharaj M, Naidu R, Chen Z (2015) An integrated biodegradation and nano-oxidation used for the remediation of naphthalene from aqueous solution. Chemosphere 141:205–211. doi:10.1016/j.chemosphere.2015.07.050

Chemosphere 213 (2018) 568–577

Contents lists available at ScienceDirect

Chemosphere

journal homepage: www.elsevier.com/locate/chemosphere

Novel assay for the toxicity evaluation of nanoscale zero-valent iron and derived nanomaterials based on lipid peroxidation in bacterial species

Jaroslav Semerád [a, b], Monika Čvančarová [a], Jan Filip [c], Josef Kašlík [c], Jana Zlotá [a], Jana Soukupová [c], Tomáš Cajthaml [a, b, *]

[a] Institute of Microbiology, Czech Academy of Sciences, v.v.i., Vídeňská 1083, CZ-142 20, Prague 4, Czech Republic
[b] Institute for Environmental Studies, Faculty of Science, Charles University, Benátská 2, CZ-128 01, Prague 2, Czech Republic
[c] Regional Centre of Advanced Technologies and Materials, Faculty of Science, Palacký University, 17. listopadu 1192/12, CZ-771 46, Olomouc, Czech Republic

ARTICLE INFO

Article history:
Received 5 June 2018
Received in revised form
5 August 2018
Accepted 4 September 2018
Available online 13 September 2018

Handling editor: Tamara S. Galloway

Keywords:
Oxidative stress
nZVI
Toxicity assay
Malondialdehyde
Remediation
Reactive oxygen species

ABSTRACT

Nano-scale zero-valent iron (nZVI) began attracting research attention in remediation practice in recent decades as a prospective nanomaterial applicable to various contaminated matrices. Despite concerns about the negative effects of nanomaterials on ecosystems, the number of reliable toxicity tests is limited. We have developed a test based on the evaluation of oxidative stress (OS). The test employed the analysis of a typical OS marker (malondialdehyde, MDA), after exposure of six bacterial strains to the tested nanomaterial. We also attempted to use other OS and cell membrane damage assays, including the determination of glutathione and lactate dehydrogenase, respectively. However, we found that the components of these assays interfered with nZVI; therefore, these tests were not applicable. The MDA assay was tested using nZVI and three newly engineered oxide shell nZVI materials with different oxide thicknesses. Six different bacterial species were employed, and the results showed that the test was fully applicable for the concentrations of nanomaterials used in remediation practice (0.1–10 g/L). MDA was produced in a dose-response manner, and the bacteria showed a similar response toward pure pyrophoric nZVI, reaching EC_{50} values of 0.3–1.1 g/L. We observed different responses in the absolute production of MDA; however, the MDA concentrations were correlated with the cell membrane surfaces of the individual strains ($R > 0.75$; $P < 0.09$). Additionally, the EC_{50} values correlated with the thickness of the oxide shells (except for *Escherichia coli*: $R > 0.95$; $P < 0.05$), documenting the reliability of the assay, where reactivity was confirmed to be an important factor for reactive oxygen species production.

1. Introduction

Nanoscale zero-valent iron (nZVI) represents a highly reactive material that was invented for remediation purposes to clean up polluted areas in situ (Li et al., 2006; Tratnyek and Johnson, 2006). The applicability of nZVI toward the aquatic phase, including groundwater, and its effectivity against various types of pollutants, including chlorinated compounds, pesticides, and heavy metals, has been documented in numerous publications (Mueller et al., 2012; Nemecek et al., 2014, 2015), even in the case of commingled plumes containing different pollutants (Nemecek et al., 2016). Typical concentrations of nZVI range from 0.1 to 10 g/L (in some cases up to 50.0 g/L) (Grieger et al., 2010). To date, many studies have also focused on the development of surface-modified nZVI to improve the remediation properties, including altered mobility, reactivity and possible combination with bioremediation mechanisms (McPherson et al., 2013; Yan et al., 2010). Due to the increasing number of nanomaterial applications, the ecotoxicity and toxicity of engineered nanoparticles have been a subject of many studies; however, there are certain concerns about their negative effect on soil ecosystems, and the toxic effects of nZVI (especially at higher doses mimicking the real concentration) have not been well described (Lefere et al., 2016; Dong et al., 2016; Semerad and Cajthaml, 2016; Ye et al., 2017). One of the possible

* Corresponding author. Institute of Microbiology, Czech Academy of Sciences, v.v.i., Prague 4, Czech Republic.
E-mail address: cajthaml@biomed.cas.cz (T. Cajthaml).

https://doi.org/10.1016/j.chemosphere.2018.09.029
0045-6535/

reasons is the certain specificity of nanomaterials in manipulation and their bioavailability, which very often precludes the use of classical standardized ecotoxicity tests. In contrast, it is known that (engineered) nanoparticles produce reactive oxygen species (ROS) as one of their main toxic effects, and possible mechanisms of their formation have been described in many publications (Xia et al., 2006, 2008). In the case of imbalanced ROS metabolism, an undesirable state called oxidative stress (OS) is established (Sies, 1997). Additionally, the toxic properties of nZVI are linked to its reactivity and primary ability to produce ROS. The results of several studies have documented an increase in ROS levels in nZVI-exposed bacterial cultures (Lv et al., 2017; Le et al., 2015; Chen et al., 2013; Ravikumar et al., 2016; Kim et al., 2010). Additionally, the overexpression of specific genes (e.g., *sodA*, *sodB* and *catB*) indicates that nZVI exposure causes oxidative stress in bacterial cultures (Fajardo et al., 2013; Sacca et al., 2014). In other studies, the authors have described a higher toxicity toward genetically modified bacteria lacking genes for the OS defense mechanism (*rpoS*, *katG*, *katE*, *sodA*, *sodB* and *sodC*) corresponding to the involvement of OS as the main nZVI toxicity factor toward bacteria (Keenan et al., 2009; Chaithawiwat et al., 2016). The overproduction of tryptophanase associated with the OS response published in the work by Sacca et al. (2014) also support this suggestion. Possible OS mechanisms induced by nZVI have been reviewed, but a deeper and detailed evaluation of OS caused by nZVI using microorganisms is lacking (Sevcu et al., 2011).

In this study, two markers of OS, namely, glutathione (GSH) and malondialdehyde (MDA), as well as one marker of membrane integrity, lactate dehydrogenase (LDH), were monitored after nZVI exposure to several various bacterial species. These three markers are routinely used to evaluate toxicity and OS induced by other nanoparticles (Kumar et al., 2011; Xiong et al., 2011). Tripeptide glutathione is used to monitor the state of antioxidant defense, and the ratio of reduced glutathione (GSH) to its oxidized dimer (GSSG) is frequently used as a marker of OS. The intracellular enzyme LDH is a marker of membrane damage. In the case of membrane disruption, enzyme leakage is determined. Another OS marker, MDA, is widely used to monitor and evaluate lipid peroxidation. MDA, a toxic and mutagenic product of fatty acid degradation, is typically detected as a colored complex with thiobarbituric acid using a UV/VIS or fluorescence spectrophotometer (Kumar et al., 2011; Kil et al., 2014). Although this is a common colorimetric assay (usually called TBA-reactive substances test - TBARS test), a lack of sensitivity and specificity is the main limitation of the test (Liu et al., 1997). TBA reacts with a whole range of compounds, and a chromatography separation step is essential to achieve reproducible and reliable results (Grotto et al., 2009). For the separation and quantification of MDA from biological samples (cells in culture, blood tissue), RP-HPLC-FL methods are frequently used (Domijan et al., 2015).

The main purpose of this study was to investigate the possible use of various common bacterial species to develop a simple protocol and to optimize an assay based on OS that would be applicable for the toxicity determination of pure newly developed nanomaterials based on nZVI. A secondary objective was to compare the short-term toxicity of pure nZVI and three core-shell nZVI-derived nanomaterials to evaluate the reliability and feasibility of the assay using core-shell materials with reduced reactivity.

2. Materials and methods

2.1. Chemicals and assays

$Na_2B_4O_7 \cdot 10\ H_2O$, dithiothreitol, o-phthalaldehyde, LDH kit TOX7, 2-thiobarbituric acid (TBA), trichloracetic acid, Hoechst 33258 and 1-butanol were obtained from Sigma-Aldrich (Steinheim, Germany). The standard solution of LDH from bovine heart, Hoechst 33258, and reduced and oxidized glutathione were purchased also from Sigma-Aldrich (Steinheim, Germany). Methanol (absolute LC-MS) was purchased from Biosolve (Valkenswaard, Nederland). Nutrient Broth w/1% peptone and nutrient Agar No. 2 were obtained from Himedia (Mumbai, India). $NaHCO_3$ and Na_2CO_3 were obtained from Chemapol (Prague, Czech Republic). HCl 35%, $Na_2HPO_4 \cdot 12\ H_2O$ and $NaH_2PO_4 \cdot 2\ H_2O$ were purchased from Lachner (Prague, Czech Republic). H_3BO_3 was from HiChem (Prague, Czech Republic). Absolute counting beads for flow cytometry (CountBright) were obtained from Thermo Fisher Scientific (Prague, Czech Republic).

2.2. Nanomaterial synthesis and characterization

Pyrophoric NANOFER 25P particles (nZVI; purchased from NANO IRON Company, Rajhrad, Czech Republic) were synthesized by thermal reduction of the iron oxide precursor according to a previously described procedure (Zboril et al., 2012; Filip et al., 2014). An oxide shell of variable thickness, passivating the nZVI particles, was prepared by controlled nZVI oxidation under variable temperature conditions and duration (see Table 1 and Results and discussion section) (Kašlík et al., 2018).

2.3. Preparation of the nanoparticle suspension

Air-stable nanoparticles based on nZVI (A, B, and C) were weighed (0.1; 0.5; 1.0; 2.0; 3.0; 5.0; 10.0; 20.0; 50.0 and 100.0 mg) in Eppendorf tubes and then mixed with 100 μL of MilliQ water. Pure pyrophoric nZVI stock solutions were weighed under a nitrogen atmosphere in a glove box (Jacomex, Dagneux, France) and mixed with MilliQ water immediately before the assay. The stock solutions were prepared at tenfold higher concentrations than the finally tested concentrations. The solutions were immediately used (within a few minutes) for exposition to the bacterial cultures.

2.4. Cultivation and preparation of bacteria

Escherichia coli (strain CCM 3988), *Bacillus subtilis* (strain CCM 1999), and *Serratia marcescens* (strain CCM 303) were obtained from the Czech Collection of Microorganisms (CCM, Brno, Czech Republic). *Bacillus cereus* (strain DBM 3035), *Staphylococcus epidermidis* (strain DBM 3072) and *Enterobacter cloacae* (strain DBM 3126) were obtained from the Collection of Yeasts and Industrial Microorganisms (DBM, Prague, Czech Republic). All the bacterial strains were cultivated at 37 °C using the following protocol. First, the bacterial culture was cultivated on bacterial agar plates, and then one colony forming unit was used to inoculate 50 mL of nutrient broth prepared according to the supplier's instructions. After 24 h of cultivation, the bacterial suspension was centrifuged for 10 min at 5000 × g, the supernatant was removed, and the pellet was resuspended in 5 mL of 2 mM bicarbonate buffer (pH 8). The final concentration in the stock suspension used for following experiments was 10^9–10^{10} bacteria/mL.

Table 1
Conditions of nZVI passivation of NANOFER 25P.

Sample	Conditions of passivation		
	Temperature (°C)	Duration (min)	Atmosphere
A	20	150	N_2 + air (−0.03 bar)
B	130	240	98% N_2 + 2% O_2 (0.5 bar)
C	165	240	98% N_2 + 2% O_2 (0.5 bar)

2.5. Exposure of bacteria to nanoparticles

A series of nZVI concentrations was tested: 0.1, 0.5, 1.0, 2.0, 3.0, 5.0, 10.0, 20.0, 50.0, and 100.0 g/L, when 100 μL of the tenfold concentrated nanoparticle stock suspension was mixed with 900 μL of the respective bacterial suspension to reach the final exposure volume of 1 mL. Exposure of the bacterial cultures to nanoparticles was then carried out in triplicate at 37 °C for 1 or 3 h. The samples were incubated on a reciprocal shaker at 150 RPM to achieve homogeneity of the suspension and to facilitate direct contact of the bacteria with the nanoparticles to prevent sedimentation. For each exposition, the cell concentration in the bacterial suspension was determined before the experiment using flow cytometry according to the following protocol.

2.6. Flow cytometry and confocal microscopy

Before analysis by flow cytometry, bacterial cultures in bicarbonate buffer were fixed and then diluted. With respect to the cell wall structure, the bacterial suspensions of Gram-positive bacteria and Gram-negative bacteria were fixed for 15 min using methanol and 99.5% ethanol (1:1, V:V) because this mixture provided the best results compared with pure methanol, ethanol, formaldehyde and various other mixtures. The fixed cultures were diluted 1000× in phosphate-buffered saline (PBS). Thereafter, 20 μL of Hoechst 33258 stain (10 μg/mL) was added to 180 μL of the diluted cultures in PBS. Next, 100 μL of the resulting solution was mixed with 10 μL of 10,000/μL of counting beads and then analyzed using the BD LSR II flow cytometer (BD Biosciences, San Jose, CA, USA). The settings for the forward scatter, side scatter and Hoechst fluorescence were adjusted according to each bacterial strain, thresholded by the Hoechst fluorescence, to measure only the stained events. When a clear population of Hoechst-stained bacteria and green fluorescent beads were obtained, the experimental samples were analyzed, and the bacterial counts were calculated based on the number of collected beads per sample. For microscopic observation, a confocal microscope Olympus FV1000 TIRF (Olympus, Prague, Czech Republic) was used.

2.7. Determination and quantification of malondialdehyde by HPLC-FLD

MDA was determined by HPLC using the derivatized MDA-TBA_2 form to facilitate sensitive fluorescence detection. The analyte concentration was estimated using a protocol previously described by Kumar et al. (2011) with several modifications (extraction of the MDA-TBA_2 complex, HPLC separation, and fluorescence detection). After exposure to the nZVI materials, 500 μL of the sample was mixed with 1 mL of 10% trichloracetic acid and left for 10 min at 25 °C. The suspension was centrifuged at 12000 g for 40 min, and then 1 mL of the supernatant was mixed with a mixture (2 mL) consisting of 0.67% TBA in 0.1 M HCl. The resulting solution was heated to 90 °C for 25 min in a water bath. Thereafter, the reaction with TBA was stopped by cooling the samples on ice. The complex MDA-TBA_2 was extracted using 1-butanol (1:1; v:v). The extracts were diluted two times with methanol and analyzed by HPLC/FLD.

An Alliance Waters HPLC system (Prague, Czech Republic) equipped with a fluorescence detector was employed, and the data were processed using Empower software. Separation of the MDA-TBA_2 complex was carried out on a reversed-phase column Waters Nova-Pak C18 4 μm 3.9 × 150 mm cartridge equipped with a C18 precolumn. The column temperature was maintained at 30 °C and a flow rate of 1 mL/min. Next, 60 μL of each sample solution was injected into the HPLC system. An isocratic HPLC program was employed consisting of 80% phosphate buffer (10 mM; pH 7; filtered through a 0.22 μm filter) and 20% methanol (HPLC grade). The excitation and emission wavelengths were set at 532 nm and 551 nm, respectively.

Due to MDA reactivity and instability, the MDA standard for the calibration stock solution was prepared by a chemical reaction from 1,1,3,3-tetramethoxypropane. 500 μL of 1,1,3,3-tetramethoxypropane and 100 μL of 1 M HCl were added to 99.4 mL of MilliQ water, and the solution was mixed and heated at 50 °C for 60 min in a water bath according to an acid hydrolysis method by Csallany et al. (1984). The MDA stock solution (30 mM) was then cooled to laboratory temperature and stored at 4 °C for less than 2 weeks (stability tested). The calibration standard solutions (ranging from 0.1 mM to 10 mM) were prepared fresh daily by dilution with MilliQ water.

2.8. Determination of lactate dehydrogenase

The amount of LDH leakage after cell membrane disruption was measured using an LDH kit (LDH kit TOX7) according to the manufacturer's protocol. The absorbance of the colored product was measured at 490 and 690 nm using the Infinite PRO multi-well plate spectrometer (Tecan, Männedorf, Switzerland). LDH from the bovine heart was used as the standard for calibration and other experiments, including the reactivity and stability of LDH.

2.9. Determination of glutathione by HPLC-FLD

The GSH concentration was determined after derivatization with o-phthalaldehyde as previously described by Gawlik et al. (2014) using another HPLC-FLD method. GSSG was reduced by dithiothreitol, and the resulting GSH was determined using the same HPLC method. The HPLC instrument was used as described above for MDA; however, the employed gradient program for GSH was different. The gradient conditions were as follows (min, %A): 0, 5; 3, 5; 5, 100; 8, 100. The duration of the analysis was 8 min, and the flow rate was 0.8 mL/min. The mobile phases were also the same as described above except for the molarity of the buffer. In this case, 20 mM phosphate buffer (pH 7) was used.

2.10. Data analysis and presentation

The determined amount of MDA by HPLC-FLD was related to several of the exposed bacterial cells, which were counted using the flow cytometry method prior to exposure. The final results were then expressed as the concentration of MDA normalized to 10^7 of bacteria. The amounts of MDA produced by control cultivations without nZVI materials reached a maximum of 4.9%, and the respective concentrations detected in the individual strains were subtracted from the results.

For the graphic presentation of the results, correlation analysis and dose-response curve modeling, OriginPro 8.5 software was used, and the EC_{50} values were calculated via sigmoidal fitting using the same software. $EC_{50\text{-corrected}}$ values were calculated for the oxide shell materials using nZVI as the reference material (see the Results and discussion section) with respect to the maxima of the individual dose-response curves. The calculation was carried out according to Ezechiáš and Cajthaml (2018) using the following formula:

$$EC_{50\text{-corrected}} = EC_{50} \times MAX_{nZVI}/MAX$$

where EC_{50} is the original value of a material obtained from the respective dose response curve, MAX_{nZVI} is the maximum response reached by nZVI under the same conditions, and MAX is the maximum value reached by the respective oxide shell material.

3. Results and discussion

3.1. Properties of the tested nanomaterials

Adopting the nanomaterial preparation procedure (Zboril et al., 2012; Kašlík et al., 2018; see 2.2. section), the particle diameter remained constant (i.e., 72 nm with variations within experimental error; see Fig. 1) with the oxide shell thickness as the only variable: sample A = 3.8 nm (this material is identical to commercially available NANOFER STAR from NANO IRON Company, Czech Republic), sample B = 7.9 nm and sample C = 14.8 nm (see Fig. 1). The phase composition of all nZVI samples was rather similar: α-Fe

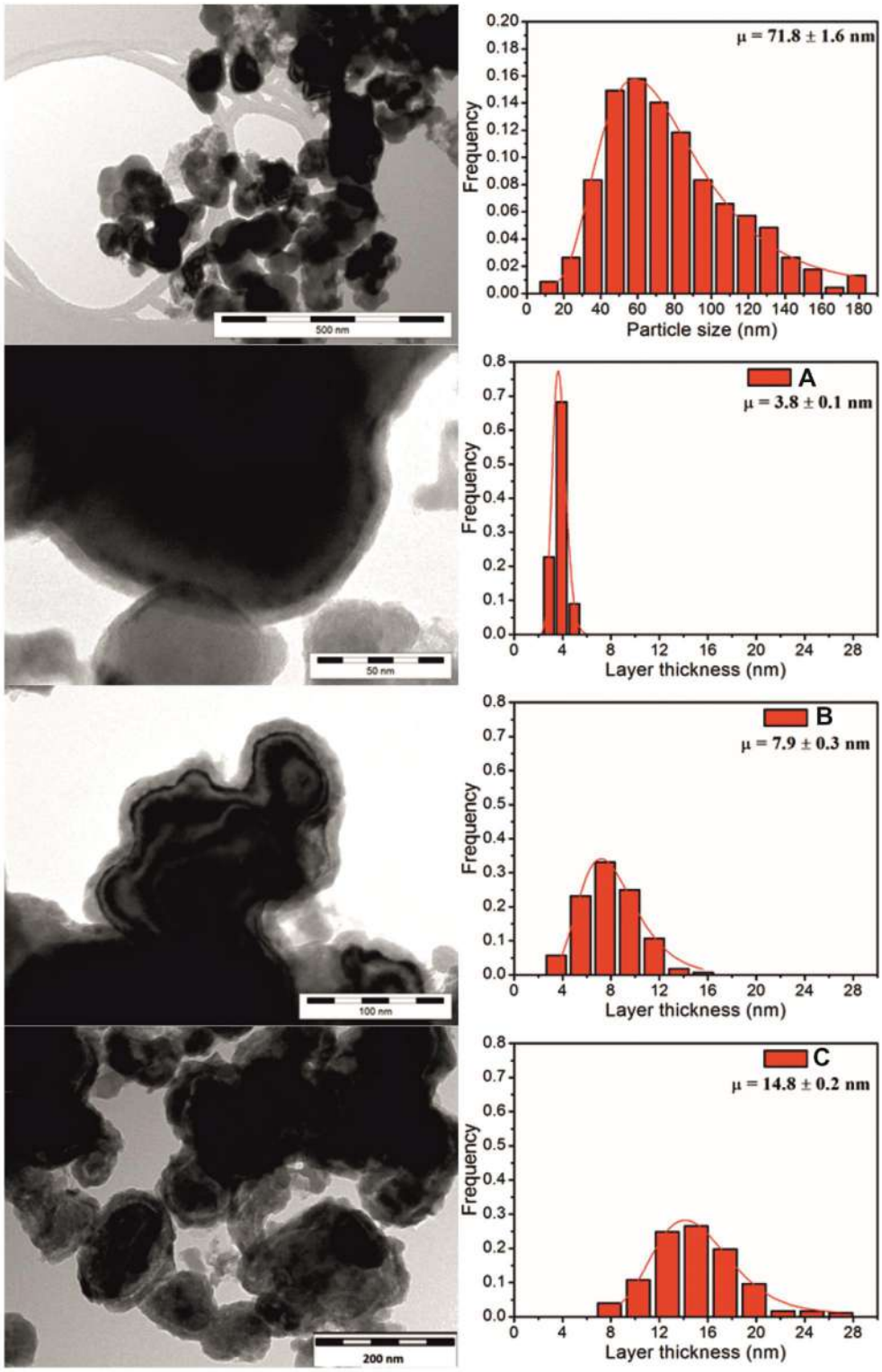

Fig. 1. TEM images and distribution of the oxide shell of the tested nanomaterial.

(>90 wt% for pyrophoric nZVI, 89 wt% for sample A, 84 wt% for sample B and 68 wt% for sample C), FeO/Fe_3O_4 as artifacts of the nZVI preparation, while the same phases (but significantly more nanocrystalline according to the respective XRD patterns; Fig. S1 in Supporting information) appeared more pronounced along with the increased oxide shell thickness. The specific surface area (as) was close to 17 m^2/g for all samples, with variations within the experimental error of measurement by the physisorption of N_2. The zeta potential of the tested nanoparticles was measured using dynamic/electrophoretic light at a concentration of 0.4 g/L. The recorded values of the Zeta potential were −22.90, −18.30, −18.00, and −3.77 mV for nZVI, A, B and C, respectively.

3.2. Membrane damage – LDH

Bacterial membrane damage after exposure to nZVI (0.1, 0.5 and 1.0 g/L) was monitored via the determination of leaked LDH from the intracellular space. In preliminary experiments in which the culture of *E. coli* was exposed to nanoparticles for 1 h, we noted that the entire nZVI concentration range caused lower production of LDH than the respective bacterial control without nZVI. In fact, the concentrations of LDH showed an inverse proportion to the nZVI concentrations. The data are shown in Supplementary Table 1. The drop in concentrations of LDH with increasing concentrations of nZVI suggested that the nanoparticles negatively affected enzyme activity. To test this hypothesis, a standard solution of purified LDH (500 mU/mL) in 2 mM bicarbonate buffer (pH 8.0) was exposed to the lowest tested concentration of nZVI. The results showed a decrease in enzymatic activity by 79% even at a dose of 0.1 g/L of nZVI, confirming the hypothesis of LDH-nanomaterial interference (Supplementary Table 2).

Inhibition of purified LDH by the various types of nanoparticles (Si, Au, Cd, Se) with surface modifications has already been described by Maccormack et al. (2012). The authors also warned about possible interference using this standard test. However, to our knowledge, LDH inhibition by nZVI has not yet been described. The interaction documented in this study suggests that this assay is not applicable for the evaluation of toxicity induced by the real concentrations of nZVI used in remediation practice. Nevertheless, in several studies, the authors used LDH assays for toxicity evaluation of various types of nZVI (Keenan et al., 2009; Nadagouda et al., 2010; Wu et al., 2013). For example, Keenan et al. (2009) tested very low concentrations of nZVI (up to 11 mg/L), where the interference does not need to be significant.

3.3. State of antioxidant defense – glutathione

Based on our previous results from the LDH assay, we performed a stability test. A standard solution of GSH (9 μmol/L) was exposed to nZVI (1 g/L) for various time periods. After 10 and 20 min of exposure to nZVI, we observed the transformation of GSH. To evaluate the stoichiometry of the GSH transformation to GSSG, we converted the created GSSG via consequent reduction by dithiothreitol to release GSH. We found that we recovered only 61.4 and 62.9% of the GSH after 10 and 20 min of nZVI exposure, respectively. These results document that, in the presence of iron nanoparticles, the GSH monomer was transformed nonstoichiometrically to its oxidized dimer GSSG and to an unknown product (Supplementary Table 3). The transformation of one of the main cellular antioxidant documents that nZVI can induce an oxidative stress response. However, the results clearly show that this assay is also inapplicable for toxicity evaluations of nZVI materials.

A possible explanation for the negative results after the application of the GSH assay is the instant GSH oxidation by the reactive products originating from nZVI. The basic reaction of nZVI is the oxidation of Fe^0. In water, Fe^0 is oxidized to Fe^{2+} by the dissolved oxygen (can be further oxidized to Fe^{3+}) during the simultaneous formation of ROS (e.g., OH· and OOH·) (Sevcu et al., 2011). Through a single electron transfer or hydrogen transfer, ROS can react with GSH, forming a GSH radical (i.e., $GSH\cdot^+$ or GSH(-H)·) (Galano and Alvarez-Idaboy, 2011). Two GSH radical species can further form the oxidized dimer GSSG (Franco et al., 2007). Another possibility for the dimer formation is the reduction of Fe^{3+} by GSH to Fe^{2+}. This nonenzymatic reduction of Fe^{3+} to Fe^{2+} by GSH is described as the retransformation of methemoglobin to hemoglobin in erythrocytes (Mansouri, 1985) Nonquantitative transformation of the GSH standard to GSSG in the presence of nZVI is probably caused by the high reactivity or sorption ability of Fe^0. By testing the real remediation concentrations of nZVI (up to grams per liter), GSH is transformed (or adsorbed) in a short time (≤10 min); therefore, it is impossible to monitor the state of oxidative defense (i.e., OS) using this assay.

There is still a lack of suitable, comprehensive, and standardized tests for the ecotoxicological evaluation of novel nanomaterials. The toxic properties of nZVI materials are linked to their reactivity and mainly to their ability to produce ROS (Semerad and Cajthaml, 2016). However, most of the commonly used in vitro assays for the evaluation of OS have been designed for conventional organic and inorganic compounds. Because of the need to monitor possible undesirable effects of nanoparticles, the standard tests were adapted for this purpose (Hund-Rinke et al., 2016). However, regarding the diversity of nanoparticles and their chemical behavior, some of the tests interfere with optical method readouts or assay components (Tournebize et al., 2013). The inapplicability of two routinely used OS/toxicity tests in the case of nZVI-based materials was documented and explained in this study. The determination of LDH and the GSH/GSSG ratio both failed in tests of real applied concentrations of nZVI for remediation purposes (Supplementary Table 1–3).

3.4. Lipid peroxidation – malondialdehyde

Regarding our previous finding, the stability of MDA was tested at five concentrations (from 0.03 to 3 mM) of MDA standard solutions using exposure to all types of the studied nanomaterials at several concentrations up to 10 g/L for 3 h. In all cases, the recovery was greater than 90%. Three hours of exposure of the 6 bacterial species to the nZVI-based nanomaterials showed a dose-dependent increase in the formation of MDA (Fig. 2). The dose-dependent curves were observed for all the bacteria and tested nanomaterials. The EC_{50} values were calculated via sigmoidal fitting, and the results are shown in Fig. 3A. nZVI without the oxide shell generally exhibited the lowest EC_{50} and highest maximum responses using all the tested bacterial strains. In contrast, the highest EC_{50} showed nanomaterials with a thicker oxide shell (9 nm and 12 nm). The EC_{50} values of both nanomaterials (B and C) were similar; however, the maximum response differed and strictly followed the order of the oxide shell thickness (nZVI>4 nm > 9 nm > 14 nm). The same pattern of maximum responses was observed for all the tested bacteria (see Fig. 2 and Supplementary Fig. 2). The maximum MDA response results also substantially differed among the individual bacterial strains, although the data were normalized to the same amount of bacterial cells (10^7). Therefore, we attempted to investigate the reasons for such different maximum responses that are important for the sensitivity of the assay. We noted that the maximum values corresponded to the size of the individual bacterial strain cells, i.e., with the surface of the bacterial membrane. Thus, we calculated approximate surfaces of the bacterial cells using confocal microscopy with respect to the shape of the strains (spheres or cylinders)

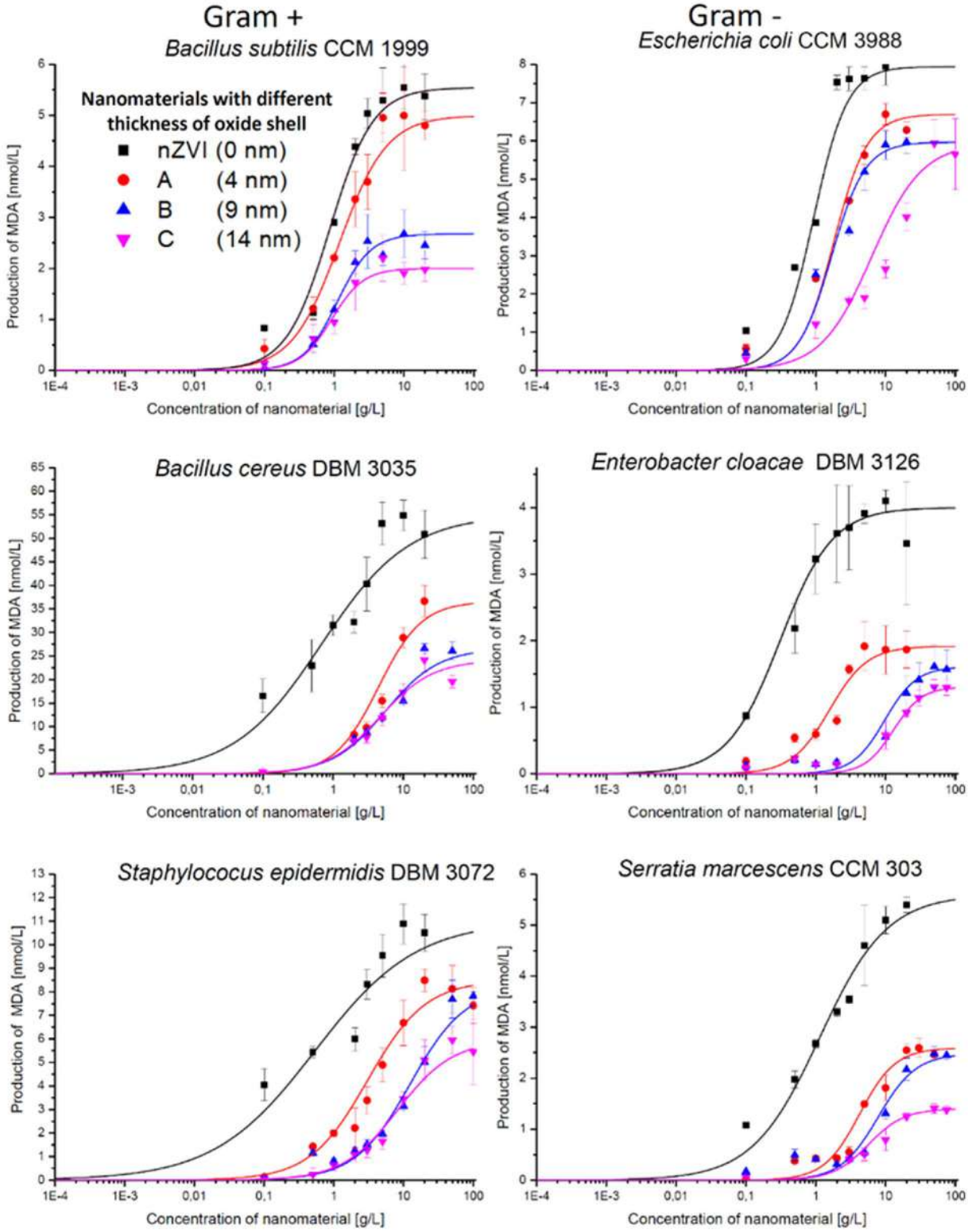

Fig. 2. Dose response curves of MDA production after 3 h of exposure of the bacteria to the nanoparticles. The MDA concentrations were recalculated to 10^7 bacteria. The individual points represent the means of three independent experiments, and the error bars represent the standard deviations.

using 50 individuals (see Supplementary Fig. 3; relative standard deviation did not exceed 20%). Thereafter, we performed a simple correlation analysis of the cell-membrane area with maximum MDA production. The Pearson correlation coefficient was, in all cases, higher than 0.75, and the P-values reached 0.05, 0.05, 0.09 and 0.07 for the nZVI, A, B and C materials, respectively.

In contrast, the optimized MDA assay for the determination of lipid peroxidation in bacteria species provided positive results in terms of OS evaluation. It is the only test, in this study, that is fully applicable to the whole range of real concentrations of nZVI-based

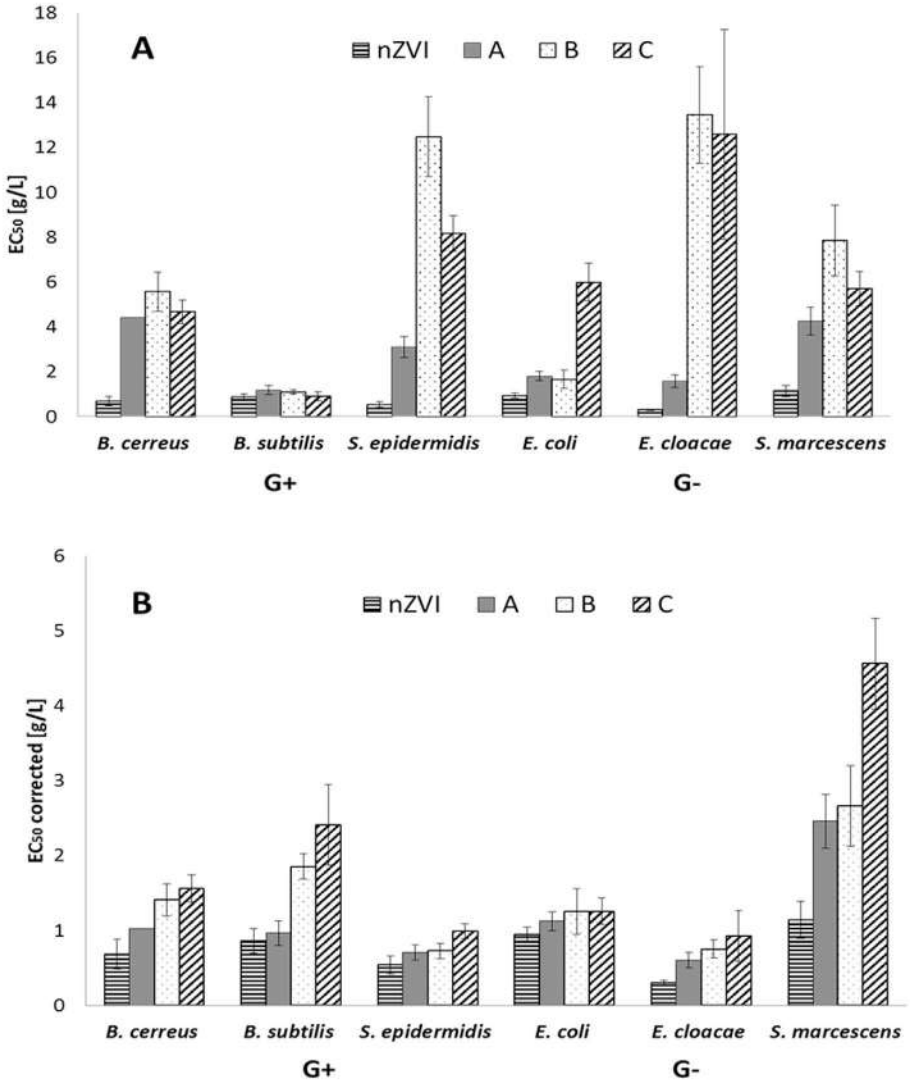

Fig. 3. A – EC50 values of MDA production calculated via sigmoidal fitting after 3-h exposure of the bacteria to the nanomaterials. B – Corrected EC50 values of MDA production regarding the maximum of the individual dose-response curves. The error bars stand for the standard deviations.

nanomaterials. To employ the phenomenon of lipid peroxidation by nZVI for toxicity assessment, it is necessary to understand the redox behavior of Fe^0 in the water and potential pathways of ROS generation via nZVI-based nanoparticles (Semerad and Cajthaml, 2016). The basic reaction of Fe^0 is its oxidation with the simultaneous reduction of various species. In the absence of free oxygen, Fe^0 can be oxidized by water to Fe^{2+} accompanied by H_2 generation (Filip et al., 2014). In water with the presence of dissolved oxygen, Fe^0 is oxidized to Fe^{2+}, which can be further oxidized to Fe^{3+}. In both cases, via one or two electron transfers, H_2O_2 can be formed (Keenan and Sedlak, 2008). Fe^{2+}, and eventually Fe^{3+}, can then enter the Fenton process and form hydroxyl radicals from H_2O_2 (Sevcu et al., 2011). In addition, radicals such as ·OH or ·OOH can react with lipids in the bacterial membrane and initiate the lipid peroxidation cascade (Esterbauer et al., 1991). One of the final products of lipid degradation (peroxidation) is MDA, the marker monitored in this study.

The results of the lipid peroxidation analysis (Fig. 2) clearly documented that the production of MDA was dose-dependent and closely associated with a specific organism. Regardless of the difference in EC_{50} values, the formation of MDA showed the same tendency in cases of all the tested bacteria. The lowest EC_{50} values were observed after exposure to the most reactive nZVI, and the production was gradually decreased following the order of A, B and C, with few exceptions (Fig. 3A). The same pattern was observed for the maximum responses, where the values of maximum MDA production greatly varied among the bacterial strains (Supplementary Fig. 1). A possible and logical explanation for the different levels of OS after exposure to the different materials is that the production of MDA corresponds to the reactivity of the particles, where a higher coating (i.e., passivation, see Fig. 1) results in a lower OS. These results in fact verify the suitability of the optimized test. The results from the present study, in general, support this hypothesis, although no additional analyses were performed. A direct connection between the bacterial inactivation and cell damage resulting from nZVI reactivity has been described in several publications (Auffan et al., 2008; Le et al., 2015; Chen et al., 2013; Ravikumar et al., 2016).

As shown in Fig. 2, the calculated EC_{50} values of the nanomaterials were probably influenced by the maxima of the individual dose-response curves. Based on the results, some of the EC_{50} values were underestimated only because the dose-response

curves reached lower maximum values than those of the more reactive materials. Therefore, we attempted to correct these EC_{50} values regarding their maxima by applying a simple formula resulting from the receptor theory (Ezechias and Cajthaml, 2018; Ehlert et al., 1999) where nZVI was used as the reference material, revealing the maximum response of the individual bacteria under the used conditions (Fig. 3B). Such an approach clearly enables the comparison of material in a better way because the value of $EC_{50\text{-corrected}}$ represents the potency of the material to trigger OS better than EC_{50} alone. When we performed the correlation analysis of the $EC_{50\text{-corrected}}$ values with the thickness of the oxide shells, we found that, except for *E. coli*, the Pearson correlation coefficients were higher than 0.951, and the P values were lower than 0.049. In the case of *E. coli*, the Pearson correlation coefficients and P values were 0.870 and 0.130, respectively.

In this study, we tested the acute toxicity of the nZVI-based materials on various species of bacteria, and a certain species-specific toxic effect was observed. However, there was no clear difference between the toxicity to gram-positive and gram-negative bacteria. In this context, there are several articles in the literature documenting different nZVI effects on specific bacterial populations (Lefevre et al., 2016; Semerad and Cajthaml, 2016; Jang et al., 2014) or even at species and strain levels (Chaithawiwat et al., 2016). However, the results of this study documented that, considering only OS, MDA production was highly correlated with the size (surface) of the respective bacterial strains (see the results). A possible explanation for this phenomenon is that larger bacterial species have a larger surface area and, therefore, higher amounts of unsaturated fatty acids that are precursors of MDA. The highest formation of MDA after exposure to the nanomaterials was observed in the case of *B. cereus* and the lowest for *E. cloacae*. Regarding the applicability of the assay, the results suggest that any easily cultivated bacterial strain can be employed, and use is not restricted to special soil or pathogenic bacteria.

Another important parameter frequently mentioned in the literature that influences the toxicity of nanoparticles is aggregation (Renzi and Guerranti, 2015). The aggregation of nanoparticles increases the size of particles and decreases their bioavailability (Rodea-Palomares et al., 2011). The key indicator of the stability of colloidal dispersions is the Zeta potential, which predicts the aggregation of nanoparticles due to Van Der Waals inter-particle attractions. The recorded Zeta potentials of our tested nanoparticles indicate that with an increasing oxide shell, particles are more likely to aggregate. Correlation analysis of the $EC_{50\text{-corrected}}$ values with the Zeta potentials of the nanomaterials again revealed that, except for *E. coli*, the Pearson correlation coefficients were better than −0.81 and the P values lower than 0.18. The Pearson correlation coefficients for *E. coli* and the P-value were −0.70 and 0.30, respectively. Documented correlation of the $EC_{50\text{-corrected}}$ values and the Zeta potential showed that aggregation of the tested nanoparticles could also influence their toxicity. In the environment, nZVI undergoes spontaneous oxidation. The effect of passivation, when Fe^0 is oxidized and iron-oxides (e.g., magnetite, maghemite, hematite, and goethite) are formed on the surface of the nanoparticles, is usually called "aging". How full/partial oxidation "aging" could affect the toxicity of nZVI has already been studied by many authors (Li et al., 2010; Phenrat et al., 2009; Wang et al., 2016). Another study has shown that with increasing oxidation of nZVI, the absolute value of the Zeta potential decreases together with the negative effects on bacteria (Ortega-Calvo et al., 2016). The authors stated that the decrease in toxicity and the concomitant decrease in the surface charge (Zeta potential) of nZVI in time indicated that Fe^0 went through an aging process. Accordingly, the results presented in the current study showing a decrease in the toxicity of nZVI-based nanoparticles in relation to the thickness of the oxide shell can also be presented as the toxicity level of nZVI over time: nZVI without an oxide shell as fresh and nZVI-based nanoparticles with a thicker oxide shell indicative of its different stages of aging (i.e., partially aged).

4. Conclusion

In summary, we attempted to develop a novel assay for toxicity determination based on the monitoring of OS to test the toxicity of nZVI and related materials covered with an oxide shell with different thicknesses. The findings of this study demonstrate that unique and specific proprieties of nZVI materials influence the toxicity/OS determination. Specific features of nZVI, such as its high reactivity (reductive potential), coagulation, sorption on cells and general interactions with assay components, complicate toxicity determination by commonly used tests. Bacterial membrane damage and detection via the determination of LDH were found to be inapplicable due to the inactivation of LDH by nZVI materials. Additionally, monitoring of the GSH/GSSG ratio was not applicable due to the reaction of GSH with nZVI and nonstoichiometry of the GSH-GSSG transformation. These results documented that during the adaptation of any classical toxicity assay to nanomaterials, stability tests should be carried out to exclude any undesired interference of the tested materials with the respective assay components.

In contrast, the optimized OS assay employing MDA determination was shown to be a suitable solution for the fast in vivo determination of oxidative stress induced by nZVI-based nanoparticles. Using this assay, we could compare the toxicity based on OS of newly manufactured nanomaterials even before their incorporation into the environment. Additionally, the results also documented the suitability of the test for the rapid and easy monitoring of nZVI material aging in terms of toxicity determination. The results of the assay also showed that OS, which is considered one of the main nZVI toxicity mechanisms, was species specific only in terms of EC_{50} values; however, the response of the assay in terms of MDA production correlated with the size of the cell membrane surface.

Overall, the correspondence of our results to the logical prediction of a toxicity decrease using the different oxide shell materials proves that the novel assay is fully applicable to the toxicity determination/evaluation of nZVI-based nanoparticles. Based on the direct evaluation of OS, we can now monitor one of the most important adverse effects of iron nanoparticles and compare the toxicity of newly engineered core-shell structures before their use in the field.

Declaration of interest

The authors declare no competing financial interests.

Acknowledgments

This work was supported by Competence Center TE01020218 of the Technology Agency of the Czech Republic and by the Center for Geosphere Dynamics (UNCE/SCI/006). We acknowledge the Cytometry and Microscopy Facility at the Institute of Microbiology of the ASCR, v.v.i, Vídeňská 1083, Prague, CZ for the use of the cytometry equipment and support from the staff.

Appendix A. Supplementary data

Supplementary data to this article can be found online at https://doi.org/10.1016/j.chemosphere.2018.09.029.

Abbreviations

OS	oxidative stress
GSH	glutathione
MDA	malondialdehyde
nZVI	nanoscale zero-valent iron
ROS	reactive oxygen species
TBA	2-thiobarbituric acid
GSSG	glutathione oxidized dimer; as, specific surface area

References

Auffan, M., Achouak, W., Rose, J., Roncato, M.A., Chaneac, C., Waite, D.T., Masion, A., Woicik, J.C., Wiesner, M.R., Bottero, J.-Y., 2008. Relation between the redox state of iron-based nanoparticles and their cytotoxicity toward *Escherichia coli*. Environ. Sci. Technol. 42, 6730–6735.

Chaithawiwat, K., Vangnai, A., McEvoy, J.M., Pruess, B., Krajangpan, S., Khan, E., 2016. Impact of nanoscale zero valent iron on bacteria is growth phase dependent. Chemosphere 144, 352–359.

Chen, Q., Li, J., Wu, Y., Shen, F., Yao, M., 2013. Biological responses of Gram-positive and Gram-negative bacteria to nZVI (Fe-0), Fe2+ and Fe3+. RSC Adv. 3, 13835–13842.

Csallany, A.S., Derguan, M., Manwaring, J.D., Addis, P.B., 1984. Free malonaldehyde determination in tissues by high-performance liquid chromatography. Anal. Biochem. 142, 277–283.

Domijan, A.M., Ralic, J., Brkanac, S.R., Rumora, L., Zanic-Grubisic, T., 2015. Quantification of malondialdehyde by HPLC-FL - application to various biological samples. Biomed. Chromatogr. 29, 41–46.

Dong, H., Xie, Y., Zeng, G., Tang, L., Liang, J., He, Q., Zhao, F., Zeng, Y., Wu, Y., 2016. The dual effects of carboxymethyl cellulose on the colloidal stability and toxicity of nanoscale zero-valent iron. Chemosphere 144, 1682–1689.

Ehlert, F.J., Griffin, M.T., Sawyer, G.W., Bailon, R.A., 1999. A simple method for estimation of agonist activity at receptor subtypes: comparison of native and cloned M-3 muscarinic receptors in Guinea pig ileum and transfected cells. J. Pharmacol. Exp. Therapeut. 289, 981–992.

Esterbauer, H., Schaur, R.J., Zollner, H., 1991. Chemistry and biochemistry of 4-hydroxynonenal, malonaldehyde and related aldehydes. Free Radical Biol. Med. 81–128.

Ezechiáš, M., Cajthaml, T., 2018. Receptor partial agonism and method to express receptor partial activation with respect to novel Full Logistic Model of mixture toxicology. Toxicology 393, 26–33.

Fajardo, C., Sacca, M.L., Martinez-Gomariz, M., Costa, G., Nande, M., Martin, M., 2013. Transcriptional and proteomic stress responses of a soil bacterium *Bacillus cereus* to nanosized zero-valent iron (nZVI) particles. Chemosphere 93, 1077–1083.

Filip, J., Karlický, F., Marušák, Z., Lazar, P., Černík, M., Otyepka, M., Zbořil, R., 2014. Anaerobic reaction of nanoscale zerovalent iron with water: mechanism and kinetics. J. Phys. Chem. C 118, 13817–13825.

Franco, R., Schoneveld, O.J., Pappa, A., Panayiotidis, M.I., 2007. The central role of glutathione in the pathophysiology of human diseases. Arch. Physiol. Biochem. 113, 234–258.

Galano, A., Alvarez-Idaboy, J.R., 2011. Glutathione: mechanism and kinetics of its non-enzymatic defense action against free radicals. RSC Adv. 1, 1763–1771.

Gawlik, M., Krzyzanowska, W., Gawlik, M.B., Filip, M., 2014. Optimization of determination of reduced and oxidized glutathione in rat striatum by hplc method with fluorescence detection and pre-column derivatization. Acta Chromatogr. 26, 335–345.

Grieger, K.D., Fjordboge, A., Hartmann, N.B., Eriksson, E., Bjerg, P.L., Baun, A., 2010. Environmental benefits and risks of zero-valent iron nanoparticles (nZVI) for in situ remediation: risk mitigation or trade-off? J. Contam. Hydrol. 118, 165–183.

Grotto, D., Maria, L.S., Valentini, J., Paniz, C., Schmitt, G., Garcia, S.C., Pomblum, V.J., Rocha, J.B.T., Farina, M., 2009. Importance of the lipid peroxidation biomarkers and methodological aspects FOR malondialdehyde quantification. Quim. Nova 32, 169–174.

Hund-Rinke, K., Baun, A., Cupi, D., Fernandes, T.F., Handy, R., Kinross, J.H., Navas, J.M., Peijnenburg, W., Schlich, K., Shaw, B.J., Scott-Fordsmand, J.J., 2016. Regulatory ecotoxicity testing of nanomaterials - proposed modifications of OECD test guidelines based on laboratory experience with silver and titanium dioxide nanoparticles. Nanotoxicology 10, 1442–1447.

Jang, M.H., Lim, M., Hwang, Y.S., 2014. Potential environmental implications of nanoscale zero-valent iron particles for environmental remediation. Environ. Health Toxicol. 29, e2014022.

Kašlík, J., Kolařík, J., Filip, J., Medřík, I., Tomanec, O., Petr, M., Malina, O., Zbořil, R., Tratnyek, P.G., 2018. Nanoarchitecture of advanced core-shell zero-valent iron particles with controlled reactivity for contaminant removal. Chem. Eng. J. 354, 335–345.

Keenan, C.R., Sedlak, D.L., 2008. Factors affecting the yield of oxidants from the reaction of manoparticulate zero-valent iron and oxygen. Environ. Sci. Technol. 42, 1262–1267.

Keenan, C.R., Goth-Goldstein, R., Lucas, D., Sedlak, D.L., 2009. Oxidative stress induced by zero-valent iron nanoparticles and Fe(II) in human bronchial epithelial cells. Environ. Sci. Technol. 43, 4555–4560.

Kil, H.-N., Eom, S.-Y., Park, J.-D., Kawamoto, T., Kim, Y.-D., Kim, H., 2014. A rapid method for estimating the levels of urinary thiobarbituric acid reactive substances for environmental epidemiologic survey. Toxicol. Res. 30, 7–11.

Kim, J.Y., Park, H.J., Lee, C., Nelson, K.L., Sedlak, D.L., Yoon, J., 2010. Inactivation of *Escherichia coli* by nanoparticulate zerovalent iron and ferrous ion. Appl. Environ. Microbiol. 76, 7668–7670.

Kumar, A., Pandey, A.K., Singh, S.S., Shanker, R., Dhawan, A., 2011. Engineered ZnO and TiO2 nanoparticles induce oxidative stress and DNA damage leading to reduced viability of *Escherichia coli*. Free Radical Biol. Med. 51, 1872–1881.

Le, T.T., Nguyen, K.H., Jeon, J.R., Francis, A.J., Chang, Y.S., 2015. Nano/bio treatment of polychlorinated biphenyls with evaluation of comparative toxicity. J. Hazard Mater. 287, 335–341.

Lefevre, E., Bossa, N., Wiesner, M.R., Gunsch, C.K., 2016. A review of the environmental implications of in situ remediation by nanoscale zero valent iron (nZVI). Sci. Total Environ. 889–901.

Li, X.Q., Elliott, D.W., Zhang, W.X., 2006. Zero-valent iron nanoparticles for abatement of environmental pollutants: materials and engineering aspects. Crc. Cr. Rev. Sol. State 31, 111–122.

Li, Z.Q., Greden, K., Alvarez, P.J.J., Gregory, K.B., Lowry, G.V., 2010. Adsorbed polymer and NOM limits adhesion and toxicity of nano scale zerovalent iron to *E. coli*. Environ. Sci. Technol. 44, 3462–3467.

Liu, J.K., Yeo, H.C., Doniger, S.J., Ames, B.N., 1997. Assay of aldehydes from lipid peroxidation: gas chromatography – mass spectrometry compared to thiobarbituric acid. Anal. Biochem. 245, 161–166.

Lv, Y.C., Niu, Z.Y., Chen, Y.C., Hu, Y.Y., 2017. Bacterial effects and interfacial inactivation mechanism of nZVI/Pd on *Pseudomonas putida* strain. Water Res. 115, 297–308.

Maccormack, T.J., Clark, R.J., Dang, M.K.M., Ma, G., Kelly, J.A., Veinot, J.G.C., Goss, G.G., 2012. Inhibition of enzyme activity by nanomaterials: potential mechanisms and implications for nanotoxicity testing. Nanotoxicology 6, 514–525.

Mansouri, A., 1985. Methemoglobinemia. Am. J. Med. Sci. 289, 200–209.

McPherson, A.W., Goltz, M.N., Agrawal, A., 2013. Pollutant degradation by nanoscale zero valent iron (nZVI): role of polyelectrolyte stabilization and catalytic modification on nZVI performance. ACS Symp. Ser. 1150, 159–191.

Mueller, N.C., Braun, J., Bruns, J., Černík, M., Rissing, P., Rickerby, D., Nowack, B., 2012. Application of nanoscale zero valent iron (NZVI) for groundwater remediation in Europe. Environ. Sci. Pollut. Res. 19, 550–558.

Nadagouda, M.N., Castle, A.B., Murdock, R.C., Hussain, S.M., Varma, R.S., 2010. In vitro biocompatibility of nanoscale zerovalent iron particles (NZVI) synthesized using tea polyphenols. ACS Symp. Ser. 12, 114–122.

Němeček, J., Lhotský, O., Cajthaml, T., 2014. Nanoscale zero-valent iron application for in situ reduction of hexavalent chromium and its effects on indigenous microorganism populations. Sci. Total Environ. 485, 739–747.

Němeček, J., Pokorný, P., Lacinová, L., Černík, M., Masopustová, Z., Lhotský, O., Filipová, A., Cajthaml, T., 2015. Combined abiotic and biotic in-situ reduction of hexavalent chromium in groundwater using nZVI and whey: a remedial pilot test. J. Hazard Mater. 300, 670–679.

Němeček, J., Pokorný, P., Lhotský, O., Knytl, V., Najmanová, P., Steinová, J., Černík, M., Filipová, A., Filip, J., Cajthaml, T., 2016. Combined nano-biotechnology for in-situ remediation of mixed contamination of groundwater by hexavalent chromium and chlorinated solvents. Sci. Total Environ. 822–834.

Ortega-Calvo, J.-J., Jimenez-Sanchez, C., Pratarolo, P., Pullin, H., Scott, T.B., Thompson, I.P., 2016. Tactic response of bacteria to zero-valent iron nanoparticles. Environ. Pollut. 213, 438–445.

Phenrat, T., Long, T.C., Lowry, G.V., Veronesi, B., 2009. Partial oxidation ("sging") and surface modification decrease the toxicity of nanosized zerovalent iron. Environ. Sci. Technol. 43, 195–200.

Ravikumar, K.V.G., Kumar, D., Rajeshwari, A., Madhu, G.M., Mrudula, P., Chandrasekaran, N., Mukherjee, A., 2016. A comparative study with biologically and chemically synthesized nZVI: applications in Cr (VI) removal and ecotoxicity assessment using indigenous microorganisms from chromium-contaminated site. Environ. Sci. Pollut. Res. 23, 2613–2627.

Renzi, M., Guerranti, C., 2015. Ecotoxicity of nanoparticles in aquatic environments: a review based on multivariate statistics of meta-data. Int. J. Environ. Anal. Chem. 2, 149.

Rodea-Palomares, I., Boltes, K., Fernandez-Pinas, F., Leganes, F., Garcıa-Calvo, E., Santiago, J., Rosal, R., 2011. Physicochemical characterization and ecotoxicological assessment of CeO_2 nanoparticles using two aquatic microorganisms. Toxicol. Sci. 119, 135–145.

Sacca, M.L., Fajardo, C., Martinez-Gomariz, M., Costa, G., Nande, M., Martin, M., 2014. Molecular stress responses to nano-sized zero-valent iron (nZVI) particles in the soil bacterium *Pseudomonas stutzeri*. PLoS One 9, e89677.

Semerád, J., Cajthaml, T., 2016. Ecotoxicity and environmental safety related to nano-scale zerovalent iron remediation applications. Appl. Microbiol. Biotechnol. 100, 9809–9819.

Ševců, A., El-Temsah, Y.S., Joner, E.J., Černík, M., 2011. Oxidative stress induced in microorganisms by zero-valent iron nanoparticles. Microb. Environ. 26, 271–281.

Sies, H., 1997. Oxidative stress: oxidants and antioxidants. Exp. Physiol. 82, 291–295.

Tournebize, J., Sapin-Minet, A., Bartosz, G., Leroy, P., Boudier, A., 2013. Pitfalls of assays devoted to evaluation of oxidative stress induced by inorganic nanoparticles. Talanta 116, 753–763.

Tratnyek, P.G., Johnson, R.L., 2006. Nanotechnologies for environmental cleanup.

Nano Today 1, 44–48.
Wang, J., Fang, Z.Q., Cheng, W., Tsang, P.E., Zhao, D.Y., 2016. Ageing decreases the phytotoxicity of zero-valent iron nanoparticles in soil cultivated with *Oryza sativa*. Ecotoxicology 25, 1202–1210.
Wu, D.L., Shen, Y.H., Ding, A.Q., Mahmood, Q., Liu, S., Tu, Q.P., 2013. Effects of nanoscale zero-valent iron particles on biological nitrogen and phosphorus removal and microorganisms in activated sludge. J. Hazard Mater. 262, 649–655.
Xia, T., Kovochich, M., Brant, J., Hotze, M., Sempf, J., Oberley, T., Sioutas, C., Yeh, J.I., Wiesner, M.R., Nel, A.E., 2006. Comparison of the abilities of ambient and manufactured nanoparticles to induce cellular toxicity according to an oxidative stress paradigm. Nano Lett. 6, 1794–1807.
Xia, T., Kovochich, M., Liong, M., Maedler, L., Gilbert, B., Shi, H., Yeh, J.I., Zink, J.I., Nel, A.E., 2008. Comparison of the mechanism of toxicity of zinc oxide and cerium oxide nanoparticles based on dissolution and oxidative stress properties. ACS Nano 2, 2121–2134.
Xiong, D., Fang, T., Yu, L., Sima, X., Zhu, W., 2011. Effects of nano-scale TiO2, ZnO and their bulk counterparts on zebrafish: acute toxicity, oxidative stress and oxidative damage. Sci. Total Environ. 409, 1444–1452.
Yan, W.L., Herzing, A.A., Li, X.Q., Kiely, C.J., Zhang, W.X., 2010. Structural evolution of Pd-doped nanoscale zero-valent iron (nZVI) in aqueous media and implications for particle aging and reactivity. Environ. Sci. Technol. 44, 4288–4294.
Ye, S., Zeng, G., Wu, H., Zhang, C., Liang, J., Dai, J., Liu, Z., Xiong, W., Wan, J., Xu, P., Cheng, M., 2017. Co-occurrence and interactions of pollutants, and their impacts on soil remediation—a review. Crit. Rev. Environ. Sci. Technol. 47, 1528–1553.
Zbořil, R., Andrle, M., Oplustil, F., Machala, L., Tuček, J., Filip, J., Marušák, Z., Sharma, V.K., 2012. Treatment of chemical warfare agents by zero-valent iron nanoparticles and ferrate(VI)/(III) composite. J. Hazard Mater. 211, 126–130.

Environmental Science and Pollution Research

Oxidative stress in microbes after exposure to iron nanoparticles: Analysis of aldehydes as oxidative damage products of lipids and proteins

--Manuscript Draft--

Manuscript Number:	
Full Title:	Oxidative stress in microbes after exposure to iron nanoparticles: Analysis of aldehydes as oxidative damage products of lipids and proteins
Article Type:	Research Article
Keywords:	nanomaterial; oxidative stress; toxicity assay; SPME; yeast; remediation
Corresponding Author:	Tomas Cajthaml Institute of Microbiology, ASCR CZECH REPUBLIC
Corresponding Author Secondary Information:	
Corresponding Author's Institution:	Institute of Microbiology, ASCR
Corresponding Author's Secondary Institution:	
First Author:	Jaroslav Semerád
First Author Secondary Information:	
Order of Authors:	Jaroslav Semerád
	Monika Moeder
	Jan Filip
	Martin Pivokonský
	Alena Filipová
	Tomas Cajthaml
Order of Authors Secondary Information:	
Funding Information:	Technology Agency of the Czech Republic (TE01020218) — prof. Tomas Cajthaml
Abstract:	Due to their enhanced reactivity, metal and metal-oxide nanoscale zero-valent iron (nZVI) nanomaterials have been introduced into remediation practice. To ensure that environmental applications of nanomaterials are safe, their possible toxic effects should be described. However, there is still a lack of suitable toxicity tests that address the specific mode of action of nanoparticles, especially for nZVI. This contribution presents a novel approach for monitoring one of the most discussed adverse effects of nanoparticles, i.e., oxidative stress (OS). We optimized and developed an assay based on head-SPME-GC-MS analysis that enables the direct determination of volatile oxidative damage products (aldehydes) of lipids and proteins in microbial cultures after exposure to commercial types of nZVI. The method employs PDMS/DVB SPME fibers and pentafluorobenzyl derivatization, and the protocol was successfully tested using representatives of bacteria, fungi and algae. Six aldehydes, namely, formaldehyde, acrolein, methional, benzaldehyde, glyoxal and methylglyoxal, were detected in the cultures, and all of them exhibited dose-dependent sigmoidal responses. The presence of methional, which was detected in all cultures except those including an algal strain, documents that nZVI also caused oxidative damage to proteins in addition to lipids. The most sensitive toward nZVI exposure in terms of aldehyde production was the yeast strain Saccharomyces cerevisiae, which had an EC50 value of 0.08 g/L nZVI. To the best of our knowledge, this paper is the first to document the production of aldehydes resulting from lipids and proteins as a result of OS in microorganisms from different kingdoms after exposure to iron nanoparticles.

Suggested Reviewers:	Anne Kahru National Institute of Chemical Physics and Biophysics, Estonia anne.kahru@kbfi.ee Expert in ecotoxicology of nanomaterials
	Joachim Sturve Department of Biological and Environmental Sciences, University of Gothenburg, Sweden joachim.sturve@bioenv.gu.se Expert in aquatic toxicology and ecotoxicology, biomarker and antioxidant defense systems
	Patryk Oleszczuk Maria Environmental Chemistry Department Curie-Sklodowska University in Lublin, Poland patryk.oleszczuk@poczta.umcs.lublin.pl Expert in environmental chemistry, ecotoxicology and nZVi
Opposed Reviewers:	
Additional Information:	
Question	**Response**
§Are you submitting to a Special Issue?	No

Oxidative stress in microbes after exposure to iron nanoparticles: Analysis of aldehydes as oxidative damage products of lipids and proteins

Jaroslav Semerád[1,2], Monika Moeder [3], Jan Filip[4], Martin Pivokonský[5], Alena Filipová[1,2] and Tomáš Cajthaml[1,2]

[1] Institute of Microbiology of the Czech Academy of Sciences, Vídeňská 1083, CZ-142 20, Prague 4, Czech Republic

[2] Institute for Environmental Studies, Faculty of Science, Charles University, Benátská 2, CZ-128 01, Prague 2, Czech Republic

[3] Helmholtz-Center for Environmental Research – UFZ, Department of Analytical Chemistry, Permoserstr. 15, 04318, Leipzig, Germany

[4] Regional Centre of Advanced Technologies and Materials, Palacký University, Šlechtitelů 27, CZ-783 71, Olomouc, Czech Republic

[5] Institute of Hydrodynamics of the Czech Academy of Sciences, Pod Patankou 30/5, CZ-166 12, Prague 6, Czech Republic

Corresponding author: Tomáš Cajthaml; E-mail: cajthaml@biomed.cas.cz; Telephone: +420241062498; ORCID: 0000-0002-3393-1333

Keywords: nanomaterial, oxidative stress, toxicity assay, SPME, yeast, remediation

Abstract

Due to their enhanced reactivity, metal and metal-oxide nanoscale zero-valent iron (nZVI) nanomaterials have been introduced into remediation practice. To ensure that environmental applications of nanomaterials are safe, their possible toxic effects should be described. However, there is still a lack of suitable toxicity tests that address the specific mode of action of nanoparticles, especially for nZVI. This contribution presents a novel approach for monitoring one of the most discussed adverse effects of nanoparticles, i.e., oxidative stress (OS). We optimized and developed an assay based on head-SPME-GC-MS analysis that enables the direct determination of volatile oxidative damage products (aldehydes) of lipids and proteins in microbial cultures after exposure to commercial types of nZVI. The method employs PDMS/DVB SPME fibers and pentafluorobenzyl derivatization, and the protocol was successfully tested using representatives of bacteria, fungi and algae. Six aldehydes, namely, formaldehyde, acrolein, methional, benzaldehyde, glyoxal and methylglyoxal, were detected in the cultures, and all of them exhibited dose-dependent sigmoidal responses. The presence of methional, which was detected in all cultures except those including an algal strain, documents that nZVI also caused oxidative damage to proteins in addition to lipids. The most sensitive toward nZVI exposure in terms of aldehyde production was the yeast strain *Saccharomyces cerevisiae,* which had an EC_{50} value of 0.08 g/L nZVI. To the best of our knowledge, this paper is the first to document the production of aldehydes resulting from lipids and proteins as a result of OS in microorganisms from different kingdoms after exposure to iron nanoparticles.

Introduction:

Nanoremediation represents an emerging branch of remediation and employs various nanomaterials to treat contaminated waters, sediments and soils (Dong et al. 2019; Xue et al. 2018). Despite the large spectrum of nanoparticles in use, nanoscale zero-valent iron (nZVI) and its related materials are the most commonly applied nanomaterials in environmental remediation practice (Karn et al. 2011). Application of nZVI and full-scale cleanup operations have been successfully used to demonstrate its efficiency in the decontamination of various pollutants (Nemecek et al. 2014; Nemecek et al. 2015; Nemecek et al. 2016). The high degradation efficiency and cost-effectiveness of nZVI production indicate increasing applications of nZVI. However, despite the known positive aspects of nZVI, detailed information of its potential influence on resident living species is still limited or has barely been explored (Semerad and Cajthaml 2016).

One of the most cited mechanisms of nanoparticle toxicity is oxidative stress (OS; (Sevcu et al. 2011)). This undesirable state of an organism is established when an imbalance of reactive oxygen species (ROS) occurs. The presence of elevated ROS concentrations or their insufficient catabolism can lead to their interaction with cellular biomolecules, such as lipids, proteins, carbohydrates and nucleic acids, leading to the formation of (sometimes toxic and mutagenic) end-products. Oxidative degradation of lipids is called lipid peroxidation, and through a cascade of radical reactions, various aldehydes (such as 4-hydroxynonenal, acrolein, malondialdehyde, glyoxal, etc.) can be formed from unsaturated fatty acids (Esterbauer et al. 1991; O'Brien et al. 2005). In addition, ROS can react with proteins and oxidize or degrade amino acids during the concurrent formation of their oxidation products containing carbonyl groups (methional, 2-aminoadipic semialdehyde, glutamic semialdehyde, etc.; (Grimsrud et al. 2008)). Some protein oxidation markers (e.g., methional, benzaldehyde, formaldehyde, etc.) can also be formed by Strecker-type degradation induced by lipid oxidation products or directly by oxidative Strecker degradation of amino acids (Schonberg and Moubacher 1952).

Zero-valent iron-based nanoparticles are redox-active catalysts that can be used for *in situ* remediations (Soukupova et al. 2015) and are highly reactive particles, and the reactivity of nZVI lies in its strong reductive potential. Fe^0 undergoes oxidation (to Fe^{2+} and Fe^{3+}) while reducing its counterparts, including pollutants, oxygen or water (Stefaniuk et al. 2016). In the case of side reactions with nontargeted molecules (e.g., water; (Filip et al. 2014)), a large amount of ROS are formed. Many studies describe possible pathways of nZVI interactions with microorganisms or living species, and the majority of them suggest that membrane disruption and oxidative stress are the main mechanisms that contribute to the cytotoxicity of nZVI (Lefevre et al. 2016; Semerad and Cajthaml 2016; Wu et al. 2019). The generation of Fe^{2+} via Fe^0 oxidation and ROS produced by the Fenton reaction also play a crucial role in the induction of OS. Several authors were able to detect and monitor nZVI-induced OS *in vitro* in bacterial species by measuring ROS, ROS catabolic enzyme activity or other markers of OS (Le et al. 2015; Lv et al. 2017; Semerád et al. 2018).

Generally, there is a demand for the development of toxicity assays to measure the adverse effects of nanoparticles that are specifically aimed at their mode of action. Moreover, the development and application of novel nZVI-derived nanomaterials calls for more intense studies of its possible adverse effects, either at the molecular level or directly at the site during nanoremediation applications.

In this study, we present a novel approach for monitoring oxidative stress damage in microorganisms from different kingdoms, which enables an estimation of the toxicity of pure newly isolated nanoparticles and monitoring of real remediated sites where nZVI is typically used, to ensure its safe application. Based on many published applications of carbonyl compound analysis in various matrices, we developed a novel, sensitive and simple method for the determination of aldehydes using microbial cultures. Aldehydes, which are typical markers of oxidative stress, are routinely determined and quantified by HPLC or GC coupled with mass spectrometry (MS) after derivatization (Nishikawa and Sakai 1995; Uchiyama et al. 2011). To avoid matrix effects and laborious sample preparation, solid

phase microextraction (SPME) is often used (Bao et al. 1998; Schmarr et al. 2008a; Schmarr et al. 2008b; Wang et al. 2005).

Therefore, the aim of this article was to optimize and develop an assay based on head-space (HS)-SPME-GC-MS method for rapid and sensitive screening of volatile oxidative damage products (aldehydes) of lipids and proteins in various microbes, including bacteria, fungi and algae, after exposure to commercial nZVI particles. To the best of our knowledge, this is the first study documenting the production of aldehydes from lipids and proteins by nZVI-induced OS in microorganisms from different kingdoms.

Materials and Methods

Materials (chemicals)

Air-stable nZVI particles, NANOFER STAR, a commercially available form of nZVI, were obtained from NANO IRON Company (Rajhrad, Czech Republic). The cultivation medium for bacteria, Nutrient broth No. 2, was acquired from Himedia (Mumbai, India). Other chemicals, including standard solutions of each aldehyde, 65 μm PDMS/DVB SPME fibers and derivatization reagent O-(2,3,4,5,6-Pentafluorobenzyl)hydroxylamine hydrochloride (PFBHA), were purchased from Sigma-Aldrich (Steinheim, Germany).

Character of nZVI-based nanoparticles

The NANOFER STAR nZVI particles used in this study were prepared by solid-gas thermal reduction of an iron oxide precursor, followed by surface passivation (to obtain air-stable particles), and were recently well characterized (Kaslik et al. 2018). Briefly, the core-shell of the nanoparticles consists of a metallic iron core (α-Fe, bcc crystal structure) and approximately 4 nm thick iron oxide shell (Fig. 1); the shell is dominantly formed by magnetite. The mean particle size of the nearly spherical particles is approximately 70 nm, and their specific surface area is close to 20 m^2/g; the particles contain approximately 90 wt.% of iron atoms in the metallic state. These nanoparticles were recently used in numerous environmental and mechanistic studies (Nemecek et al. 2016; Ribas et al. 2017; Tucek et al. 2017; Zboril et al. 2012).

Microbial cultivation and pretreatment before exposure

All microbial species were cultivated according to their specific requirements. The bacterial strains *Bacillus cereus* DBM 3035 and *Serratia marcescens* CCM 303 were grown in Nutrient broth No. 2 at 37 °C as described previously (Semerád et al. 2018). A yeast culture of *Saccharomyces cerevisiae* BY 4742 was cultivated at 30 °C in YPD medium (composition: glucose, 20 g/L; bacterial peptone, 10 g/L; yeast extract, 10 g/L; and, agar, 15 g/L) as follows. One single CFU was added to a 500 mL Erlenmeyer flask containing 50 mL of YPD medium, and the yeast culture was cultivated for 18 hours. The last microbial species, the algal strain *Desmodesmus subspicatus* CCALA 688, was purchased from the Institute of Botany of the Czech Academy of Sciences (Czech Republic) and cultivated in Bold's basal medium (21 °C, 72 hours, and 8000 lux). After cultivation, all microbial cultures were washed twice with phosphate-buffered saline (PBS) and concentrated 10x as follows: 50 mL of cellular suspension was centrifuged for 10 min at 5000 *g*, the supernatant was removed, and the pellet was resuspended in 50 mL of PBS and then centrifuged again. The final pellet was resuspended in 5 mL of PBS.

Cell counting by flow cytometry

The number of microbial cells used in this study was counted by flow cytometry. The instrumental setup for bacterial counting was the same as in a previously study (Semerád et al. 2018). The yeast culture was fixed with

ethanol (1:1; yeast: ethanol absolute) and diluted 100x in PBS. Prior to flow cytometry, 180 µL of the diluted cultures in PBS were mixed with 20 µL of stain (Hoechst 33258; 10 µg/mL) and 10 µL of counting beads (green fluorescence beads; 10,000 beads/µL). The algal strain exhibited auto-fluorescence, and, therefore, this culture was directly measured without staining after the addition of 10 µL of counting beads to 100 µL of the algal samples. The prepared samples were further analyzed using a BD LSR II flow cytometer (BD Biosciences, San Jose, CA, USA). The settings of forward scatter, side scatter and Hoechst fluorescence or auto-fluorescence were adjusted and thresholded by Hoechst fluorescence or auto-fluorescence, respectively. Finally, the stained or auto-fluorescent events were recorded, and cell counts were calculated from the number of collected beads and events per sample. The cell concentrations of the stock suspensions used for subsequent experiments were 10^9–10^{10} cells/mL for bacteria, 10^9 cells/mL for yeast and 10^7 cells/mL for algae.

Exposition to nanoparticles and sample preparation prior to HS-SPME-GC-MS

Exposure to the nanoparticles was based on a previously described protocol (Semerád et al. 2018) with slight modifications. The respective biotic controls were prepared without exposure to nZVI. The tested concentrations of iron nanoparticles were 0.1, 0.5, 1.0, 2.5, 5, 10, and 20 g/L. Air-stable nZVI nanoparticles were weighed (1, 5, 10, 25, 50, 100, and 200 mg) in centrifugation tubes and mixed with 1 mL of Milli-Q water. The nanoparticle suspension (1 mL) was mixed with 9 mL of the respective microbial suspension to reach a final exposure volume of 10 mL. Exposure of the microbial cultures to iron nanoparticles was carried out in triplicate under the specific growth conditions for each species for 24 hours. To reach homogeneity of the suspension and to prevent sedimentation of nanoparticles, exposure was carried out on a reciprocal shaker at 150 oscillations per minute.

Thereafter, the exposed samples were prepared for HS-SPME-GC-MS analysis according to the following protocol. First, after the exposure, microbial cells were lysed by mechanical disruption of their membranes; 1 mL of the exposed sample was added to 0.5 g glass beads and vigorously shaken on a high-throughput cell homogenizer MP FastPrep-24 (MP Biomedicals, Santa Ana, CA, USA). Subsequently to lysis, the samples were centrifuged for 10 min at 12,000 *g* to achieve complete sedimentation of the nanoparticles.
Finally, 1850 µL of the centrifuged sample supernatant, 100 µL of an internal standard (ISTD; D6-cyclohexanon, 20 µg/L) and 50 µL of the derivatization reagent (PFBHA·HCl; 1 g/L) were transferred to 20 mL headspace vials that were sealed with PTFE caps prior to HS-SPME-GC-MS analysis.

HS-SPME-GC-MS method

GC-MS analysis was performed using gas chromatography-mass spectrometry (GC–MS; 450-GC, 240-MS ion trap detector, Varian, Walnut Creek, CA, USA). The automated HS-SPME technique was performed using a CombiPal autosampler (CTC Analytics AG, MN, USA) equipped with an SPME fiber holder and a heating station for incubation (i.e., derivatization) and extraction of the derivatized aldehydes. MS workstation software was used for data acquisition, data processing and to control the GC-MS and CombiPal autosampler. The temperature of the injector, equipped with an SPME liner (Topaz, Restek, Bellefonte, PA, USA), was set to 250 °C to desorb the derivatized aldehydes from the SPME fiber. A constant flow of helium, 1.2 mL/min, was used as the carrier gas for GC-MS analysis. The temperature ramp started from 40 °C (2 min isothermal) to 120 °C at 12 °C/min (6 min isothermal) and then to 240 °C at 5 °C/min (1 min isothermal). The temperature of the mass spectrometer was set to 220 °C for the ion trap, 50 °C for the manifold and 280 °C for the transferline. The data were collected within a mass range of 50–500 *m/z*, and selected ions (see below) were used for quantification with respect to each carbonyl compound. All aldehydes were quantified by the sum of the peak areas of two geometric isomers as previously described (Cullere et al. 2004; Vesely et al. 2003) with the exception of formaldehyde, for which the separation of the two oximes was not achieved.
According to previously published methods of aldehyde determination in various samples, a 65 µm PDMS/DVB fiber was selected for its affinity for PFBHA oximes (Martos and Pawliszyn 1998). HS-SPME derivatization was

based on methods recently described in the literature (Ferreira et al. 2004) and modified and optimized for our purpose (derivatization time: 30, 60, 90, and 180 min; extraction time: 15, 30 and 45 min; temperature: 40, 60, and 80 °C; and carryover effect). The optimized conditions were as follows. Each headspace vial containing a sample was transferred to the heating station and conditioned for 60 minutes at 80 °C. Then, the SPME fiber was inserted into the headspace of the heated sample for 30 min (at the same temperature) to extract the derivatized aldehydes. Finally, the fiber loaded with PFBHA oximes was inserted into the injector. Prior to each sequence, the fiber was left and conditioned in the injector for 15 minutes at 250 °C to avoid sample cross-contamination and potential background/carryover effects.

Data analysis

Dose-response curves were modelled using OriginPro 8.5, and the EC_{50} values were calculated via sigmoidal fitting using the same software. For further statistical testing, a t-test was employed ($p < 0.05$).
Dose response curves were constructed after subtracting the background concentrations of aldehydes in the biotic control samples without exposure to nZVI.
The lowest observed effect concentration (LOEC) was the lowest tested concentration that was significantly different from the control ($p < 0.05$) within the given exposure time.
The limit of quantification (LOQ) of the whole method was determined as the lowest point of the calibration curve with precision lower than 20 %, comprising the whole process, including SPME and the derivatization process. The reproducibility of the instrument was determined using 10 replicated injections of the individual analytes at a concentration level of 100 µg/L.

Results

Method optimization and validation

The HS-SPME-GC-MS method, which is the standard method for aldehyde determination in clinical and food matrices, was adapted and optimized. According to previous studies, the PDMS-DVB SPME fiber was selected because of its suitable selectivity and extraction/desorption ability. To more deeply explore the oxidative stress damage caused by nZVI, 16 aldehyde representatives, as potential biomarkers of oxidative stress selected according to the literature, were derivatized with PFBHA, and the GC-MS method has been optimized to analyze the respective PBHA-oximes. The optimized parameters selected as the most efficient are mentioned in Materials and Methods. The final method was then validated, and the reproducibility of the selected aldehydes was tested. The reproducibility at a concentration level of 100 µg/L was lower than 13.6 % for each aldehyde. All other parameters, including the retention times of all the derivatization products, quantification ions, and the LOQ of the whole process, are presented in Table 1.

Microbial samples after exposure to different concentrations of nZVI

In this study, 4 microbial cultures were exposed to different concentrations of the commercially available form of nZVI as typical representatives of different kingdoms, including bacteria (Gram + *B. subtilis*; Gram – *S. marcescens*), fungi (yeast *S. cerevisiae*) and plantae (alga *D. subspicatus*). Microbes can potentially be affected by nZVI during remediation processes when nanoparticles of Fe^0 are applied at concentrations of approximately 2 g/L (Nemecek et al. 2014) and, sometimes, at even higher concentrations (Grieger et al. 2010). After 24 h of exposure of the microbial cultures to nZVI, several short chain aldehydes and dialdehydes were detected and identified as markers of oxidative damage of various biomolecules. Two aldehyde markers were detected in the algal culture:

formaldehyde and glyoxal. Both detected markers showed a similar dose-dependent sigmoidal trend (Fig. 2). The EC_{50} values are shown in Table 2.

The number of aldehyde markers of OS damage found in the yeast and bacterial cultures was higher than that found in the algal culture. In the culture of *S. cerevisiae* exposed to the concentration range of nZVI, 6 aldehydes were detected: formaldehyde, acrolein, methional, benzaldehyde, glyoxal and methylglyoxal (Fig. 3). All of the detected markers showed a statistically significant increase ($p < 0.05$) in their concentrations in nZVI-exposed samples compared with the biotic nZVI-free control; for formaldehyde, acrolein, benzaldehyde, and glyoxal, a statistically significant increase in their concentrations was even found at the lowest tested concentration of 0.1 g/L. A significant increase in the concentration of methional in this microbial culture was found at a concentration of 5 g/L, and the LOEC for methylglyoxal production was 1 g/L.

S. marcescens and *B. cereus*, as representatives of Gram-negative and Gram-positive bacteria, respectively, were also used in our study. After exposure of the bacterial culture of *S. marcescens* to the concentration range of nZVI, dose-dependent responses of formaldehyde, acrolein, methional and benzaldehyde were observed (Fig. 4). In comparison to the biotic control samples, the production of all of the detected OS markers except for methional were significantly higher, even at the lowest nZVI concentration used in the experiment, 0.1 g/L; the LOEC for methional was 0.5 g/L. The Gram-negative strain *S. marcescens* exhibited 10x higher total production of aldehydes compared to the Gram-positive strain *B. cereus*.

Screening of aldehydes in the culture of *B. cereus* after exposure to nZVI showed an increase in the concentrations of 5 aldehydes (i.e., formaldehyde, acrolein, methional, glyoxal, and benzaldehyde); see Fig. 5. As for the previous microbes exposed to nZVI, the aldehydes detected after exposure to *B. cereus* exhibited a sigmoidal dose-response trend (see Table 2).

Discussion

During the last three decades, lipid peroxidation, one of the main forms of oxidative damage caused by ROS, has been extensively studied, and several degradation pathways of fatty acids have been described. A series of iterative oxidation and cleavage reactions produce carbonyl compounds that are frequently highly reactive, toxic and, in some cases, even mutagenic. The most explored products of lipid peroxidation are aldehydes (e.g., malondialdehyde, 4-hydroxynonenal, acrolein, and glyoxal), and elevated levels of aldehydes are often observed in biological systems (Esterbauer et al. 1991). Short-chain aldehydes and dicarbonyls can also be formed via glycoxidation caused by high levels of oxidants or by degradation of glycated proteins. The formation of short-chain aldehydes resulting from the oxidation of amino acids also occurs. Therefore, analysis of aldehydes could provide insight into oxidative damage and be used to evaluate the current level of OS in living species (Kohen and Nyska 2002). OS is frequently connected with many pathological states of several diseases in clinical studies (Hussain et al. 2003; Jenner 2003; Markesbery 1997). Consequently, many authors have focused on discovering new markers of oxidative stress, and new methods have been developed for their quantification, which could allow a better understanding of disease progression and help in diagnosis (Chen et al. 2016). The undesirable state of disbalance in ROS metabolism can occur in all living cells, including microbes. Accordingly, some of the OS markers used in clinical studies can also be found in different organisms and be used as monitoring tools of their vitality.

The most common markers of lipid peroxidation are TBARS (thiobarbituric acid reactive species) derivatives, which are measured by UV/fluorescent spectrometry (Kohen and Nyska 2002). To separate and identify each marker/carbonyl/aldehyde, analytical methods, such as liquid chromatography or gas chromatography with mass detection, are typically employed (Shibamoto 2006; Spiteller et al. 1999). For both separation techniques, derivatization of aldehydes is used. Recently published studies on the derivatization of aldehydes with PFBHA and

subsequent headspace extraction by SPME fibers and analysis by gas chromatography coupled with mass detection showed that even trace levels of aldehydes could be feasibly determined under concurrent suppression of matrix effects (Cancho et al. 2002; Iglesias et al. 2010; Moreira et al. 2013; Schmarr et al. 2008a).

Due to their high reactivity and toxicity, the most studied products of lipid degradation in living systems are malondialdehyde, 4-hydroxynonenal and acrolein (Dalle-Donne et al. 2006; Hauck and Bernlohr 2016). Malondialdehyde and 4-hydroxynonenal were not detected in the current study, even though the presence of malondialdehyde was confirmed by HPLC-FL in our previous work using another analytical technique (Semerád et al. 2018). The possible explanation for the lack of detection of malondialdehyde and 4-hydroxynonenal is that the PFBHA oximes of several carbonyls are polar and non-volatile, and only a minor portion will be present in the sample headspace. Another explanation is the high reactivity of malondialdehyde, which can bind to large biomolecules, resulting in a low partial pressure of the compound in the head space (Esterbauer et al. 1991).

The only typical marker of lipid peroxidation and, at the same time, the most reactive product of lipid degradation detected in this study, was acrolein (Perluigi et al. 2012). This short, unsaturated aldehyde was present in both bacterial strains as well as in the yeast strain after exposure to nZVI. Moreover, glyoxal, a short and reactive dialdehyde, was detected in all the tested microbial species. This marker of OS is standardly described to be a product of the decomposition of lipid hydroperoxides, which are products of the oxidative breakdown of deoxyribose or the autoxidation of other sugars (Mistry et al. 2003). However, all of the described mechanisms of glyoxal formation occur during or are involved with OS and therefore can be used to quantify unspecific oxidative damage. For instance, the formation of glyoxal during ozonization of algal/natural organic matter has also been described (Huang et al. 2008). In addition, a methylated form of glyoxal was found in the yeast culture. The endogenous metabolite methylglyoxal could be formed like glyoxal via glucose metabolism, protein catabolism and fatty acid oxidation (Voulgaridou et al. 2011). Methylglyoxal is considered a marker of OS and it is a precursor of advanced glycation products that is often found in studies dealing with age-related diseases (Maessen et al. 2015). Nevertheless, the most abundant aldehyde of the detected carbonyls, which was found in all the exposed microbial cultures, was formaldehyde. Formaldehyde, the shortest aldehyde, was detected at concentrations several times higher than the other detected markers (see the Results section). The occurrence of formaldehyde is also connected to OS and is related to oxidative damage in many studies (Shara et al. 1992; Voulgaridou et al. 2011). Some authors have suggested potential pathways of formaldehyde formation via lipid peroxidation or endogenous processes, such as amino acid metabolism. We also found endogenous formaldehyde production in the nZVI-free microbial control samples.

In addition to lipid peroxidation, protein breakdown or oxidation of free amino acids could also result in carbonyl formation. The direct reaction of proteins and ROS can result in the carbonylation of the side chains of polypeptides and, in some cases, the formation of peptide fragments with a carbonyl group. Another mechanism of the oxidative damage of proteins leading to the formation of the carbonyl moiety was described by Stadtman and Levine (Stadtman and Levine 2003). Another possible pathway of carbonyl generation is the direct oxidation of free alpha amino acids via process called Strecker degradation. This degradation process involves a series of reactions in which alpha amino acids undergo oxidation by a large number of different oxidizing agents for the subsequent formation of an aldehyde. Strecker degradation could be caused by inorganic agents (e.g., H_2O_2, O_2 or O_3, etc.) or by organic compounds, such as other carbonyls (Schonberg and Moubacher 1952). Oxidation of glycine will lead to formaldehyde production. The large difference in the concentrations of formaldehyde and the rest of the detected markers could also be explained by the uncertainty of the formaldehyde origin – there are many potential pathways/precursors for its formation. Benzaldehyde, another aldehyde connected to OS damage, was detected in both bacterial and yeast cultures. Direct oxidation of amino acids is one of the probable explanations for the increase in the benzaldehyde concentration in microbial samples exposed to nZVI, as well as in the case of formaldehyde. The formation of benzaldehyde via a hydroxyl radical attack has been described, and oxidation of phenylalanine results in the production of phenylacetaldehyde and benzaldehyde (Chu and Yaylayan 2008). The last marker of

oxidative damage found in all three nonphotosynthetic species was methional. Oxidative degradation of methionine leads to methional formation the previously mentioned Strecker reaction. Methionine is the only aldehyde that contains sulfur which was detected during the exposure of microbes to nZVI; methionine has been shown to induce apoptosis in murine lymphoid cells (Roch et al. 1998). Apart from this, the majority of OS-derived carbonyls have been shown to be able to cause some toxic effects or to induce damage to biomolecules (Esterbauer 1993; Moghe et al. 2015; Voulgaridou et al. 2011).

It is worth noting that the detected carbonyls connected to oxidative damage are unstable and, in some cases, highly reactive. Therefore, aliphatic or aromatic carbonyls can interact with biomolecules inside cells. The toxicity of endogenous aldehydes has been well described as well as their interactions with macromolecules, such as proteins, and their ability to cause protein carbonylation/oxidation (by alkenals) or protein glycation (by glyoxals) (Grimsrud et al. 2008; Stadtman and Levine 2003). In addition to proteins, macromolecules of nucleic acids are also targeted by aldehydes (Voulgaridou et al. 2011). Highly reactive carbonyls could be intercalated into macromolecules of DNA (as well as into protein structure), and the formed adducts could then be metabolically degraded (Mistry et al. 2003). DNA or RNA could even be oxidized by hydroperoxyaldehydes formed by the peroxidation of some unsaturated fatty acids. Moreover, both oxidation and adduction could result in mutagenicity.

Conclusion:

Sublethal effects, such as oxidative stress and subsequent oxidative damage, play crucial roles in the cytotoxicity induced by nanoparticles and many other chemicals/compounds. The development of new assays based on oxidative stress will enable the discovery of mechanisms and help to better understand the adverse effects of xenobiotics in exposed microbial cells. The whole range of the detected and quantified markers of lipid peroxidation shows that the assay described in this study can easily be used as a suitable tool for oxidative stress/toxicity evaluation in microbes. Moreover, an example nanoparticle known to trigger OS (e.g., nZVI) was used to evaluate the assay. It is worth noting that the potential of nZVI to cause OS has already been proven by many authors, and the method for its quantification in bacteria species was recently published (Semerád et al. 2018). However, we were only concerned with performing a toxicity evaluation of nZVI using a single marker of bacterial lipid peroxidation, i.e., malondialdehyde in bacteria species. The present work is an extended study of the OS damage caused by nZVI in 3 different microbial species in which other volatile markers of lipid peroxidation and protein oxidation were monitored. All the detected markers exhibited dose-dependent sigmoidal responses. To avoid matrix effects and simplify sample preparation and derivatization, the abovementioned method based on HS-SPME-GC-MS was selected, optimized and applied. The results of the detected changes in aldehyde fractions prove that this fast, effective and automated approach is applicable to OS determination in microbial cultures. The composition of the detected aldehydes, including sulfur-containing methional, proves that nZVI can also cause oxidative damage to proteins apart from lipids. This study presents a novel approach for the determination of OS in microbes from different kingdoms after exposure to a nanomaterial. Moreover, the presented assay is applicable for the evaluation of unspecific OS damage in microbes caused by other nanoparticles and xenobiotics as well.

Acknowledgments

This work was supported by Competence Center TE01020218 of the Technology Agency of the Czech Republic and by the Center for Geosphere Dynamics (UNCE/SCI/006). We acknowledge the Cytometry and Microscopy Facility at the Institute of Microbiology of the ASCR, v.v.i, Vídeňská 1083, Prague, CZ for the use of the cytometry equipment and support from the staff, as well as J. Kašlík for technical assistance.

Compliance with ethical standards

Conflict of interest The authors declare that they have no conflict of interest.

References:

Bao ML, Pantani F, Griffini O, Burrini D, Santianni D, Barbieri K (1998) Determination of carbonyl compounds in water by derivatization - solid-phase microextraction and gas chromatographic analysis. J Chromatogr A. https://doi.org/10.1016/s0021-9673(98)00188-5

Cancho B, Ventura F, Galceran MT (2002) Determination of aldehydes in drinking water using pentafluorobenzylhydroxylamine derivatization and solid-phase microextraction. J Chromatogr A. https://doi.org/10.1016/S0021-9673(01)01437-6

Chen XQ, Wang F, Hyun JY, Wei TW, Qiang J, Ren XT et al. (2016) Recent progress in the development of fluorescent, luminescent and colorimetric probes for detection of reactive oxygen and nitrogen species. Chem Soc Rev. https://doi.org/10.1039/c6cs00192k

Chu FL, Yaylayan VA (2008) Model Studies on the Oxygen-Induced Formation of Benzaldehyde from Phenylacetaldehyde Using Pyrolysis GC-MS and FTIR. J Agric Food Chem. https://doi.org/10.1021/jf8022468

Cullere L, Cacho J, Ferreira V (2004) Analysis for wine C5-C8 aldehydes through the determination of their O-(2,3,4,5,6-pentafluorobenzyl)oximes formed directly in the solid phase extraction cartridge. Anal Chim Acta. https://doi.org/10.1016/j.aca.2004.03.025

Dalle-Donne I, Rossi R, Colombo R, Giustarini D, Milzani A (2006) Biomarkers of oxidative damage in human disease. Clin Chem. https://doi.org/10.1373/clinchem.2005.061408

Dong HR, Li L, Lu Y, Cheng YJ, Wang YY, Ning Q et al. (2019) Integration of nanoscale zero-valent iron and functional anaerobic bacteria for groundwater remediation: A review. Environ Int. https://doi.org/10.1016/j.envint.2019.01.030

Esterbauer H, Schaur RJ, Zollner H (1991) Chemistry and biochemistry of 4-hydroxynonenal, malonaldehyde and related aldehydes. Free Radic Biol Med. https://doi.org/10.1016/0891-5849(91)90192-6

Esterbauer H (1993) Cytotoxicity and genotoxicity of lipid-oxidation products. Am J Clin Nutr. https://doi.org/10.1093/ajcn/57.5.779S

Ferreira V, Cullere L, Lopez R, Cacho J (2004) Determination of important odor-active aldehydes of wine through gas chromatography-mass spectrometry of their O-(2,3,4,5,6-pentafluorobenzyl)oximes formed directly in the solid phase extraction cartridge used for selective isolation. J Chromatogr A. https://doi.org/10.1016/j.chroma.2003.11.104

Filip J, Karlicky F, Marusak Z, Lazar P, Cernik M, Otyepka M et al. (2014) Anaerobic Reaction of Nanoscale Zerovalent Iron with Water: Mechanism and Kinetics. J Phys Chem C. https://doi.org/10.1021/jp501846f

Grieger KD, Fjordboge A, Hartmann NB, Eriksson E, Bjerg PL, Baun A (2010) Environmental benefits and risks of zero-valent iron nanoparticles (nZVI) for in situ remediation: Risk mitigation or trade-off? J Contam Hydrol. https://doi.org/10.1016/j.jconhyd.2010.07.011

Grimsrud PA, Xie HW, Griffin TJ, Bernlohr DA (2008) Oxidative stress and covalent modification of protein with bioactive aldehydes. J Biol Chem. https://doi.org/10.1074/jbc.R700019200

Hauck AK, Bernlohr DA (2016) Oxidative stress and lipotoxicity. J Lipid Res. https://doi.org/10.1194/jlr.R066597

Huang WJ, Cheng YL, Cheng BL (2008) Ozonation byproducts and determination of extracellular release in freshwater algae and cyanobacteria. Environ Eng Sci. https://doi.org/10.1089/ees.2006.0113

Hussain SP, Hofseth LJ, Harris CC (2003) Radical causes of cancer. Nat. Rev. Cancer. https://doi.org/10.1038/nrc1046

Iglesias J, Gallardo JM, Medina I (2010) Determination of carbonyl compounds in fish species samples with solid-phase microextraction with on-fibre derivatization. Food Chem. https://doi.org/10.1016/j.foodchem.2010.05.025

Jenner P (2003) Oxidative stress in Parkinson's disease. Ann Neurol. https://doi.org/10.1002/ana.10483

Karn B, Kuiken T, Otto M (2011) Nanotechnology and in situ remediation: a review of the benefits and potential risks. Cienc Saude Coletiva. https://doi.org/10.1590/s1413-81232011000100020

Kaslik J, Kolarik J, Filip J, Medrik I, Tomanec O, Petr M et al. (2018) Nanoarchitecture of advanced core-shell zero-valent iron particles with controlled reactivity for contaminant removal. Chem Eng J. https://doi.org/10.1016/j.cej.2018.08.015

Kohen R, Nyska A (2002) Oxidation of Biological Systems: oxidative stress phenomena, antioxidants, redox reactions, and methods for their quantification. Toxicol Pathol. https://doi.org/10.1080/01926230290166724

Le TT, Nguyen K-H, Jeon J-R, Francis AJ, Chang Y-S (2015) Nano/bio treatment of polychlorinated biphenyls with evaluation of comparative toxicity. J Hazard Mater. https://doi.org/10.1016/j.jhazmat.2015.02.001

Lefevre E, Bossa N, Wiesner MR, Gunsch CK (2016) A review of the environmental implications of in situ remediation by nanoscale zero valent iron (nZVI): Behavior, transport and impacts on microbial communities. Sci Total Environ. https://doi.org/10.1016/j.scitotenv.2016.02.003

Lv YC, Niu ZY, Chen YC, Hu YY (2017) Bacterial effects and interfacial inactivation mechanism of nZVI/Pd on Pseudomonas putida strain. Water Res. https://doi.org/10.1016/j.watres.2017.03.012

Maessen DEM, Stehouwer CDA, Schalkwijk CG (2015) The role of methylglyoxal and the glyoxalase system in diabetes and other age-related diseases. Clin Sci. https://doi.org/10.1042/cs20140683

Markesbery WR (1997) Oxidative stress hypothesis in Alzheimer's disease. Free Radic Biol Med. https://doi.org/10.1016/s0891-5849(96)00629-6

Martos PA, Pawliszyn J (1998) Sampling and determination of formaldehyde using solid-phase microextraction with on-fiber derivatization. Anal Chem. https://doi.org/10.1021/ac9711394

Mistry N, Podmore I, Cooke M, Butler P, Griffiths H, Herbert K et al. (2003) Novel monoclonal antibody recognition of oxidative DNA damage adduct, deoxycytidine-glyoxal. Lab Invest. https://doi.org/10.1097/01.lab.0000053915.88556.ed

Moghe A, Ghare S, Lamoreau B, Mohammad M, Barve S, McClain C et al. (2015) Molecular Mechanisms of Acrolein Toxicity: Relevance to Human Disease. Toxicol Sci. https://doi.org/10.1093/toxsci/kfu233

Moreira N, Meireles S, Brandão T, De Pinho PG (2013) Optimization of the HS-SPME-GC-IT/MS method using a central composite design for volatile carbonyl compounds determination in beers. Talanta. https://doi.org/10.1016/j.talanta.2013.09.027

Nemecek J, Lhotsky O, Cajthaml T (2014) Nanoscale zero-valent iron application for in situ reduction of hexavalent chromium and its effects on indigenous microorganism populations. Sci Total Environ. https://doi.org/10.1016/j.scitotenv.2013.11.105

Nemecek J, Pokorny P, Lacinova L, Cernik M, Masopustova Z, Lhotsky O et al. (2015) Combined abiotic and biotic in-situ reduction of hexavalent chromium in groundwater using nZVI and whey: A remedial pilot test. J Hazard Mater. https://doi.org/10.1016/j.jhazmat.2015.07.056

Nemecek J, Pokorny P, Lhotsky O, Knytl V, Najmanova P, Steinova J et al. (2016) Combined nano-biotechnology for in-situ remediation of mixed contamination of groundwater by hexavalent chromium and chlorinated solvents. Sci Total Environ. https://doi.org/10.1016/j.scitotenv.2016.01.019

Nishikawa H, Sakai T (1995) Derivatization and chromatographic determination of aldehydes in gaseous and air samples. J Chromatogr A. https://doi.org/10.1016/0021-9673(94)01006-z

O'Brien PJ, Siraki AG, Shangari N (2005) Aldehyde sources, metabolism, molecular toxicity mechanisms, and possible effects on human health. Crit Rev Toxicol. https://doi.org/10.1080/10408440591002183

Perluigi M, Coccia R, Butterfield DA (2012) 4-Hydroxy-2-Nonenal, a Reactive Product of Lipid Peroxidation, and Neurodegenerative Diseases: A Toxic Combination Illuminated by Redox Proteomics Studies. Antioxid Redox Signal. https://doi.org/10.1089/ars.2011.4406

Ribas D, Cernik M, Benito JA, Filip J, Marti V (2017) Activation process of air stable nanoscale zero-valent iron particles. Chem Eng J. https://doi.org/10.1016/j.cej.2017.03.056

Roch AM, Panaye G, Michal Y, Quash G (1998) Methional, a cellular metabolite, induces apoptosis preferentially in G2/M-synchronized BAF3 murine lymphoid cells. Cytometry. https://doi.org/10.1002/(sici)1097-0320(19980101)31:1<10::aid-cyto2>3.0.co;2-n

Schmarr HG, Potouridis T, Ganss S, Sang W, Koepp B, Bokuz U et al. (2008) Analysis of carbonyl compounds via headspace solid-phase microextraction with on-fiber derivatization and gas chromatographic-ion trap tandem mass spectrometric determination of their O-(2,3,4,5,6-pentafluorobenzyl)oxime derivatives. Anal Chim Acta. https://doi.org/10.1016/j.aca.2008.02.002

Schmarr HG, Sang W, Ganss S, Fischer U, Kopp B, Schulz C et al. (2008) Analysis of aldehydes via headspace SPME with on-fiber derivatization to their O-(2,3,4,5,6-pentafluorobenzyl)oxime derivatives and comprehensive 2D-GC-MS. J Sep Sci. https://doi.org/10.1002/jssc.200800294

Schonberg A, Moubacher R (1952) The Strecker Degradation of α-Amino Acids. Chem Rev. https://doi.org/10.1021/cr60156a002

Semerad J, Cajthaml T (2016) Ecotoxicity and environmental safety related to nano-scale zerovalent iron remediation applications. Appl Microbiol Biotechnol. https://doi.org/10.1007/s00253-016-7901-1

Semerád J, Čvančarová M, Filip J, Kašlík J, Zlotá J, Soukupová J et al. (2018) Novel assay for the toxicity evaluation of nanoscale zero-valent iron and derived nanomaterials based on lipid peroxidation in bacterial species. Chemosphere. https://doi.org/10.1016/j.chemosphere.2018.09.029

Sevcu A, El-Temsah YS, Joner EJ, Cernik M (2011) Oxidative Stress Induced in Microorganisms by Zero-valent Iron Nanoparticles. Microbes Environ. https://doi.org/10.1264/jsme2.ME11126

Shara MA, Dickson PH, Bagchi D, Stohs SJ (1992) Excretion of formaldehyde, malondialdehyde, acetaldehyde and acetone in the urine of rats in response to 2,3,7,8-tetrachlorodibenzo-p-dioxin, paraquat, endrin and carbon tetrachloride. J Chromatogr B Biomed Sci Appl. https://doi.org/10.1016/0378-4347(92)80196-w

Shibamoto T (2006) Analytical methods for trace levels of reactive carbonyl compounds formed in lipid peroxidation systems. J Pharm Biomed Anal. https://doi.org/10.1016/j.jpba.2006.01.047

Soukupova J, Zboril R, Medrik I, Filip J, Safarova K, Ledl R et al. (2015) Highly concentrated, reactive and stable dispersion of zero-valent iron nanoparticles: Direct surface modification and site application. Chem Eng J. https://doi.org/10.1016/j.cej.2014.10.024

Spiteller G, Kern W, Spiteller P (1999) Investigation of aldehydic lipid peroxidation products by gas chromatography-mass spectrometry. J Chromatogr A. https://doi.org/10.1016/s0021-9673(98)01078-4

Stadtman ER, Levine RL (2003) Free radical-mediated oxidation of free amino acids and amino acid residues in proteins. Amino Acids. https://doi.org/10.1007/s00726-003-0011-2

Stefaniuk M, Oleszczuk P, Ok YS (2016) Review on nano zerovalent iron (nZVI): From synthesis to environmental applications. Chem Eng J. https://doi.org/10.1016/j.cej.2015.11.046

Tucek J, Prucek R, Kolarik J, Zoppellaro G, Petr M, Filip J et al. (2017) Zero-Valent Iron Nanoparticles Reduce Arsenites and Arsenates to As(0) Firmly Embedded in Core-Shell Superstructure: Challenging Strategy of Arsenic Treatment under Anoxic Conditions. ACS Sustain Chem Eng. https://doi.org/10.1021/acssuschemeng.6b02698

Uchiyama S, Inaba Y, Kunugita N (2011) Derivatization of carbonyl compounds with 2,4-dinitrophenylhydrazine and their subsequent determination by high-performance liquid chromatography. J Chromatogr B. https://doi.org/10.1016/j.jchromb.2010.09.028

Vesely P, Lusk L, Basarova G, Seabrooks J, Ryder D (2003) Analysis of Aldehydes in Beer Using Solid-Phase Microextraction with On-Fiber Derivatization and Gas Chromatography/Mass Spectrometry. J Agric Food Chem. https://doi.org/10.1021/jf034410t

Voulgaridou G-P, Anestopoulos I, Franco R, Panayiotidis MI, Pappa A (2011) DNA damage induced by endogenous aldehydes: Current state of knowledge. Mutat Res-Fundam Mol Mech Mutagen. https://doi.org/10.1016/j.mrfmmm.2011.03.006

Wang Q, O'Reilly J, Pawliszyn J (2005) Determination of low-molecular mass aldehydes by automated headspace solid-phase microextraction with in-fibre derivatisation. J Chromatogr A. https://doi.org/10.1016/j.chroma.2004.09.031

Wu S, Cajthaml T, Semerad J, Filipova A, Klementova M, Skala R et al. (2019) Nano zero-valent iron aging interacts with the soil microbial community: a microcosm study. Environ Sci-Nano. doi:10.1039/C8EN01328D

Xue WJ, Huang DL, Zeng GM, Wan J, Cheng M, Zhang C et al. (2018) Performance and toxicity assessment of nanoscale zero valent iron particles in the remediation of contaminated soil: A review. Chemosphere. https://doi.org/10.1016/j.chemosphere.2018.07.118

Zboril R, Andrle M, Oplustil F, Machala L, Tucek J, Filip J et al. (2012) Treatment of chemical warfare agents by zero-valent iron nanoparticles and ferrate(VI)/(III) composite. J Hazard Mater. https://doi.org/10.1016/j.jhazmat.2011.10.094

Figure and Table captions

Fig. 1 Transmission electron microscope (TEM) image (left) and TEM-derived particle-size distribution (right) of the NANOFER STAR particles used in this study

Fig. 2 Production of aldehydes after exposure of an algal representative, *D. suspicatus*, to several concentrations of nZVI

Fig. 3 Production of aldehydes after exposure of a yeast representative, *S. cerevisiae*, to several concentrations of nZVI

Fig. 4 Production of aldehydes after exposure of a Gram - bacteria representative, *S. marcescens*, to several concentrations of nZVI

Fig. 5 Production of aldehydes after exposure of a Gram + bacteria representative, *B. cereus*, to several concentrations of nZVI

Table 1 HS-SPME-GC-MS method parameters

Table 2 EC50 obtained via sigmoidal fitting by OriginPro 8.5

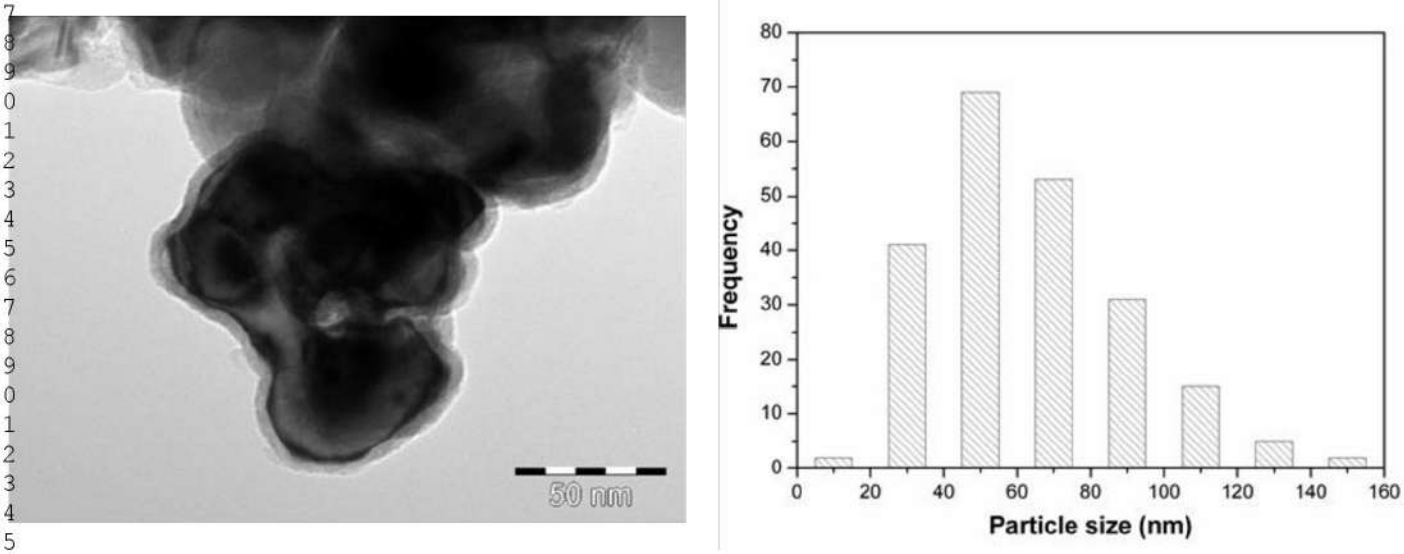

Fig. 1 Transmission electron microscope (TEM) image (left) and TEM-derived particle-size distribution (right) of the NANOFER STAR particles used in this study

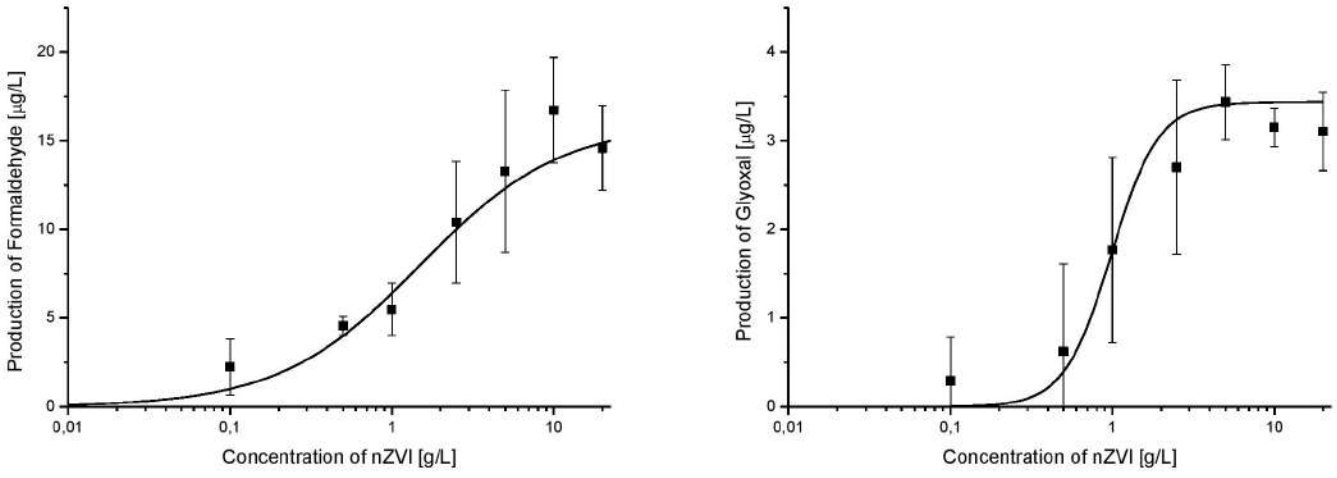

Fig. 2 Production of aldehydes after exposure of an algal representative, *D. subspicatus*, to several concentrations of nZVI

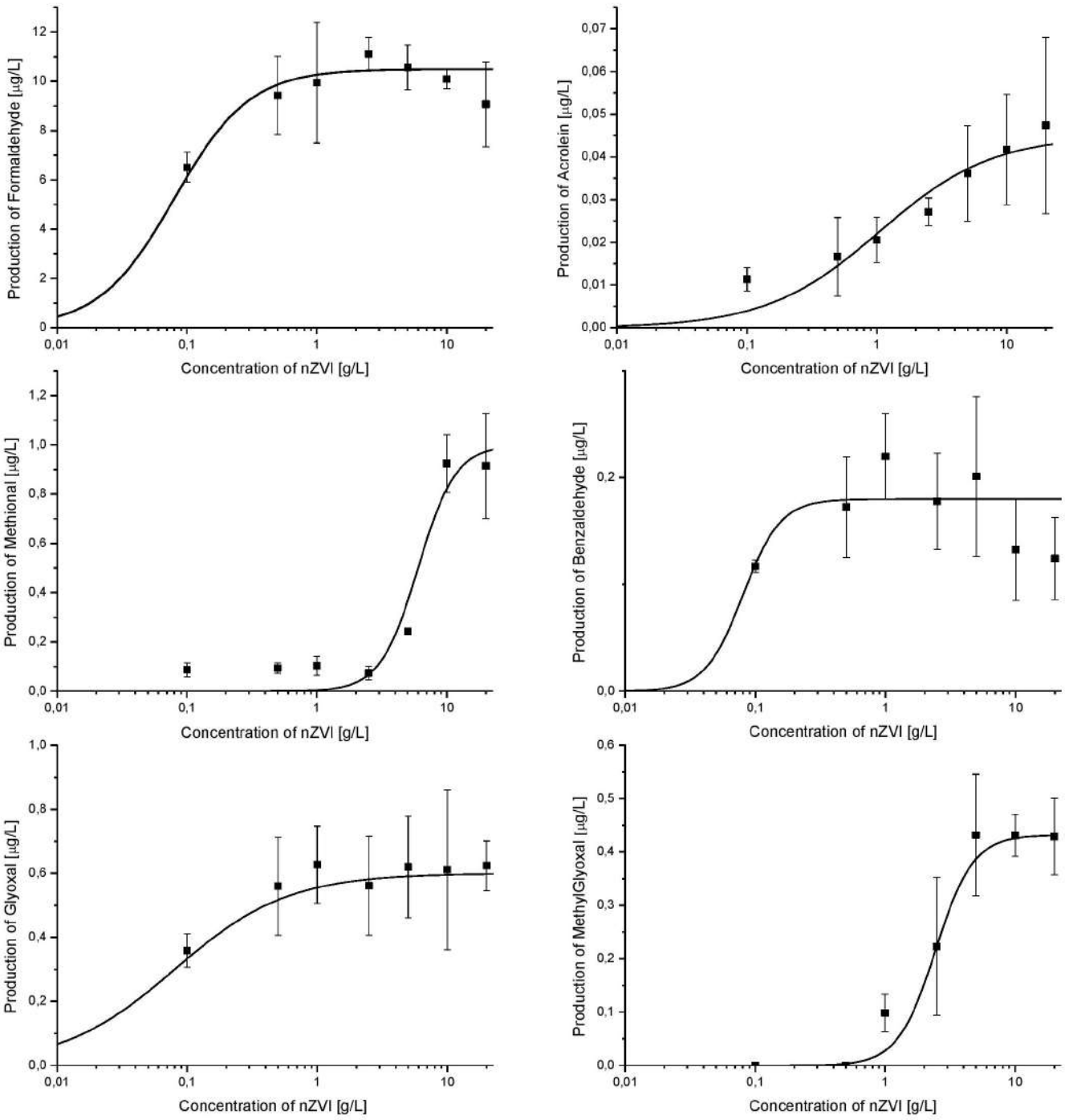

Fig. 3 Production of aldehydes after exposure of a yeast representative, *S. cerevisiae*, to several concentrations of nZVI

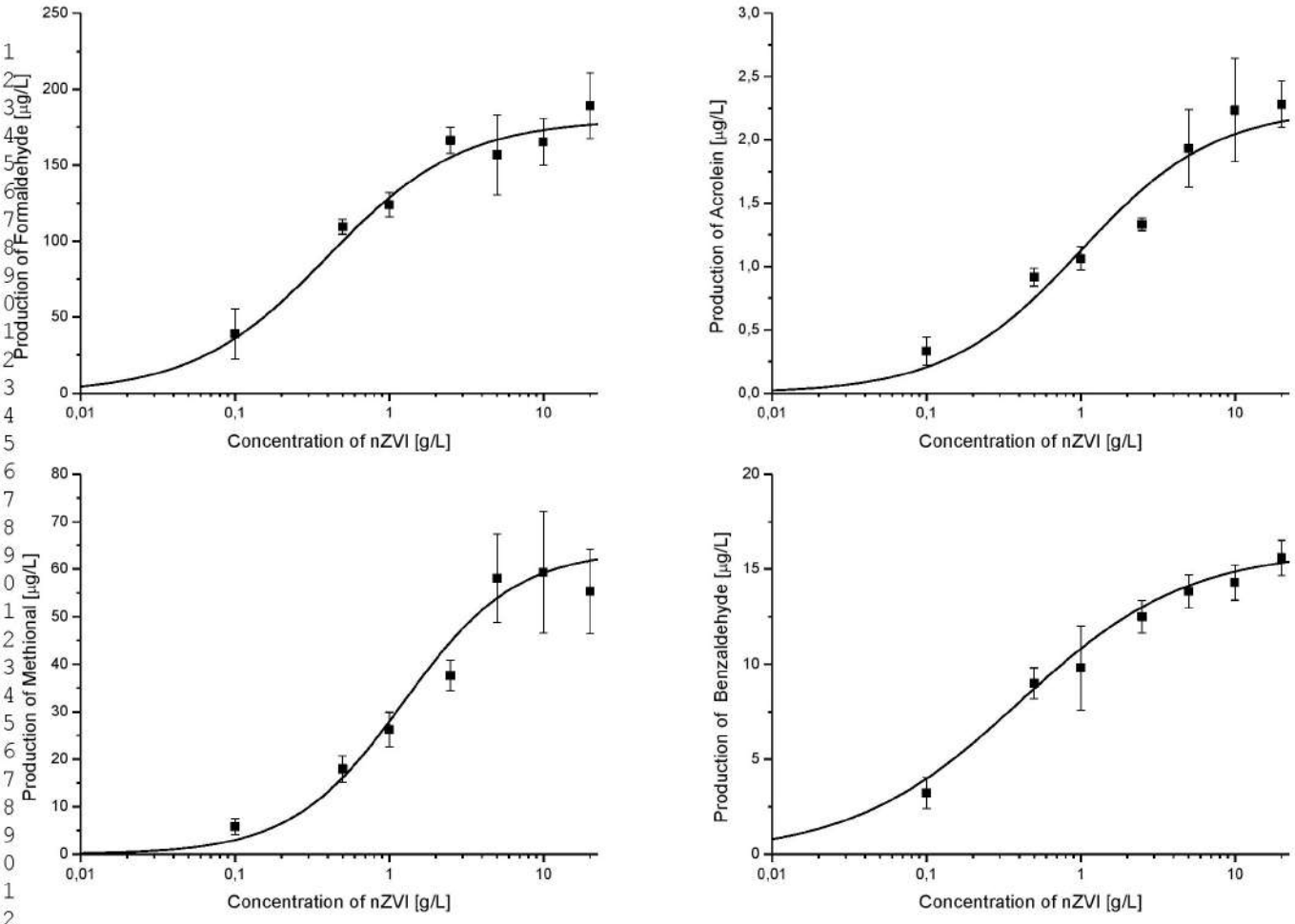

Fig. 4 Production of aldehydes after exposure of a Gram - bacteria representative, *S. marcescens*, to several concentrations of nZVI

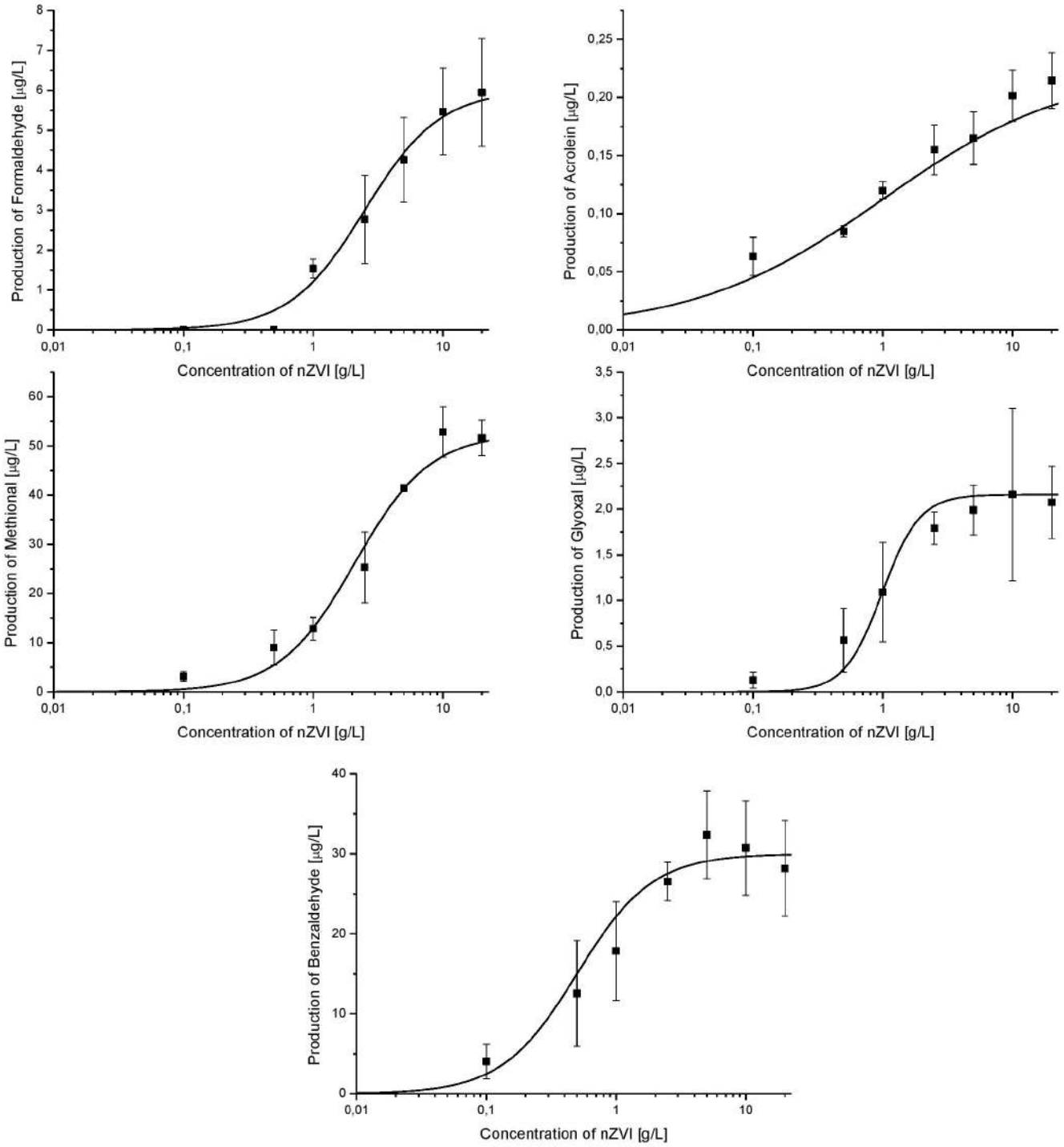

Fig. 5 Production of aldehydes after exposure of a Gram + bacteria representative, *B. cereus*, to several concentrations of nZVI

Table 1 HS-SPME-GC-MS method parameters

	RT [min] PFBHA-oxime 1	RT [min] PFBHA-oxime 2	Quantification ion	R^2	Reproducibility [%] 100 µg/L	LOQ [µg/L]
Formaldehyde	7.8	-	181	0.9966	4.3	0.1
Acetaldehyd	9.15	9.25	181	0.9922	8.1	0.1
Acrolein	10.65	10.95	250	0.9972	1.3	0.01
Butanal	12.85	13.05	181	0.9987	3.8	0.2
Pentanal	16.25	16.5	181	0.9961	3.6	0.5
Trans-2-hexenal	18.55	18.62	181	0.9880	11.5	0.2
Hexanal	19.53	19.68	181	0.9970	4.4	0.2
ISTD	21.65	-	181	-	-	-
Heptanal	22.15	22.25	181	0.9858	6.8	0.5
Methional	23.3	23.4	299	0.9995	2.8	0.05
Octanal	24.93	25.01	181	0.9998	10.1	0.1
Benzaldehyde	25.4	25.6	181	0.9985	12.3	0.5
Nonanal	27.3	-	181	0.9935	9.7	0.05
Trans-2-nonenal	28.8	29.1	181	0.9949	9.0	0.05
Decanal	29.49	-	181	0.9966	9.6	0.1
Glyoxal	31.3	31.45	181	0.9935	12.8	0.05
Methylglyoxal	31.6	32.05	181	0.9981	13.6	0.1

Table 2 EC50 obtained *via* sigmoidal fitting by OriginPro 8.5

EC_{50} [g/L]				
	Algae *D. subspicatus*	Yeasts *S. cerevisiae*	Gram + bacteria *B. cereus*	Gram – bacteria *S. marcescens*
Formaldehyde	1.50	0.08	2.51	0.40
Acrolein	N.D.	1.05	1.01	1.05
Methional	N.D.	6.00	2.10	1.24
Benzaldehyde	N.D.	0.08	0.52	0.40
Glyoxal	1.98	0.08	0.99	N.D.
MethylGlyoxal	N.D.	2.44	N.D.	N.D.

Environmental Science Nano

Environmental fate of sulfidated nZVI particles: the interplay of nanoparticle corrosion and toxicity during aging

Journal:	*Environmental Science: Nano*
Manuscript ID	EN-ART-07-2019-000771
Article Type:	Paper
Date Submitted by the Author:	09-Jul-2019

Complete List of Authors:	Semerád, Jaroslav; Institute of Microbiology AS CR, v.v.i., Filip, Jan; Palacky University, RCPTM Ševců, Alena; University of Liberec, Brumovský, Miroslav; Palacky University, RCPTM Šlechtitelů 27 Olomouc, CZ 78371 Nguyen, Nhung; Technicka Univerzita v Liberci, Institute for Nanomaterials, Advanced Technologies and Innovation Mikšíček, Jiří; University of Liberec Studentska 2 Liberec, CZ 46117 Lederer, Tomáš; Technical University of Liberec, Centre for Nanomaterials, Nanotechnologies and Innovation Filipová, Alena; Institute of Microbiology AS CR, v.v.i. Holecová, Jana; Institute of Microbiology AS CR, v.v.i. Prague, CZ 14200 Cajthaml, Tomas; Institute of Microbiology AS CR, v.v.i.,

Environmental Significance Statement

This work describes an important, environmentally relevant phenomenon of metal nanoparticle aging in relation to the toxicity of nanomaterials; in this case, novel sulfidated nanoscale zero-valent materials intended for remediation purposes. To document the safety and relevance of nanomaterials together with maximal remediation efficiency, such a study is of extreme importance. The main finding of this paper is that sulfidated nanomaterials are more stable and generally less toxic in terms of oxidative stress. Nevertheless, the sulfidated nZVI particles exhibited elevated toxic properties after 7 days of aging. We performed aging experiments under different conditions that are relevant to standard ecotoxicity tests, and the results of the material analyses showed that aging must be considered during ecotoxicity testing.

ARTICLE

Environmental fate of sulfidated nZVI particles: the interplay of nanoparticle corrosion and toxicity during aging

Received 00th January 20xx,
Accepted 00th January 20xx

DOI: 10.1039/x0xx00000x

Jaroslav Semerád [a,b], Jan Filip[c], Alena Ševců[d], Miroslav Brumovský[c], Nhung Nguyen[d], Jiří Mikšíček[c], Tomáš Lederer[d], Alena Filipová [a,b], Jana Holecová [a,b] and Tomáš Cajthaml *[a,b]

Nanomaterials have attracted research attention due to their unique properties, which have also made them increasingly useful for various applications, including remediation technologies. In this work, we tried to explore the aging phenomenon of several newly developed nanoscale zero-valent iron (nZVI) particles containing 0.25, 1, and 5% sulfur and to monitor the possible toxicity changes related to the nZVI particles before and during the aging period. We used several relevant techniques for monitoring nZVI aging, including transmission electron microscopy, X-ray powder diffraction, and particle size analysis. The toxicity of the nZVI particles was monitored using a new oxidative stress assay based on lipid peroxidation, a simple bacterial cultivation test. A test using activated sludge respiration and phospholipid fatty acid analysis of microbial populations was also employed. The results of the material analyses showed that the sulfidated nZVI particles were more stable than bare nZVI particles in terms of Fe^0 content and particle diameter. The stability was more pronounced with the increasing content of sulfur in the nanoparticles; the content of α-Fe was only 35.3% in the nZVI particles compared with 78.6% in the 5% sulfur-doped nanoparticles after 60 days of aging. The results of the oxidative stress assay revealed that the toxicity was also lower with increasing sulfur content; nevertheless, the oxidative stress marker increased substantially after 7 days of aging, reaching a similar level to that caused by bare nZVI in some cases. Other results showed that even incubation in media used for the respective tests caused extensive aging; therefore, this information must be considered before the selection of toxicity assays for nanomaterial evaluation.

Introduction

Over the last two decades, nanoscale zero-valent iron (nZVI) particles have been abundantly used in environmental applications, especially for soil and groundwater clean-up, and rarely in wastewater treatment processes [1]. This material, most likely the most applied nanomaterial for remediation purposes, has shown its high efficiency in the degradation or geofixation of various pollutants, including (poly)chlorinated organic compounds and heavy metals [2–6]. Despite the high potential of nZVI particles for contaminant removal, their applicability is still limited. The main limitation of the extensive use of nZVI particles lies in the nonspecific reactivity leading to a low efficiency of the nZVI-based remediation technology. Nonmodified nZVI undergoes oxidation under the concurrent reduction of natural reducible species that compete with the targeted pollutants. Under anoxic conditions, nZVI can even reduce water to hydrogen [7]. However, surface modification can alleviate the limitations of bare nZVI and improve its mobility and selectivity [8,9]. Aside from the well-known modifications (e.g., surface oxidation, palladization, etc.), surface modifications with sulfur compounds of low oxidation states, such as sulfidation, has recently shown the most promising results and suitability for real applications [10,11]. Sulfidation of nZVI prevents the spontaneous reaction with water and therefore improves the selectivity to pollutants [12]. The improved degradation efficiency of sulfidated nZVI (S-nZVI), especially towards chlorinated ethenes, has been shown by many authors and has shown its potential for on-site applications [12–15].

However, the fate of S-nZVI, which has shown great potential for future applications, has not yet been well described, and a deeper evaluation of the structural changes as well as the evaluation of its toxicity during aging is desirable. Resident microorganisms in the contaminated site are the first to be exposed to the nZVI and thus are directly affected during the remediation process [16,17]. Therefore, the majority of recent studies dealing with the toxicity of nZVI have been performed on resident microbes and especially on bacterial species. Many in vitro tests on single bacterial species have shown some degree of toxicity, but the mechanisms behind the toxic actions are still not well explored [18,19]. Several authors have observed changes in the microbial population during the in vitro tests as well as during the in situ application of nZVI. Detected population changes suggest that in the long term, nZVI

[a] Institute of Microbiology, Czech Academy of Sciences, v.v.i., Vídeňská 1083, CZ-142 20, Prague 4, Czech RepublicAddress here.
[b] Institute for Environmental Studies, Faculty of Science, Charles University, Benátská 2, CZ-128 01, Prague 2, Czech Republic
[c] Regional Centre of Advanced Technologies and Materials, Palacký University, Šlechtitelů 27, CZ-783 71, Olomouc, Czech Republic
[d] Institute for Nanomaterials, Advanced Technologies and Innovation, Technical University of Liberec, Studentská 2, CZ-461 17, Liberec, Czech Republic
* cajthaml@biomed.cas.cz

decreases the overall toxicity of contaminated sites and improves the living environment for microbes [5,20]. After exposure to water or oxygen, nZVI changes its chemical nature and crystal structure related to the oxidation/corrosion of nZVI. This process is called aging and plays a crucial role in the decrease in both remediation efficiency and mobility of nZVI. These physical and chemical changes reduce nZVI bioavailability and thus its toxicity. Only a few studies have addressed the changes in nZVI toxicity during its aging [8,21–23]. Moreover, none of these studies have focused on the influence of different exposition media on material characteristics during the aging process, which could affect both reactivity and toxicity.

Therefore, the main goals of the present study are to i) evaluate the toxicity of bare nZVI particles and their sulfidated counterparts on a single bacterial species and a microbial community of activated sludge and ii) quantify the structural and toxicity changes of nZVI and S-nZVI particles during the course of aging using field-relevant nanoparticle concentrations of 1 and 100 mg/L. To the best of our knowledge, the present study is the first to evaluate the toxicity and structural changes of S-nZVI particles during aging and could help uncover the environmental fate of nZVI particles and their sulfide modifications after their application in groundwater treatment.

Materials and methods

Synthesis, aging and characterization of S-nZVI particles

The commercially available nZVI particles NANOFER 25P (pyrophoric nanoparticles in the form of a powder; NANO IRON, Czech Republic) were used in all experiments. Prior to use, dry nZVI powder was stored in an airtight container under inert atmosphere inside a N_2-filled glove box. Sodium sulfide nonahydrate (≥98.0%, Sigma-Aldrich) was used as the sulfidation agent. Water was purified in the laboratory using a Milli-Q water system (Millipore). S-nZVI particles were prepared by the wet treatment of nZVI particles in aqueous solutions of different concentrations of sodium sulfide. These solutions were added to NANOFER 25P type nZVI particles to yield an nZVI concentration of 242 g/L and nominal S/Fe mass ratios of 0.0025, 0.01 and 0.05 (0.25%, 1% and 5% S-nZVI, respectively). After the addition of the sodium sulfide solutions, the mixtures were immediately dispersed using a T25 ULTRA-TURRAX® disperser (IKA) at 11,000 rpm for 2 min. The vials were then sealed and allowed to react for 60 min on an orbital shaker (160 rpm). Reference pristine nZVI was prepared by dispersing NANOFER 25P particles in purified water using the same procedure. Subsequently, all nZVI-based materials were diluted to a final concentration of 100 or 10 mg/L in purified water and placed in a dark refrigerator (5 °C) without mixing and allowed to age for 7, 14, 30 or 60 days. Static aging at low temperature was chosen to simulate the behavior of a material injected into an underground well with limited water flow. The aged particles were diluted in exposure medium prior to toxicity tests to reach the tested concentrations (i.e., 100 and 1 mg/L).

The key material characteristics were determined by a combination of X-ray powder diffraction (XRD), electron microscopy, and particle size distribution on freshly prepared samples as well as on samples collected during the aging experiment. The X-ray powder diffractometer EMPYREAN (PANalytical, B. V.) operating in Bragg-Brentano geometry was equipped with an iron-filtered CoK_α radiation source, programmable divergence and diffracted beam antiscatter slits and a fast PIXcel detector. The XRD patterns were measured in a 2θ range from 5 to 105°. Data were processed using High Score Plus software in conjunction with the PDF-4+ and ICSD databases, and the relative contribution of the individual crystalline phases was calculated. The morphology and elemental distribution of the S-nZVI/nZVI particles were characterized with transmission electron microscopy (TEM) with a JEOL 2100 microscope at an electron acceleration voltage of 200 kV. The elemental analysis was performed with an X-MaxN 80T SDD EDS detector (Oxford Instruments). Moreover, the particle size distribution was determined by Zetasizer Nano (Malvern Instruments Ltd), and final results were obtained using a 10 second autocorrelation function. Finally, each liquid/suspension sample was quantitatively examined for the dissolved iron and dissolved sulfur species (i.e., sulfide) by ICP-MS.

Experimental setup

The aging experiment was designed to monitor the physicochemical characteristics (see above) and to evaluate the changes in toxicity of the S-nZVI particles using a model bacteria species, i.e., aerobic Pseudomonas putida during two months of aging. Two other routine tests were also used to evaluate the possible negative impact of these nanoparticles on the microbial communities of activated sludge. The whole experimental setup for the toxicity evaluation is summarized in Table 1.

Bacterial culture and growth conditions

Gram-negative *P. putida* (CCM 7156) was obtained from the Czech Collection of Microorganisms, Masaryk University, Brno, Czech Republic. The bacterial inoculum was always prepared fresh from a single colony grown overnight in soya nutrient broth (Sigma Aldrich) (aerobic conditions at 27 °C).

Exposure of the bacterial culture to the nZVI and spot test

The method of exposure was recently described elsewhere [24,25]. The cultures were diluted to achieve an optical density OD = 0.01–0.02 at 600 nm (OD600) using a UV–Vis spectrophotometer (Hach Lange DR6000). Briefly, each nZVI suspension was added to the fresh bacterial culture to obtain final particle concentrations of 1 or 100 mg/L. Cell growth without nZVI was considered a control. Each experiment was performed in triplicate. Afterwards, the exposition plates were kept in the incubator at the above-mentioned growing conditions. The sampling was performed after 6 h and 24 h, and the spot test was carried out following a previously described method [26,27].

Table 1 The experimental design of the toxicity tests.

Microorganisms	Exposure time	Exposure medium	Growth/exposure conditions	Toxicity test
P. putida	24 h	Soya broth	Aerobic, 27 °C	Growth inhibition
	3 h	Carbonate buffer		Oxidative stress – malondialdehyde production
Microbial community in activated sludge	24 h 7 d, 14 d	Activated sludge	Aerobic, 22 °C	Respiration of activated sludge Phospholipid fatty acid analysis

Determination of malondialdehyde

The determination of malondialdehyde as an oxidative stress product was performed according to a previously developed protocol [19]. Briefly, the bacterial culture was cultivated overnight and then concentrated by centrifugation to reach a final concentration of 10^9 cells/ml. Final resuspension was performed using an exposition buffer (carbonate buffer; pH 7), and the bacterial suspension was exposed to nanoparticles with different extents of aging (9:1 bacteria:nanoparticle suspension). At the beginning of the whole aging experiment (i.e., aging time 0 days), the dose-response curve was measured for each nanomaterial, and the EC_{50} was calculated as well as $EC_{50corrected}$ according to our previously published protocol [19]. The production of malondialdehyde during the nanoparticle aging process was measured only for two particle concentrations, i.e., 1 mg/L and 100 mg/L.

Respiratory activity and PLFA analysis of activated sludge

The effect of S-nZVI on the microbial community in activated sludge was assessed following a modified version of the method according to ISO 9408 (ISO, 1999) described in detail in Esquivel-Gaon et al. [28] To determine the production and consumption of respiratory gases such as oxygen and carbon dioxide, the respiratory activity was measured with a Micro-Oxymax respirometer (Columbus Instruments International, USA). The samples were exposed to 100 mg/L of the nanomaterials and prepared in duplicate, and the results were evaluated as the mean of the total oxygen accumulation detected in two individual samples (48 h).

After the respiration test, the samples of activated sludge were further incubated under aerobic conditions for 7 or 14 days. Then, phospholipid fatty acid (PLFA) analysis was performed to estimate the active bacterial biomass. All samples were first freeze-dried, and afterward, the pellet was processed according to a standardly used protocol consisting of extraction, purification, transmethylation and analysis of the formed methyl esters by GC-MS (EVOQ, Bruker) [29]. Each monitored group of microbial biomass was quantified as a sum of the methyl ester markers (for G+ bacteria: i14:0, i15:0, a15:0, i16:0, i17:0 and a17:0; for G- bacteria: 16:1ω7, 18:1ω7, cy17:0, cy19:0; for anaerobic bacteria: cy17:0, cy19:0; for fungi: 18:1ω9; and for actinobacteria: 10Me18:0, 10Me16:0, 10Me17:0).

Results and discussion

The corrosion of S-nZVI during the aging process

The main goal of the present study was to evaluate the extent of corrosion and the changes in the toxicity of variously sulfidated nZVI particles over a 2-month aging period. To the best of our knowledge, only several authors have studied the toxicity of S-nZVI or the toxicity profile over time, and none of these studies provided a detailed material characterization during the aging process, which is crucial for understanding the behavior of the nanoparticles [30,31]. Moreover, the present study is the first to describe the toxicity evaluation of 3 novel materials (0.25, 1 and 5% S-nZVI) along with the structural changes of S-nZVI during a two-month aging period.

The XRD patterns of bare nZVI and S-nZVI particles (Tab. 2) revealed that the major phase forming in the nanoparticles was α-Fe (>90%), with characteristic peaks at 52.5° and 99.5° 2θ. Magnetite ($Fe^{2+}Fe^{3+}{}_2O_4$) and wustite (FeO) were the minor crystalline phases representing artifacts from the manufacturing procedure [32]. No sulfur-containing phases were observed in the XRD pattern of fresh S-nZVI due to its low concentration and/or low degree of crystallinity of FeSx, forming a thin shell [11]. Over the course of aging, the abundance of the α-Fe phase decreased gradually in all of the synthesized materials (see Table 2) as a result of iron corrosion in water. The main corrosion products included magnetite, lepidocrocite and trébeurdenite for nZVI, and magnetite and trebeurdenite/green rust/iron hydroxide for S-nZVI. The differences in the abundance of iron oxidation products among the different materials are likely due to the different surface properties of the variously treated nZVI particles (i.e., the extent of coverage on the nZVI surface by iron sulfides) and possibly also by different physicochemical conditions (pH and ORP) and the concentration of dissolved Fe in the aged suspensions.

Table 2 The phase composition of nZVI and S-nZVI samples aged for up to 60 days in water at 5 °C. The data are derived from XRD measurements (i.e., from quantitative phase analysis).

		% Abundance of crystalline phase						
Material type	**Aged (days)**	**α-Fe**	**Lepidocrocite**	**Magnetite**	**Trébeurdenite**	**Green rust**	**Wustite**	**Iron hydroxide**
nZVI	freshly prepared	95.6	0	3.5	0	0	0.9	0
	7	86.7	2.0	9.3	0.9	0	1.1	0
	30	83.6	8.1	6.0	1.3	0	1.0	0
	60	35.3	36.7	23.9	1.3	0	0.9	1.9
0.25% S-nZVI	freshly prepared	96.4	0	2.9	0	0	0.8	0
	7	86.8	0	12.0	0.5	0	0.7	0
	30	74.3	0	23.6	0.9	0	0	1.2
	60	43.6	4.0	48.8	0	0	0	3.5
1% S-nZVI	freshly prepared	95.4	0	3.5	0	0	1.1	0
	7	90.7	0	8.0	0	0	1.3	0
	30	82.6	0	15.1	0	1.4	0.9	0
	60	71.3	0	22.0	0	1.7	1.0	4.1
5% S-nZVI	freshly prepared	95.2	0	4.1	0	0	0.7	0
	7	96.1	0	3.9	0	0	0	0
	30	76.5	0	4.3	19.2	0	0	0
	60	78.6	0	6.0	15.4	0	0	0

The abundance of magnetite, a typical product of long-term iron oxidation, increased, and it was most dominant oxidation product formed, except for a few samples of bare nZVI and 5% S-nZVI. In the case of nZVI, lepidocrocite (γ-FeO(OH)) was found to be the dominant oxidation product formed after 30 and 60 days of aging. Interestingly, the abundance of this mineral was mostly negligible in all S-nZVI samples except the 0.25% S-nZVI sample, which had the lowest content of sulfide. Trébeurdenite ($Fe^{2+}_2Fe^{3+}_4O_2(OH)_{10}CO_3{\cdot}3H_2O$), a member of the fougérite mineral group, represented 19.2% and 15.4% of the crystalline phase in the 5% S-nZVI sample after 30 and 60 days, respectively. A higher contribution of α-Fe was observed at the end of the aging experiment for materials with an increasing sulfur dose, thus confirming the inhibitory effect of sulfur treatment on iron corrosion [10,12,14]. TEM micrographs of freshly prepared nZVI and 5% S-nZVI particles reveal that both materials are composed of nearly isometric particles that are approximately 80 nm in size. While the S-nZVI particles after 60 days of aging are covered by sheet-like nanocrystals of corrosion products, the nZVI particles are nearly completely transformed into lamellar reaction products due to extensive corrosion (Fig. 1).

The results of the particle size distribution analysis of the nZVI particles performed in the carbonate buffer showed an increasing trend in the size of the nanomaterials during the aging process, which corresponds with the TEM observations (i.e., the growth of relatively large reaction products; Fig. 2). The obtained results confirm that during the course of aging, nZVI undergoes intensive oxidation, resulting in the formation of larger crystals of iron oxides and their aggregates. It is worth noting that the size distribution of all the S-nZVI materials showed a similar pattern that was significantly different from the bare nZVI (Fig. 2). After one week of aging, the apexes of the size distribution curves of the sulfidated materials surprisingly shifted to slightly lower values. This effect was observed in all tested S-nZVI materials and suggests that after a short time of aging, the particles and/or aggregates of S-nZVI decrease in size. This effect seems to be analogous to the so-called activation process observed on surface-passivated air-stable nZVI particles [33]. The activation is explained as partial degradation/reductive dissolution of the compact iron oxide shell on nZVI (i.e., in this case, partial dissolution of FeS or iron oxides/hydroxides that could be expected at higher concentrations of S-nZVI particles in water), leading to the partial disintegration of the nZVI particle aggregates. Nevertheless, this downsizing effect was not permanent, and the particle size reached the same distribution as at the beginning of the experiment within two weeks and remained similar until the end of the aging experiment. Comparing the S-nZVI materials with bare nZVI, it is obvious that the nZVI curves correspond to substantially larger particles after 2 weeks of aging. The size distribution of the S-nZVI particles also supports the results of XRD and confirms the stabilization of nZVI via sulfidation, thus being in full accordance with the previously proposed mechanisms of S-nZVI interaction with water (e.g., Fan et al., 2017 [11]).

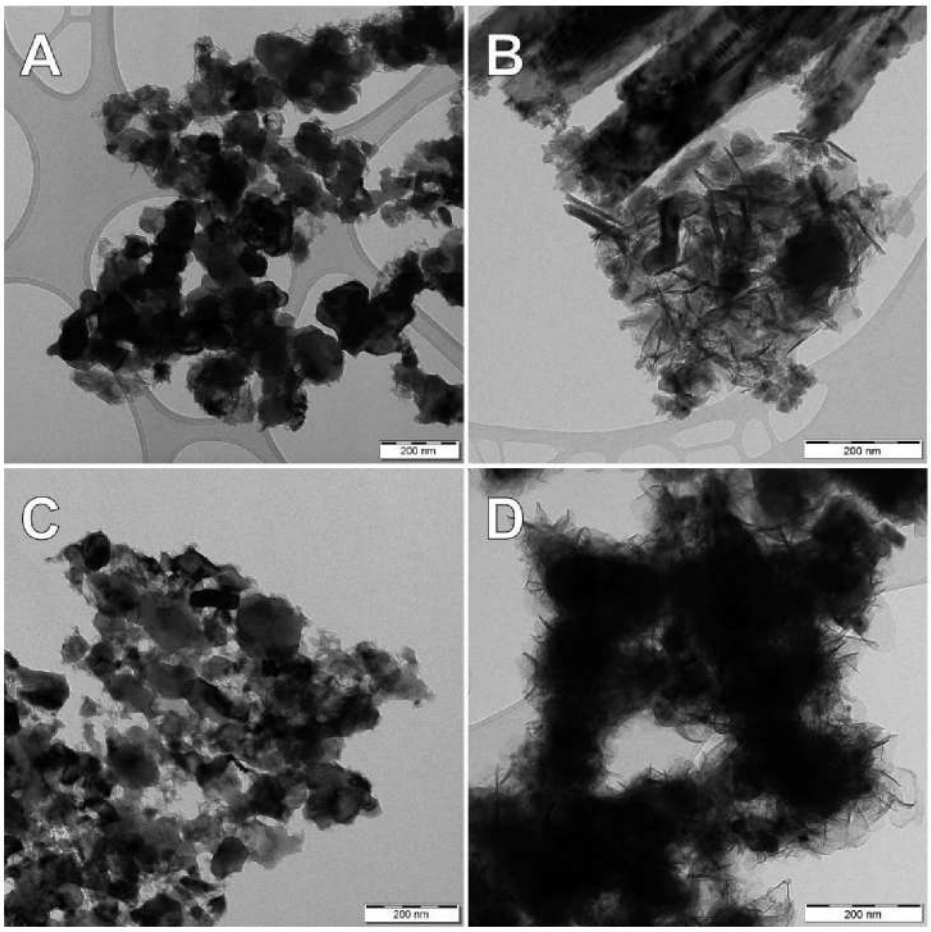

Fig. 1 TEM micrographs and corresponding mineral phase abundance determined using XRD: A) fresh nZVI, B) nZVI aged 60 days, C) fresh 5% S-nZVI, D) 5% S-nZVI aged 60 days.

Toxicity of fresh S-nZVI particles

The toxicity results, expressed as the production of malondialdehyde after exposure to the fresh non-aged materials, document the dose-dependent production of malondialdehyde representing the level of oxidative stress (Fig. 3). The $EC_{50corrected}$ values were calculated according to a formula resulting from the receptor theory where the correction was performed with respect to different maximal production values of malondialdehyde [34]. This already verified protocol enables the direct evaluation of EC values regardless of the maxima of the dose-dependent curves [19]. At the beginning of the aging experiment, the highest toxicity was observed for bare nZVI and then decreased with increasing sulfur content in the shell of the nanoparticles as follows: 0.25% S-nZVI> 1% S-nZVI > 5% S-nZVI. The tendency of the decrease in the toxicity clearly corresponds to the sulfur content in the shell of the nanoparticles and, thus, to the extent of the protection of the Fe^0 core against the direct interaction of the iron atoms with the surrounding media (i.e., causing the oxidative stress). This is again in full accordance with the observed trends for the corrosion of the nZVI/S-nZVI particles (see above).

Since other oxidative stress assays (glutathione and lactate dehydrogenase) are not applicable for nZVI materials due to undesired interactions with the assay components, malondialdehyde, as well as other aldehydes, appeared to be suitable markers to evaluate this mode of action caused by the nanoparticles. When employing the same protocol to compare bare nZVI and three nZVI types coated with oxide shells of different thicknesses, the oxidative stress marker was substantially lowered by increasing the shell thickness [19]. Similar to the present study, the concentration of the oxidative stress marker was substantially lowered by increasing the extent of nZVI coverage by iron sulfides, i.e., with increasing sulfur content.

Nevertheless, the obtained data describe a possible toxicity risk related only to the freshly applied materials. It is noteworthy that the exposure of nZVI to many environmental factors during the remediation process leads to structural changes caused mainly by its oxidation, sorption and aggregation. Several days or weeks after injection into groundwater, only a small amount of nZVI (i.e., Fe^0 in the remaining particles) typically persists in the reactive form, and therefore, the respective toxicity will no longer be the same as in the case of the freshly prepared nZVI particles 5. Therefore, the logical assumption supported by the results from recent studies [19,23,35] is that the nanoparticle toxicity significantly decreases over time.

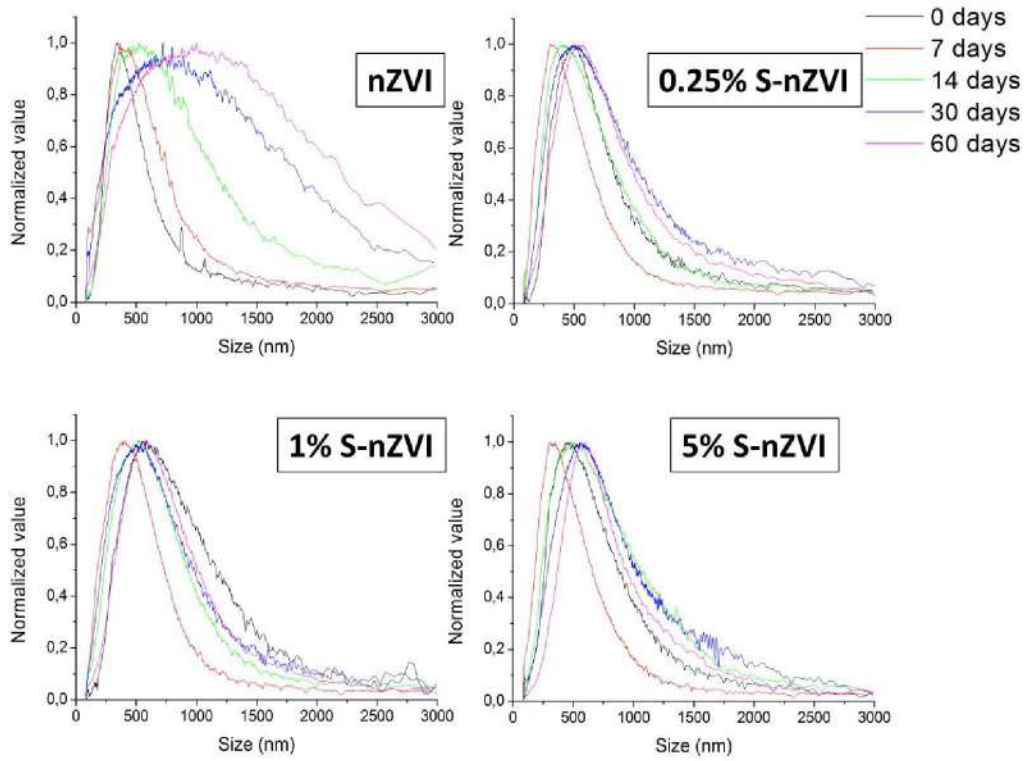

Fig. 2 The evolution of the particle size distribution for nZVI/S-nZVI samples during the course of aging in carbonate buffer.

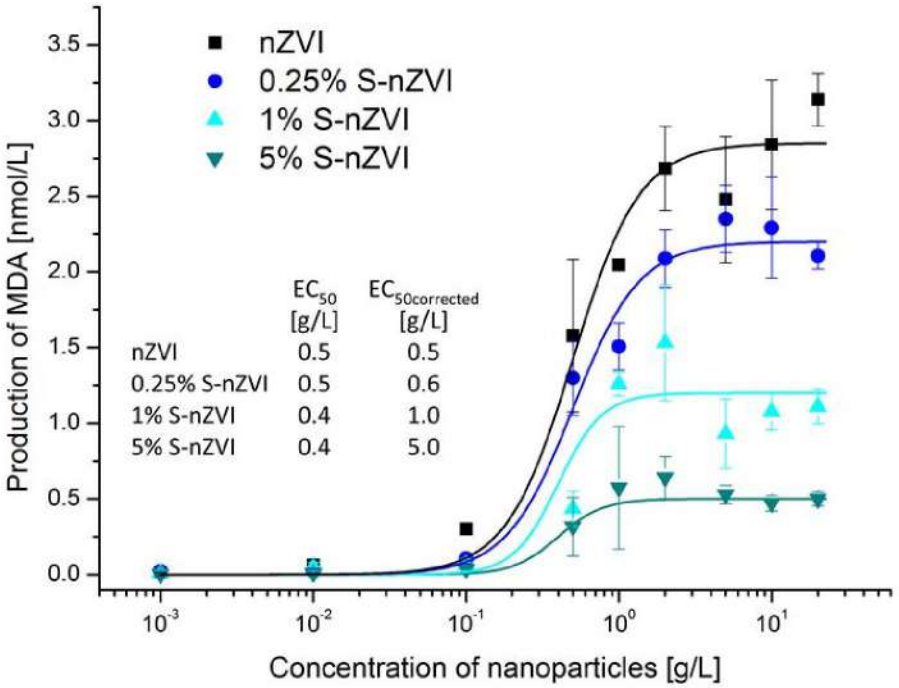

Fig. 3 The dose-response curves of malondialdehyde production with the corresponding EC_{50} and corrected EC_{50} values for sulfidated and bare nZVI materials at the beginning of the aging experiment (0 days, *P. putida*). The data are the mean ± standard deviation of three replicates.

Toxicity of S-nZVI particles during the aging process

To investigate the possible course of toxicity caused by chemical and physical changes during aging of the nZVI particles, a 60-day experiment was performed in water. The toxicity levels of the sulfide-modified nZVI particles expressed as malondialdehyde production during the aging processes are shown in Fig. 4. Contrary to our original assumption that the nanoparticle toxicity will constantly decrease over the course of nZVI aging, the results are not in agreement with the aforementioned hypothesis. The influence of the aging process on the oxidative stress level was tested at two concentration levels. It is worth noting that even the low particle concentration (1 mg/L) indicated a certain increase in malondialdehyde production compared to the control samples (i.e., those not exposed to the nanoparticles); however, the results are burdened with very high experimental error and are thus not interpretable and applicable. However, we obtained more interpretable results with the higher concentration of the particles (100 mg/L). The toxicity of bare nZVI was not significantly different ($P = 0.05$) after 7 days of incubation in comparison with the initial values, and the toxicity of the bare particles started decreasing during further aging. However, the malondialdehyde production caused by all the sulfide-modified materials increased substantially after the first 7 days. Oxidative stress reached similar levels in the cases of 0.25 and 1% S-nZVI and bare nZVI. Nevertheless, the concentration of malondialdehyde dropped with a further increase in time and a further increase in the content of sulfur in the nZVI particles.

A similar pattern of increasing toxicity during the aging of the S-nZVI particles was determined by the cultivation spot test using the same bacterial species. A concentration of 1 mg/L did not exhibit any inhibition, and the results after exposure to 100 mg/L are shown in Table 3.

No negative effects were observed at the nZVI concentration of 1 mg/L using the spot test. However, at the beginning of the experiment with the 100 mg/L nZVI particles, an inhibitory effect was observed after a 6 h of exposure to the iron nanoparticles (except for the 5% S-nZVI). Similar to malondialdehyde, the inhibitory effect lasted for 7 days and decreased below the limit of observation within two weeks. The observed negative effect after 24 h of exposure to S-nZVI supports the previous results and suggests an increase in toxicity after the first few days.

Finally, to evaluate the potential negative effects of the tested nanomaterials on the microbial community present in the activated sludge from water treatment plants, two assays were used. First, a commonly used test that indicates the vitality of activated sludge (inhibition of respiration of the activated sludge) was applied. Then, PLFA analysis was performed to investigate potential changes in the microbial community. With respect to the conditions of the test and possible necessary exposure time, all of the nZVI-based materials were incubated for 48 h with respirometric detection and incubated for another 7 and 14 days for PLFA analyses. During the respiration test, no negative effects were observed at any concentration of the tested nZVI particles (data not shown). Additionally, no significant negative effects, i.e., a shift in the microbial community or any decrease in the microbial biomass compared to the control sample during the whole aging process were observed using the PLFA method (data not shown). Although the respiration test and the PLFA method are routinely used for similar studies [36–38], obviously in this case, the methods with sludge cultivation were not applicable. A possible explanation is the complex microbial community with high biomass in the sludge that is less sensitive to the adverse effects of the tested nanoparticles, together with the high content of organic substances that can interact preferentially with the reactive species originating from the nZVI materials. Another possible explanation for this phenomenon that can contribute to the lower toxic effects in the sludge was obtained from the XRD analyses of aging in the sludge medium (see discussion below, Table 4). These results document accelerated aging even after 48 h. A similar lack of negative effects or minimal impacts of nanoparticles on the sludge microbiome at lower concentrations were observed in many studies [39,40]. During aging of the nZVI particles, α-Fe is mainly oxidized into iron oxides and hydroxides. However, this process is also accompanied by the release of soluble ferrous ions and the formation of radical oxygen species. Many authors therefore connect the toxicity of nZVI to the generation of Fe^{2+} ions during the oxidation [41–43]. Considering the low solubility of Fe^{3+} hydroxides, the iron determined by ICP-MS will be predominantly in the form of Fe^{2+}, which is much more soluble [44]. The results showed that in the case of the carbonate buffer, the background level of dissolved iron was below the LOD (LOD = 0.02 mg/L), and the Fe^{2+} ions started to appear after one month of aging and were detected at the same level even after two months of aging (30 and 60 days: 3.56 ± 2.50 and 3.68 ± 0.93 mg/L, respectively), which does not correlate with the decreasing toxicity trend. The exposition media used for the spot test (soya broth) originally contained a trace concentration of Fe^{2+} (0.81 mg/L). The increasing concentration of Fe^{2+} ions in this case also did not correspond to the toxicity results where the toxic effect is the most pronounced after the first week of aging and decreased over the course of aging. Overall, the results of the dissolved iron and 4 independent toxicity tests showed that at the tested concentrations, the toxicity was not affected by the dissolved iron ions.

Other inorganic compounds that could have a toxic effect on the tested microorganisms are sulfide species (H_2S, HS^- and S^{2-}) that could leach from the sulfidated nZVI materials or that could be created by the reduction of the present sulfate by nZVI in exposure media. Nevertheless, dissolved sulfur was not detected (LOD=0.025 mg/L) in the exposure media without or with low inorganic sulfur content (in the carbonated buffer, nor in the activated sludge), which suggests that the toxicity is also not caused by dissolved sulfur evolving from S-nZVI.

The toxicity results could be affected by many factors, and it is important to bear in mind that even the time necessary for the exposure for a respective assay can influence the tested nanomaterials. Aggregation of nanoparticles in exposure medium is one of the most discussed factors that could lead to the underestimation or overestimation of the nanotoxicological

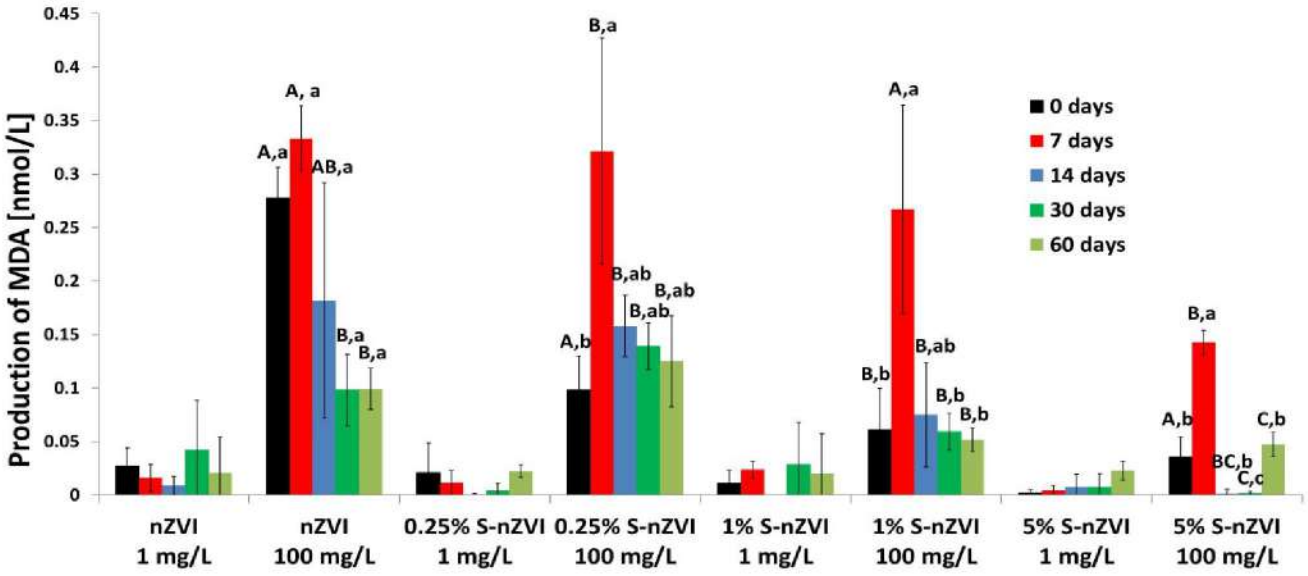

Fig. 4 The production of malondialdehyde (recalculated to 10^7 cells) induced by S-nZVI in different stages of aging up to 60 days of exposure. P. putida cultures were exposed at two concentrations, each of 4 nanomaterials. The data are the mean ± standard deviation of three replicates. Multiple pair-wise comparisons were performed by the Tukey's test ($P < 0.05$). Same uppercase letters above bars indicate that differences among the aging time within the same material were not significant. The lowercase letters describe significant differences among the materials at the same time.

results [45,46]. The present study addresses nanomaterials based on nZVI, which are known to be highly reactive/unstable.

To evaluate the influence of different media and time of the exposure on the character of the nanoparticles (nZVI and 5% S-nZVI), XRD and TEM analyses were performed. Nevertheless, the TEM analysis results (data not shown) did not differ from aging in water (Fig. 1). The results of the XRD analyses are displayed in Tab. 4. The XRD-derived phase composition of the particles exposed in the diluted soya broth and carbonate buffer after the respective exposure times necessary for the tests were generally similar to the phase compositions of the particles before the exposure, which means that the media did not significantly alter the phase composition of the particles. Therefore, the results document that the conditions (media and time of exposure) of these assays are suitable for testing the toxicity of the nZVI particles.

Nevertheless, greater corrosion after exposure of the materials was observed, particularly in the sewage sludge medium, which is likely due to i) a longer exposure (48 h) compared to the other media and ii) bicarbonate content. Bicarbonate solution was previously found to accelerate iron corrosion [47]. In the present study, the bicarbonate buffer also slightly promoted iron corrosion despite the relatively short exposure time (3 h). A higher abundance of trébeurdenite was found in the case of the particles exposed to sewage sludge (48%) and in the bicarbonate buffer (up to 6%), indicating the tendency of aqueous carbonate incorporation into the corrosion products. The complexity of the sludge medium accelerated the corrosion of the nanoparticles, better reflecting the environmental conditions, and this phenomenon could cause negative results. It is noteworthy that the nZVI-based nanomaterials are typically injected into contaminated soils and aquifers where the matrix is complex, and faster aging will decrease the risks coupled with their applications.

Table 3 Visuals of bacterial growth in colonies by the spot test exposed to 100 mL of the aged nanomaterial during the 60-day aging experiment. The inhibition of bacterial growth is marked with "-" while no effect is marked with "0".

	Day 0		Day 7		Day 14		Day 30		Day 60	
	6 h	24 h	6 h	24 h	6 h	24 h	6 h	24 h	6 h	24 h
Control	0	0	0	0	0	0	0	0	0	0
nZVI	-	0	-	0	0	0	0	0	0	0
0.25% S-nZVI	-	0	-	-	0	0	0	0	0	0
1% S-nZVI	-	0	-	-	0	0	0	0	0	0
5% S-nZVI	0	0	-	-	0	0	0	0	0	0

Table 4 The phase composition of nZVI and S-nZVI (5%) samples aged for 60 days in water and subsequently exposed to the respective media within the respective exposure times of the toxicity tests. The data are derived from XRD measurements (i.e., from quantitative phase analysis). Only the detected crystalline phases are displayed.

	% Abundance of crystalline phases			
Exposure medium/time	**α-Fe**	**Lepidocrocite**	**Magnetite**	**Trébeurdenite**
	nZVI 60 days aged			
Carbonate buffer 3 h	36.2	34.8	26.4	2.6
Soya medium 24 h	32.5	33.7	32.3	1.5
Sewage sludge 48 h	24.4	40	25.3	10.2
	5% S-nZVI 60 days aged			
Carbonate buffer 3 h	74.3	0	6.1	19.6
Soya medium 24 h	78.2	0	9.5	12.3
Sewage sludge 48 h	1.4	86.6	11.1	0.9

Conclusion

In this study, we investigated the toxicity and aging behavior of novel sulfur-containing nZVI materials in comparison with the common, commercially available bare nZVI NANOFER 25P. The first aging experiment in water revealed that the sulfidated materials were more stable and thus less susceptible to the formation of the oxidized forms of ferric/ferrous minerals. The stability was much more pronounced with an increasing sulfur content in the nanoparticles. The results were confirmed by TEM analysis and particularly by particle size distribution analysis. The size distribution analysis results showed that, contrary to the sulfidated nanoparticles, bare nZVI tended to form substantially larger aggregates represented by shifted and broader peaks as described in the size distribution curves. In other words, the sulfidated materials appeared to be greatly stabilized, with very slight changes in the distribution even after 2 months of aging. Regarding the toxicity of these materials, the sulfidated nanoparticles were tested using an optimized protocol for the estimation of oxidative stress via the analysis of malonylaldehyde. The data provided a clear comparison of corrected EC_{50} values that documented the limited toxic effects of the fresh sulfidated materials in comparison with the bare nZVI. These results with improved selectivity toward organic pollutants, as documented by other authors, support the applicability of sulfidated nZVI nanomaterials for remediation purposes.

However, attention has also been paid to the toxic effects of the aged materials. The malonyldialdehyde assay was employed at two environmentally relevant concertation levels, and at 1 mg/L, the test was not sufficiently sensitive and reliable. The result from the 100 mg/L concentration showed that the production of malonyldialdehyde caused by the sulfidated materials increased significantly after the first 7 days, reaching the same levels as the nZVI particles. Nevertheless, the concentration of malondialdehyde dropped with increases in the time and the content of sulfur in the materials and showed significantly lower toxicity in comparison with the bare nZVI. These results were confirmed with the cultivation spot test that was less sensitive; nevertheless, the results are in agreement with findings from the oxidative stress assay. Notably, we did not detect any elevated concentrations of dissolved sulfide or iron ions that could explain the toxicity changes during the course of the aging experiment. Additionally, we also employed other tests, including the respiration of activated sludge and the PLFA analysis of the microbial community in the sludge; however, we did not obtain any significantly different results after exposure to the different nanoparticles. Due to this fact, we tried to investigate the effects of the cultivation media, the conditions of the assay and the material analyses of the nanoparticles that were performed after the respective duration of the tests. The results revealed that 48 h of exposure to the activated sludge caused dramatic composition changes in the 60-day aged sulfidated materials, which is probably the reason why these tests are not applicable for the intended purposes. Nevertheless, from another perspective, the conditions of the tests reflect the environmental situations in a more realistic way.

The results of this study show several new findings regarding the possible toxic effects of nanomaterials that are used or are promising for remediation practices. The results clearly document that for the toxicity assessment, the assays must be very carefully selected, and all of the environmental factors must be taken into account, including the aging of the nanomaterials and the influence of the test conditions on the possible physicochemical parameters of the tested materials. The data also show that laboratory testing can bring some interesting preliminary data, e.g., the fact that sulfidated materials are more stable and generally less toxic than bare nZVI. For this purpose, the protocol of oxidative stress testing was proven again to be highly suitable; nevertheless, further testing and research should focus on real environmental conditions that are present directly at the contaminated sites.

Conflicts of interest

There are no conflicts to declare.

Acknowledgements

This work was supported by the Technology Agency of the Czech Republic under the project of Competence Center (TE01020218) and by the Center for Geosphere Dynamics (UNCE/SCI/006). We acknowledge the Cytometry and Microscopy Facility at the Institute of Microbiology of the ASCR, v.v.i, Vídeňská 1083, Prague, CZ for the use of the cytometry equipment and support from the staff. The work was also supported by the Ministry of Education, Youth and Sports of the Czech Republic and The European Union - European Structural and Investments Funds in the frame of Operational Programme Research Development and Education - project Pro-NanoEnviCz (Project No.CZ.02.1.01/0.0/0.0/16_013/0001821). The work was also supported by Progress Q16 of Charles University.

Notes and references

1 F. L. Fu, D. D. Dionysiou and H. Liu, The use of zero-valent iron for groundwater remediation and wastewater treatment: A review, *J. Hazard. Mater.*, 2014, **267**, 194–205.

2 J. Němeček, O. Lhotský and T. Cajthaml, Nanoscale zero-valent iron application for in situ reduction of hexavalent chromium and its effects on indigenous microorganism populations, *Sci. Total Environ.*, 2014, **485**, 739–747.

3 J. Němeček, P. Pokorný, L. Lacinová, M. Černík, Z. Masopustová, O. Lhotský, A. Filipová and T. Cajthaml, Combined abiotic and biotic in-situ reduction of hexavalent chromium in groundwater using nZVI and whey: A remedial pilot test, *J. Hazard. Mater.*, 2015, **300**, 670–679.

4 Y. S. El-Temsah, A. Sevcu, K. Bobcikova, M. Cernik and E. J. Joner, DDT degradation efficiency and ecotoxicological effects of two types of nano-sized zero-valent iron (nZVI) in water and soil, *Chemosphere*, 2016, **144**, 2221–2228.

5 J. Němeček, P. Pokorný, O. Lhotský, V. Knytl, P. Najmanová, J. Steinová, M. Černík, A. Filipová, J. Filip and T. Cajthaml, Combined nano-biotechnology for in-situ remediation of mixed contamination of groundwater by hexavalent chromium and chlorinated solvents, *Sci. Total Environ.*, 2016, **563–564**, 822–834.

6 M. Stefaniuk, P. Oleszczuk and Y. S. Ok, Review on nano zerovalent iron (nZVI): From synthesis to environmental applications, *Chem. Eng. J.*, 2016, **287**, 618–632.

7 J. Filip, F. Karlicky, Z. Marusak, P. Lazar, M. Cernik, M. Otyepka and R. Zboril, Anaerobic Reaction of Nanoscale Zerovalent Iron with Water: Mechanism and Kinetics, *J. Phys. Chem. C*, 2014, **118**, 13817–13825.

8 H. Dong, Y. Xie, G. Zeng, L. Tang, J. Liang, Q. He, F. Zhao, Y. Zeng and Y. Wu, The dual effects of carboxymethyl cellulose on the colloidal stability and toxicity of nanoscale zero-valent iron, *Chemosphere*, 2016, **144**, 1682–1689.

9 J. Liu, A. R. Liu and W. X. Zhang, The influence of polyelectrolyte modification on nanoscale zero-valent iron (nZVI): Aggregation, sedimentation, and reactivity with Ni(II) in water, *Chem. Eng. J.*, 2016, **303**, 268–274.

10 D. M. Fan, G. O. Johnson, P. G. Tratnyek and R. L. Johnson, Sulfidation of Nano Zerovalent Iron (nZVI) for Improved Selectivity During In-Situ Chemical Reduction (ISCR), *Environ. Sci. Technol.*, 2016, **50**, 9558–9565.

11 D. M. Fan, Y. Lan, P. G. Tratnyek, R. L. Johnson, J. Filip, D. M. O'Carroll, A. N. Garcia and A. Agrawal, Sulfidation of Iron-Based Materials: A Review of Processes and Implications for Water Treatment and Remediation, *Environ. Sci. Technol.*, 2017, **51**, 13070–13085.

12 Y. L. Han and W. L. Yan, Reductive Dechlorination of Trichloroethene by Zero-valent Iron Nanoparticles: Reactivity Enhancement through Sulfidation Treatment, *Environ. Sci. Technol.*, 2016, **50**, 12992–13001.

13 H. R. Dong, C. Zhang, J. M. Deng, Z. Jiang, L. H. Zhang, Y. J. Cheng, K. J. Hou, L. Tang and G. M. Zeng, Factors influencing degradation of trichloroethylene by sulfide-modified nanoscale zero-valent iron in aqueous solution, *Water Res.*, 2018, **135**, 1–10.

14 S. R. C. Rajajayavel and S. Ghoshal, Enhanced reductive dechlorination of trichloroethylene by sulfidated nanoscale zerovalent iron, *Water Res.*, 2015, **78**, 144–153.

15 Y. Y. Gong, L. S. Gai, J. C. Tang, J. Fu, Q. L. Wang and E. Y. Zeng, Reduction of Cr(VI) in simulated groundwater by FeS-coated iron magnetic nanoparticles, *Sci. Total Environ.*, 2017, **595**, 743–751.

16 J. Semerád and T. Cajthaml, Ecotoxicity and environmental safety related to nano-scale zerovalent iron remediation applications, *Appl. Microbiol. Biotechnol.*, 2016, **100**, 9809–9819.

17 R. Hjorth, C. Coutris, N. H. A. Nguyen, A. Sevcu, J. A. Gallego-Urrea, A. Baun and E. J. Joner, Ecotoxicity testing and environmental risk assessment of iron nanomaterials for sub-surface remediation – Recommendations from the FP7 project NanoRem, *Chemosphere*, 2017, **182**, 525–531.

18 E. Lefevre, N. Bossa, M. R. Wiesner and C. K. Gunsch, A review of the environmental implications of in situ remediation by nanoscale zero valent iron (nZVI): Behavior, transport and impacts on microbial communities, *Sci. Total Environ.*, 2016, **565**, 889–901.

19 J. Semerád, M. Čvančarová, J. Filip, J. Kašlík, J. Zlotá, J. Soukupová and T. Cajthaml, Novel assay for the toxicity evaluation of nanoscale zero-valent iron and derived nanomaterials based on lipid peroxidation in bacterial species., *Chemosphere*, 2018, **213**, 568–577.

20 Y. T. Sheu, P. J. Lien, K. F. Chen, J. H. Ou and C. M. Kao, Application of NZVI-contained emulsified substrate to bioremediate PCE-contaminated groundwater - A pilot-scale study, *Chem. Eng. J.*, 2016, **304**, 714–727.

21 T. Phenrat, T. C. Long, G. V Lowry and B. Veronesi, Partial Oxidation ('Aging') and Surface Modification Decrease the Toxicity of Nanosized Zerovalent Iron, *Environ. Sci. Technol.*, 2009, **43**, 195–200.

22 C. Lei, L. Q. Zhang, K. Yang, L. Z. Zhu and D. H. Lin, Toxicity of iron-based nanoparticles to green algae: Effects of particle

size, crystal phase, oxidation state and environmental aging, *Environ. Pollut.*, 2016, **218**, 505–512.

23 S. Wu, T. Cajthaml, J. Semerád, A. Filipová, M. Klementová, R. Skála, M. Vítková, Z. Michálková, M. Teodoro, Z. Wu, D. Martínez-Fernández and M. Komárek, Nano zero-valent iron aging interacts with the soil microbial community: a microcosm study, *Environ. Sci. Nano*, 2019, **6**, 1189–1206.

24 N. H. A. Nguyen, M. S. A. Darwish, I. Stibor, P. Kejzlar and A. Sevcu, Magnetic Poly(N-isopropylacrylamide) Nanocomposites: Effect of Preparation Method on Antibacterial Properties, *Nanoscale Res. Lett.*, 2017, **12**, 571.

25 M. S. A. Darwish, N. H. A. Nguyen, A. Sevcu, I. Stibor and S. K. Smoukov, Dual-modality self-heating and antibacterial polymer-coated nanoparticles for magnetic hyperthermia, *Mater. Sci. Eng. C-Materials Biol. Appl.*, 2016, **63**, 88–95.

26 S. Suppi, K. Kasemets, A. Ivask, K. Kuennis-Beres, M. Sihtmaee, I. Kurvet, V. Aruoja and A. Kahru, A novel method for comparison of biocidal properties of nanomaterials to bacteria, yeasts and algae, *J. Hazard. Mater.*, 2015, **286**, 75–84.

27 V. Aruoja, S. Pokhrel, M. Sihtmaae, M. Mortimer, L. Maedler and A. Kahru, Toxicity of 12 metal-based nanoparticles to algae, bacteria and protozoa, *Environ. Sci.*, 2015, **2**, 630–644.

28 M. Esquivel-Gaon, N. H. A. Nguyen, M. F. Sgroi, D. Pullini, F. Gili, D. Mangherini, A. I. Pruna, P. Rosicka, A. Sevcu and V. Castagnola, *In vitro* and environmental toxicity of reduced graphene oxide as an additive in automotive lubricants, *Nanoscale*, 2018, **10**, 6539–6548.

29 J. Snajdr, T. Cajthaml, V. Valaskova, V. Merhautova, M. Petrankova, P. Spetz, K. Leppanen and P. Baldrian, Transformation of Quercus petraea litter: successive changes in litter chemistry are reflected in differential enzyme activity and changes in the microbial community composition, *Fems Microbiol. Ecol.*, 2011, **75**, 291–303.

30 Y. Cheng, H. Dong, Y. Lu, K. Hou, Y. Wang, Q. Ning, L. Li, B. Wang, L. Zhang and G. Zeng, Toxicity of sulfide-modified nanoscale zero-valent iron to Escherichia coli in aqueous solutions, *Chemosphere*, 2019, **220**, 523–530.

31 Y. Han, S. Ghoshal, G. V. Lowry and J. Chen, A comparison of the effects of natural organic matter on sulfidated and nonsulfidated nanoscale zerovalent iron colloidal stability, toxicity, and reactivity to trichloroethylene, *Sci. Total Environ.*, 2019, **671**, 254–261.

32 J. Kaslik, J. Kolarik, J. Filip, I. Medrik, O. Tomanec, M. Petr, O. Malina, R. Zboril and P. G. Tratnyek, Nanoarchitecture of advanced core-shell zero-valent iron particles with controlled reactivity for contaminant removal, *Chem. Eng. J.*, 2018, **354**, 335–345.

33 D. Ribas, M. Cernik, J. A. Benito, J. Filip and V. Marti, Activation process of air stable nanoscale zero-valent iron particles, *Chem. Eng. J.*, 2017, **320**, 290–299.

34 M. Ezechiáš and T. Cajthaml, Receptor partial agonism and method to express receptor partial activation with respect to novel Full Logistic Model of mixture toxicology, *Toxicology*, 2018, **393**, 26–33.

35 N. H. A. Nguyen, R. Špánek, V. Kasalický, D. Ribas, D. Vlková, H. Řeháková, P. Kejzlar and A. Ševců, Different effects of nano-scale and micro-scale zero-valent iron particles on planktonic microorganisms from natural reservoir water, *Environ. Sci. Nano*, 2018, **5**, 1117–1129.

36 L. Svobodová, T. Lederer and P. Šubrtová, Response to Shock Loads of Engineered Nanoparticles (Tio2, Sio2 Or Zro2) on Activated Sludge Microbial Communities, 2018

37 A. García, L. Delgado, J. A. Torà, E. Casals, E. González, V. Puntes, X. Font, J. Carrera and A. Sánchez, Effect of cerium dioxide, titanium dioxide, silver, and gold nanoparticles on the activity of microbial communities intended in wastewater treatment, *J. Hazard. Mater.*, 2012, **199–200**, 64–72.

38 M. I. N. Ahamed, V. Ragul, S. Anand, K. Kaviyarasu, V. Chandru and B. Prabhavathi, Green synthesis and toxicity assessment of nano zerovalent iron against chromium contaminated surface water, *Int. J. Nanoparticles*, 2018, **10**, 312.

39 M. Durenkamp, M. Pawlett, K. Ritz, J. A. Harris, A. L. Neal and S. P. McGrath, Nanoparticles within WWTP sludges have minimal impact on leachate quality and soil microbial community structure and function, *Environ. Pollut.*, 2016, **211**, 399–405.

40 D. L. Wu, Y. H. Shen, A. Q. Ding, Q. Mahmood, S. Liu and Q. P. Tu, Effects of nanoscale zero-valent iron particles on biological nitrogen and phosphorus removal and microorganisms in activated sludge, *J. Hazard. Mater.*, 2013, **262**, 649–655.

41 J. Y. Kim, H. J. Park, C. Lee, K. L. Nelson, D. L. Sedlak and J. Yoon, Inactivation of Escherichia coli by Nanoparticulate Zerovalent Iron and Ferrous Ion, *Appl. Environ. Microbiol.*, 2010, **76**, 7668–7670.

42 C. R. Keenan, R. Goth-Goldstein, D. Lucas and D. L. Sedlak, Oxidative Stress Induced by Zero-Valent Iron Nanoparticles and Fe(II) in Human Bronchial Epithelial Cells, *Environ. Sci. Technol.*, 2009, **43**, 4555–4560.

43 Q. Chen, J. Li, Y. Wu, F. Shen and M. Yao, Biological responses of Gram-positive and Gram-negative bacteria to nZVI (Fe-0), Fe2+ and Fe3+, *Rsc Adv.*, 2013, **3**, 13835–13842.

44 K. H. Gayer and L. Woontner, The Solubility of Ferrous Hydroxide and Ferric Hydroxide in Acidic and Basic Media at 25°, *J. Phys. Chem.*, 1956, **60**, 1569–1571.

45 J. C. Y. Kah, 2013, Stability and Aggregation Assays of Nanoparticles in Biological Media, pp. 119–126.

46 A. R. M. N. Afrooz, S. M. Hussain and N. B. Saleh, Aggregate size and structure determination of nanomaterials in physiological media: importance of dynamic evolution, *J. Nanoparticle Res.*, 2014, **16**, 2771.

47 H. Pullin, R. A. Crane, D. J. Morgan and T. B. Scott, The effect of common groundwater anions on the aqueous corrosion of zero-valent iron nanoparticles and associated removal of aqueous copper and zinc, *J. Environ. Chem. Eng.*, 2017, **5**, 1166–1173.

Environmental Science Nano

PAPER

View Article Online
View Journal | View Issue

Cite this: *Environ. Sci.: Nano*, 2019, 6, 1189

Nano zero-valent iron aging interacts with the soil microbial community: a microcosm study†

Songlin Wu, *[a] Tomáš Cajthaml,[bc] Jaroslav Semerád,[bc] Alena Filipová,[b] Mariana Klementová,[d] Roman Skála,[ef] Martina Vítková,[a] Zuzana Michálková,[a] Manuel Teodoro,[a] Zhaoxiang Wu,[g] Domingo Martínez-Fernández [a] and Michael Komárek[a]

Nano zero-valent iron (nZVI) is a promising material for remediating metal(loid)-contaminated soils, but its aging in the soil ecosystem (unlike intensively studied aqueous systems) and interaction with soil microbial communities have not been resolved. In this study, three types of nZVI particles (bare nZVI, nZVI coated with carboxymethyl cellulose (CMC), or polyacrylic acid (PAA)) were incubated in soils with different microbial community compositions (realized by γ-radiation), and their aging was investigated using complementary microspectroscopic analyses. In addition, the soil microbial community in association with nZVI aging was assessed by employing DNA sequencing by using Illumina MiSeq. The results revealed a drastic morphological change of nZVI, which was transformed mainly into magnetite with a rough morphology. CMC coating decreased nZVI aging, whereas PAA coating accelerated it and facilitated magnetite, goethite and lepidocrocite formation. The γ-radiation induced soil microbial community change possibly slowed down nZVI oxidation (especially for bare nZVI). Iron-reducing/oxidizing bacteria (*Bacillus*, *Shewanella*, and *Sediminibacterium*) and fungal strains with a capacity for siderophore production may participate in nZVI aging. In return, nZVI presence and aging altered soil microbial communities. This study revealed the transformation of nZVI particles into Fe (oxy)hydroxides during aging in the soil ecosystem and their bilateral interactions with the soil microbial community, thus contributing to the assessment of nZVI use in soil remediation.

Received 25th November 2018,
Accepted 27th February 2019

DOI: 10.1039/c8en01328d

rsc.li/es-nano

Environmental significance

Nano zero-valent iron (nZVI) is a promising material for the remediation of contaminated soils, but its function is influenced by its aging and transformation in soils. To date, most studies on nZVI aging are based on aqueous systems rather than soils. This study is the first investigation on the aging of nZVI with different polymer coatings in a soil ecosystem by adoption of a "sandwich"-like soil microcosm and its interactions with soil microbial communities. The results revealed the transformation of nZVI into Fe (oxy)hydroxides regulated by different polymer coating types, as well as the bilateral interactions between nZVI aging and the microbial communities. This study could provide valuable information on engineered Fe nanoparticles' behaviour and impacts in the soil ecosystem.

1. Introduction

Nano zero-valent iron (nZVI) is a promising material for remediating soils contaminated with pollutants because of its high specific surface area, high reactivity, and strong reducing properties.[1–8] However, once in the environment, it could be easily oxidized to form Fe (oxy)hydroxides,[9,10] and such transformation can influence its reactivity and functions. As nZVI has a high reducing capacity, surface oxidation usually occurs even under anaerobic conditions, resulting in

[a] *Department of Environmental Geosciences, Faculty of Environmental Sciences, Czech University of Life Sciences Prague, Kamýcká 129, 165 00 Prague – Suchdol, Czech Republic. E-mail: wusonglin11@gmail.com; Tel: +61 7 3346 3103*
[b] *Institute of Microbiology of the Czech Academy of Sciences, Videňská 1083, 142 20 Prague 4, Czech Republic*
[c] *Institute for Environmental Studies, Faculty of Science, Charles University in Prague, Benátská 2, 128 01 Prague 2, Czech Republic*
[d] *Institute of Physics of the Czech Academy of Sciences, Na Slovance 2, 182 21 Prague 8, Czech Republic*
[e] *Institute of Geology of the Czech Academy of Sciences, Rozvojová 269, 165 00 Prague - Suchdol, Czech Republic*
[f] *Institute of Geochemistry, Mineralogy and Mineral Resources, Faculty of Science, Charles University in Prague, Albertov 6, 128 43 Prague 2, Czech Republic*
[g] *Jiangxi Engineering and Technology Research Center for Ecological Remediation of Heavy Metal Pollution, Institute of Biological Resources, Jiangxi Academy of Sciences, Nanchang 330096, China*

† Electronic supplementary information (ESI) available: Supplemental methods and additional results include PLFA, TEM-SAED, and SEM results, as well as microbial diversity and composition, and their relationship with key nZVI aging products. See DOI: 10.1039/c8en01328d

the formation of an Fe oxide layer (*e.g.*, magnetite and goethite) on the surface.[11] Furthermore, it has been reported that emulsified nZVI injected into the subsurface of a groundwater system was transformed into magnetite, lepidocrocite, and goethite.[12] Therefore nZVI oxidation and transformation (here we call it "nZVI aging") should be considered clearly before application.

Bare nZVI usually aggregates readily, owing to attractive magnetic forces.[13] To improve the mobility of nZVI, various modifications have been done, including surface coating by carboxymethyl cellulose (CMC)[14,15] and polyacrylic acid (PAA),[9,16] which are widely reported. CMC is a polyelectrolyte that carries carboxylate groups in addition to hydroxyl groups, whereas PAA has a smaller molecular weight and is reported to be less stable than CMC.[16] Besides their functions in nZVI mobility improvement, these polymer coatings can also influence the reactivity of nZVI[17,18] and thus influence nZVI aging processes. In fact, in some studies, the transformation of polymer-coated nZVI in the aquatic environment was investigated.[9,19] For instance, Dong *et al.* (2016).[19] found that CMC coating decreased nZVI aging and altered nZVI's corrosion products in water.

Currently, most studies on nZVI functions and aging are performed in the aqueous environment,[11,17,19,20] whereas nZVI aging in the soil ecosystem is seldom addressed. Different from aqueous media, such as groundwater, soil is a complex matrix comprising both solid and liquid phases, with a high organic matter content, high abundance of phyllosilicates, and with stable physical structures like aggregate hierarchy, making the aging of nZVI rather complex. More specifically, soil contains numerous microbes that can be involved in nZVI aging and Fe mineral transformation. In fact, the interactions between microbes and nZVI have been reported intensively, including nZVI toxicity to microbial strains and/or microbial communities. According to Lefevre *et al.* (2016),[21] nZVI could show cytotoxicity to microbes through production of Fe^{2+} and various reactive oxygen species (ROS) that could cause oxidative stress. For example, nZVI particles caused physical disruption of the cell membrane of *Escherichia coli* and thus inactivated the microbial cells.[22] Besides, nZVI could cause elevated malondialdehyde (MDA) levels in various bacterial strains.[23] In our recent study,[24] it was found that nZVI could reduce the colonization of arbuscular mycorrhizal (AM) fungi with maize plant roots. At the microbial community level, nZVI could also influence the soil microbial community composition.[25,26] However, in fact, the interactions between nZVI and microbes are supposed to be bilateral. Typical microbes may participate or play an important role in nZVI transformation ("aging"). For instance, Ding *et al.*[27] found that extracellular polymeric substances of *Bacillus subtilis* could complex with the Fe(II) (or Fe(III)) generated by nZVI and thus influence nZVI's aging and functions in metal (*i.e.*, U) reduction and precipitation. Thus, it is reasonable to predict that the soil microbial community may influence nZVI aging. However, little information is available on bilateral interactions between nZVI aging and soil microbial community composition, which would be of great value in the assessment of nZVI functions and its environmental impacts.

The aim of the present study is to investigate the detailed processes of the aging of nZVI particles with different polymer coatings in a typical contaminated soil ecosystem, considering its interactions with the soil microbial community. Different from aqueous media, where the aged nZVI can be easily collected through sedimentation, centrifugation, or filtration, nZVI can be hardly separated from the soil when homogenously mixed with soil particles. To solve this problem, a new three layer "sandwich" incubation system ("microcosm") was developed in the present study. Metal(loid)-contaminated soil we used previously[24] was employed, and the aging of bare nZVI was compared with CMC- and PAA-coated nZVI. The soil was partially γ-radiated to prepare a control soil with a different microbial community.[28] Morphological and mineralogical changes in nZVI particles at different stages of aging were studied *via* complementary microspectroscopic methods. In addition, the microbial communities in association with nZVI aging were also investigated using amplicon sequencing (Illumina MiSeq) and phospholipid fatty acid analysis. We had three assumptions: (1) nZVI in soils could be oxidized and transformed into various Fe (oxy)hydroxides including ferrihydrite, hematite, magnetite, and goethite; (2) different polymer coatings (CMC or PAA) could influence nZVI aging and transformation differently in the soils; (3) the aging of nZVI was different in soils with a different microbial community (realized by γ-radiation treatment), and nZVI aging could in return regulate the soil microbial community composition. This study provides important information on the transformation of nZVI particles in relation to the microbial community in the soil ecosystem and thus contribute to the understanding of nZVI behavior and impacts in the complex soil ecosystem.

2. Materials and methods

2.1. nZVI preparation

Bare nZVI was provided by Nano Iron Ltd. (Rajhrad, Czech Republic) in the form of a surface-stabilized nanopowder (NANOFER STAR). The nZVI particles were surface coated with a thin layer of Fe oxides, which protected the nZVI from immediate oxidation (Fig. S1†). To activate the nZVI particles, NANOFER STAR was put into demineralized water (solid : water = 1 : 4 (w/w)) and mixed for 10 minutes in a high-shear mixer, then the suspension was kept at room temperature (25 ± 1 °C) for 48 h, according to the manufacturer's instructions. In this way, Fe oxides on the surface could be removed (Fig. S1†), and the nZVI particles could reach the highest activity. For CMC–nZVI synthesis, active bare nZVI particles were prepared from NANOFER STAR as described above and then dispersed in a CMC (the molecular weight is 90 kg mol^{-1}, Sigma-Aldrich, Saint Louis, Missouri, USA) solution. The mixture was ultrasonicated for 30 min to facilitate CMC–nZVI formation.[19] The final nZVI concentration was 20% (w/w),

and the final CMC concentration was 3% (w/w). Polyacrylic acid (PAA)–nZVI was provided by Nano Iron (Czech Republic), with a composition of 20% (w/w) nZVI and 3% (w/w) PAA (the molecular weight is 1.8 kg mol^{-1}).[29] The newly formed nZVI, CMC–nZVI and PAA–nZVI were analyzed by attenuated total reflection Fourier-transform infrared (ATR-FTIR) spectroscopy by using a Cary 630 FTIR (Agilent Technologies) (after freeze-drying) to investigate the possible mechanisms of polymer coating adsorption on the nZVI particles. The pH values of fresh nZVI particle samples were determined in water extracts (solid : water = 1 : 10 (w/v)) by using a pH electrode (TPS 900-P). The N_2-BET (Brunauer–Emmett–Teller) specific surface area (SSA) of the CMC–nZVI particles was measured by nitrogen sorption at 77 K using a Micromeritics Tristar 3020 (Micromeritics Instrument Corporation, Norcross, GA, USA).

2.2. Soil collection and characterization

The soil was collected from the alluvium of Litavka River (Příbram District, Czech Republic), which has been contaminated *via* intensive smelting activities in the past. The soil consisted of 75% sand (50–2000 μm), 20% silt (2–50 μm), and 5% clay (<2 μm) and contained mainly quartz, albite, kaolinite, chamosite 1M, and muscovite 2M1 as revealed by XRD analysis (Fig. S2†). Details on the soil physico-chemical characteristics are shown in Table S1.† Prior to the experiment, the soil was air-dried at room temperature, homogenized and sieved through a 2 mm stainless sieve.

2.3. Experimental design

2.3.1. Assessment of colloidal stability. A sedimentation trial was set to assess the colloidal stability of nZVI with different coatings (bare nZVI, CMC-/PAA-coated nZVI). The suspensions of the three types of nZVI were diluted 10 times (2% (w/w) nZVI) using deoxygenated Milli-Q water (with N_2 supply in a closed vial) to facilitate the following absorbance detection. A volume of 20 mL of the suspensions was put into the 25 mL glass vessels (three replicates for each nZVI type), and the absorbance at 508 nm over time (0, 10, 20, 30, 40, 50, and 60 min) was determined through an ultraviolet spectrophotometer (Cary 60, Agilent Technologies, California, USA). All measurements were made at 24 ± 1 °C.

2.3.2. Microcosm experiment: nZVI aging in the soil ecosystem. To investigate nZVI aging in soils, a microcosm incubation study was performed. Rather than mixing nZVI particles with soils, those nZVI particles were put on a 37 μm nylon net bag (a "nylon net layer") in the middle of the soil column filled with 250 g of soil (Fig. 1), by which the nZVI particles and its aging products could be readily collected after different periods of incubation (Fig. 1 and S3†). Besides, the potential interactions between the microbial community and nZVI can also be investigated as the mesh of 37 μm permits penetration of nearly all bacterial and fungal cells or mycelium (the diameter of most microbes is less than 30 μm[30]). Batches of 0.8 g of the three types of fresh nZVI materials (bare nZVI, CMC–nZVI and PAA–nZVI particles, were all settled from the suspension) were prepared and deposited in the 37 μm nylon net layer. A control treatment of no nZVI in the nylon layer was also set to confirm whether soil particles could penetrate the nylon net and whether the nZVI layer could influence the microbial community in the surrounding soils. To test the influence of soil microbial communities on nZVI aging, half of the soil was treated with γ-radiation (at a dose of 20 kGrey; ^{60}Co source with an irradiation rate of *ca.* 50 Grey per min), resulting in eight treatments in total (bare nZVI, CMC–nZVI, PAA–nZVI, and no nZVI in a "nylon net layer" inserted in soil with and without γ-radiation). Here we used γ-radiation, because it was reported to be effective in

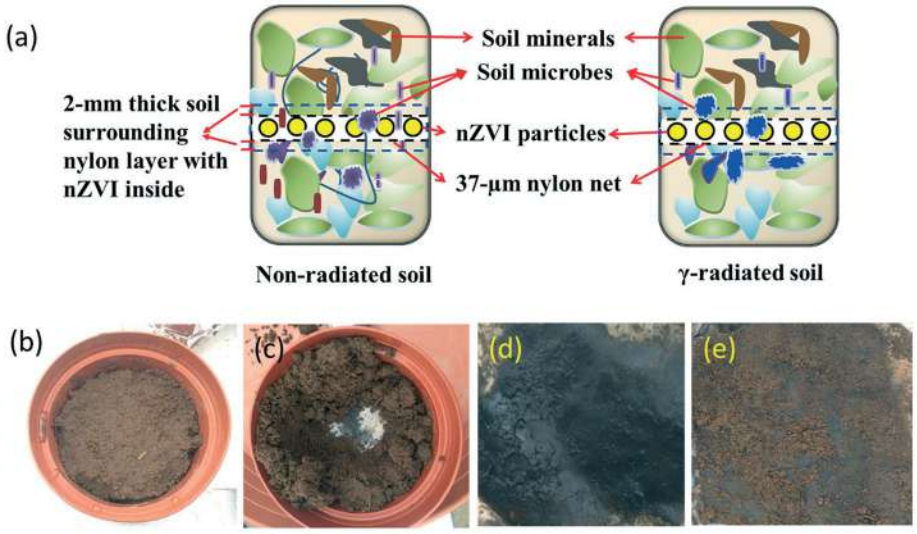

Fig. 1 Diagram showing the microcosm incubation system (a); the photos show the actual incubation system (b and c) and sampling process (d, nZVI on the nylon net; e, *ca.* 2 mm soil attached to the nylon net). At harvest, nZVI particles on the nylon net (d) and 2 mm soil layer (e) surrounding the nylon net with nZVI were collected for phospholipid fatty acid (PLFA) analysis and DNA extraction followed by sequencing (Illumina MiSeq) to characterize the bacterial and fungal communities.

the alteration of the soil microbial community (through killing most microbes) with little influence on the soil physico-chemistry (compared with other methods like autoclaving).[28] Each treatment had 24 pots (6 replicates and 4 time intervals), resulting in 192 pots in total. Within the 6 replicates, 3 were collected for spectroscopic analysis of Fe speciation and the other 3 for microbial community analysis. The pots were loosely covered with aluminum foil to allow air exchange and incubated in a temperature controlled chamber (sterilized with 75% v/v alcohol from time to time) under a constant temperature of 25 ± 1 °C for 56 days. Sterilized Milli-Q water was added into the pots regularly to maintain ~55% of the water holding capacity of the soils. It is essential to point out that the air-drying and rewetting could influence soil microbial respiration and functions towards organic matter decomposition and nitrification (known as the "Birch Effect"[31]), as well as the microbial community in the soils;[32] therefore, the present study investigated the interactions of nZVI aging with the soil microbial community that recovered from rewetting of air-dried soils. Individual nZVI samples were collected after 1, 7, 28, and 56 days. Of the 6 replicates, 3 of the original nZVI materials (and their aging products) were lyophilized for 48 h and then stored in a vacuum desiccator to avoid oxidation until spectroscopic analysis, whereas the other 3 were collected and stored at −80 °C for microbial community analysis *i.e.* phospholipid fatty acid (PLFA) analysis and DNA sequencing. It is essential to point out that we were not able to detect PLFA and isolate DNA directly from the nZVI particles and its aging products in the nylon layers even after 56 days' incubation. This may be due to the high oxidative stress of nZVI materials, resulting in low microbial colonization of the nZVI layers. To investigate potential interactions between the soil microbial community and nZVI aging, we collected samples of the soil surrounding the nZVI (within 2 mm, supposed to be intimately associated with nZVI) for microbial diversity analysis (Fig. 1 and S3†). The activities of the microbes in this soil layer may influence nZVI aging and, in return, nZVI can influence the microbial community.

The soils surrounding the nZVI layer were stored at −80 °C until PLFA and DNA extraction and amplicon sequencing analysis. Part of the soils was also air-dried for physico-chemical analysis.

2.4. SEM, TEM/SAED, XRD, ATR-FTIR, and Raman analysis

The morphology of the nZVI particles and their aging products were analyzed *via* scanning electron microscopy (SEM; TESCAN Brno, Czech Republic) and transmission electron microscopy (TEM; FEI Tecnai TF20, Massachusetts, USA) with electron dispersive X-ray spectroscopy (EDX; 125 eV, Bruker Nano, Berlin, Germany) (see details in the ESI†). The nZVI mineralogy and aging products were analyzed using X-ray diffraction (XRD; Bruker D8, Bruker, Germany), attenuated total reflection Fourier-transform infrared (ATR-FTIR, Cary 630 FTIR, Agilent Technologies Co. Ltd., California, USA) spectroscopy, and Raman analysis (MonoVista CRS+, S&I, Warstein, Germany). Detailed methods of the XRD, ATR-FTIR and Raman analysis are shown in the ESI.†

2.5. PLFA and high-throughput sequencing of the microbial community

The microbial biomass in soils of different treatments was analyzed by the phospholipid fatty acid (PLFA) method, which is shown in the ESI.† For sequencing by using Illumina MiSeq, total DNA for microbial community analysis was extracted in triplicate from all the samples using a PowerSoil DNA Isolation Kit (MoBio Laboratories Inc., Carlsbad, California, USA) and purified using a GENECLEAN Turbo Kit (MP Biomedicals, Santa Ana, California, USA), following the manufacturer's instructions. PCR amplification of the fungal ITS2 region of DNA was performed using the barcoded primers gITS7 and ITS4.[33] The V4 region of the bacterial 16S rRNA was amplified using the barcoded primers 515F and 806R.[34] PCR was performed in triplicate for each sample, and the resulting amplicons were purified, pooled, and subjected to sequencing on the Illumina MiSeq platform as an external service (GeneTiCA, Brno, Czech Republic). The amplicon sequencing data were processed using the SEED 2.1.03 pipeline.[35] Briefly, pair-end reads were merged using fastq-join.[36] Two external algorithms implemented in Vsearch[37] and Usearch[38] were used to perform clustering of similar sequences into OTUs (Operational Taxonomic Units) and chimera removal. Subsequently grouping sequences at a 97% level of identity was performed. The data were rarefied using 4808 randomly selected sequences per sample for fungi and 9906 sequences for bacteria. After clustering, it is possible to create OTU-tables and assign taxonomy to the OTUs using the alignment software BLAST,[39] which allows the retrieval of any number of best hits for each query. BLAST searches were performed remotely through the NCBI API. The generated sequences were deposited in the EMBL Nucleotide Sequence Database and are available under accession number PRJEB27806.

2.6. Soil physico-chemical characterization

Soil pH was analyzed by dispersing air-dried soils into water (solid : water = 1 : 5 w/w) and determined using an inoLab pH meter (pH 7310, WTW, Germany) coupled with a pH electrode (SenTix 41, WTW, Germany). The soil electrical conductivity (EC) was analyzed using a conductivity portable meter (ProfiLine Cond 3110, WTW, Germany). The soil redox potential (Eh) was analyzed using a digital multi-meter (Multi 3420, WTW, Germany) equipped with an IDS electrode (SenTix ORP 900, WTW, Germany). Soil dissolved organic carbon (DOC) was extracted with 0.01 mol L^{-1} $CaCl_2$ (ref. 40) and analyzed using a carbon analyzer (TOC-L CPH, SSM-5000A, Shimadzu, Japan). Key soluble elements like Al, Fe, Mn, Mg, K, Zn, and Pb were detected in a 0.01 mol L^{-1} $CaCl_2$ extract using inductively-coupled plasma optical emission spectrometry (ICP-OES, Agilent 730, Agilent Technologies, USA).

2.7. Statistical analysis

For microbial diversity analysis, the Shannon–Wiener and Simpson indices were calculated based on operational taxonomic unit (OTU) information.[41] Principal component analysis (PCA) of microbial communities in soils from different treatments was conducted by employing CANOCO 5.0 (Microcomputer Power, Ithaca, NY, USA). The multiple response permutation procedure (MRPP)[42] and permutational multivariate analysis of variance (Adonis)[43] and similarity (ANOSIM)[44] were conducted based on Bray–Curtis distances by using the VEGAN package in R.[45] Additionally, two-way clustering analysis with heat-charts (software "HemI" http://hemi.biocuckoo.org/) was used to investigate the abundance change in the identified bacterial and fungal genera in response to different treatments. Physico-chemical traits, microbial diversity indices and concentrations of microbial biomass (revealed through PLFA analysis), as well as the abundance of bacterial and fungal genus (Illumina data) in soils from different treatments, were subjected to two-way analysis of variance (ANOVA) (to address effects of γ-radiation and nZVI presence), followed by Duncan's test ($P < 0.05$), *via* the statistical package SPSS (Ver 18, IBM, Armonk, NY, USA). The relationship between physico-chemical characteristics and soil microbes was studied by canonical correspondence analysis (CCA) coupled with the Mantel test by using CANOCO 5.0 (Microcomputer Power, Ithaca, NY, USA). The bacterial and fungal abundances at the class level, as well as the physico-chemistry data used for CCA, were transformed by natural log to make sure that they were in normal distribution, which was tested by using both the quantile–quantile (Q–Q) plot and Kolmogorov–Smirnov (K–S) test using the statistical package SPSS (Ver 18, IBM, Armonk, NY, USA).

3. Results and discussion

3.1. Physico-chemical characterization of three nZVI types

All three nZVI (bare, carboxymethyl cellulose (CMC)- and polyacrylic acid (PAA)- coated) particles have a diameter of 50–100 nm according to TEM analysis, with an average size of around 60 nm (Table S2,† Fig. 2). The CMC and PAA coated nZVI show chain-like structures connecting different particles together, indicating the existence of polymers on the particle surface (Fig. 2b and c). The three nZVI types have similar N_2-BET specific surface areas (SSA, around 20 $m^2\ g^{-1}$). Bare and CMC–nZVI have a pH value of around 7.5, while PAA–nZVI has 11.0 (Table S2†), which may be due to the protonation of the negatively charged acrylic acids from the PAA coating. The molecule weight (Mw) of CMC is 90 kg mol^{-1}, which is about 50 times that of PAA. All three types of nZVI particles are negatively charged, as they have zeta potential values of below zero. In particular, PAA and CMC coating could form a higher negative charge on the surface to enhance electrostatic repulsion between particles and thus enhance nZVI stability. As showed in Fig. S4,† the bare nZVI has no specific peaks indicating organic groups, while CMC and PAA–nZVI have several peaks representing functional organic groups. In particular, the separation of the symmetric and asymmetric carboxylate positions, defined as Δv, can help identify the mechanisms of polymer adsorption on the nZVI surface.[46,47] For CMC–nZVI, there is an asymmetric COO^- at around 1559 cm^{-1} and a symmetric COO^- at 1328 cm^{-1}, with a Δv value of 231 cm^{-1}, indicating that CMC may possibly associate with nZVI particles *via* monodentate chelating.[46] For PAA–nZVI, there is an asymmetric COO^- at around 1575 cm^{-1} and a symmetric COO^- at 1393 cm^{-1}, producing a Δv value of 182 cm^{-1}, indicating that PAA may associate with nZVI *via* a bidentate bridge.[47] In addition, CMC–nZVI also has a broad peak at 1727 cm^{-1}, representing the free COO^- groups, which was not observed for PAA–nZVI.

Fig. S5† shows the relative absorbance (ratio of absorbance at some time to initial absorbance) at 508 nm for different periods of nZVI exposure. The decrease in absorbance over time indicates the reduction in the number of particles in the suspension because of aggregation and sedimentation. For bare nZVI, the relative absorbance at 508 nm was reduced by more than 90% within 10 min, indicating fast sedimentation, which may result from the aggregation of the colloidally unstable nZVI particles. This is due to the low surface charge that cannot provide significant electrostatic stabilization to resist magnetic and van der Waals attractive forces between nZVI particles.[48] As the aggregates became larger, the magnetic and van der Waals attractive forces between particles increased.[48,49] This process was faster than that observed by Dong *et al.*,[19] which may be caused by a higher Fe content in the present bare-nZVI particles, resulting in higher aggregation between nZVI particles. However, when nZVI was coated with CMC or PAA, the settling speed decreased significantly (Fig. 2). The enhanced colloidal stability of nZVI particles *via* polymer coating may be due to the reduced magnetic attraction of particles, as CMC and PAA were reported to be bound to the Fe nanoparticle surface by polar bonds between carboxylate groups, forming a physical barrier and adding negative charges to the surface.[46,50] In addition, the free polyelectrolytes from the polymer coatings can also form a bridge among polyelectrolyte covered nZVI particles and thus increase the stability of nZVI.[51] Besides, PAA or CMC coating may also increase the colloidal stability of nZVI *via* steric and depletion stabilization.[52] Similarly to the findings by Cirtiu *et al.*,[50] although both PAA and CMC could enhance the colloidal stability of nZVI, PAA–nZVI was less stable than CMC–nZVI, as indicated in the sedimentation study (Fig. S5†). This may be due to PAA having a much lower molecule weight and a less negative zeta potential compared with CMC (Table S2†), contributing thus to lower electrosteric repulsion between PAA–nZVI particles.[16,53]

3.2. Morphological changes in three nZVI types

No soil minerals were found in the control nylon net (no nZVI addition) showing that no soil minerals entered the nylon net layer during the incubation (Fig. S3†). Therefore, all the Fe minerals detected in the nylon net layer were products

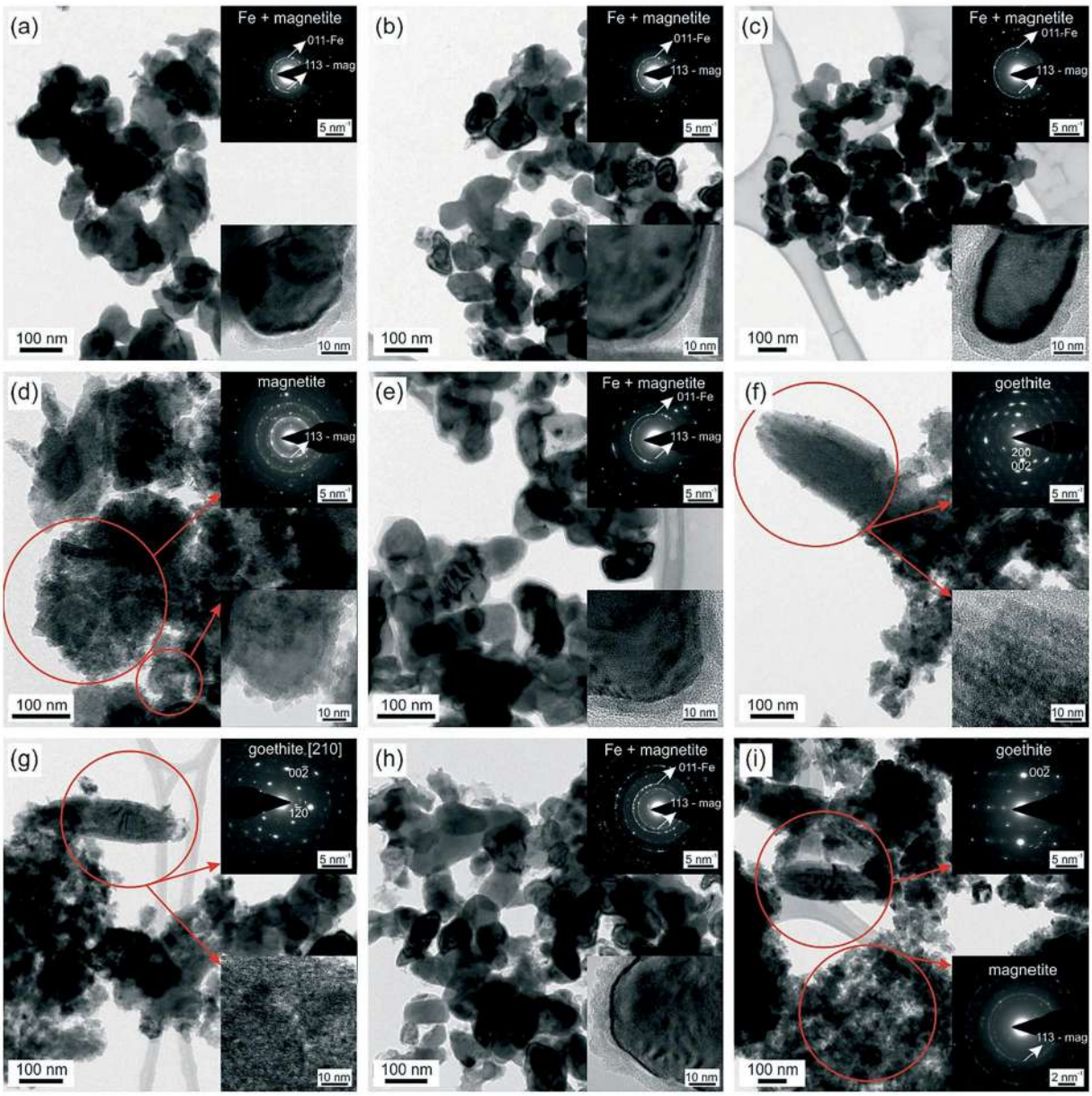

Fig. 2 Transmission electron microscopy coupled with selected area electron diffraction (TEM/SAED) results showing fresh nZVI and nZVI aging products after 56 days of aging in soils. (a), (d) and (g) bare nZVI; (b), (e) and (h) CMC-coated nZVI; (c), (f) and (i) PAA-coated nZVI. (a), (b) and (c) fresh nZVI particles; (d), (e) and (f) nZVI particles in γ-radiated soils (with altered microbial community) after 56 days of aging; (g), (h) and (i) nZVI particles in non-radiated soils (with original soil microbial community) after 56 days of aging. Note: nZVI, nano zero-valent iron; CMC, carboxymethyl cellulose; PAA, polyacrylic acid.

of the aging of nZVI particles in the soil environment. Morphological and phase changes during nZVI aging were studied *via* TEM/SAED and SEM (Fig. 2 and S6–S9†). Fresh nZVI generally formed spherically shaped nanoparticles with a diameter of about 50–100 nm, which aggregated quickly into chain structures owing to magnetic interactions.[47,54] The diffuse rings observed in the selected areas of the SAED pattern indicated that fresh nZVI (including bare and CMC- or PAA-coated nZVI) was poorly ordered and amorphous (although some indications of magnetite existed). In fact, the spherical iron (α-Fe) particles were completely covered by a magnetite shell with a thickness of a few nanometers (Fig. 2a–c). After 56 days of aging, the size and shape of particles changed significantly depending on the nZVI type.

For bare nZVI, the particle diameter increased, as did the surface area (Fig. 2d and g), indicating oxidation of the particles. Residual nZVI particles covered by irregular magnetite particles (above 200 nm) were observed after 56 days of aging (Fig. 2d and g). Besides, in the non-radiated soil, rod-like particles formed by goethite nanoparticles ordered in a single-crystal manner were revealed (Fig. 2g). Moreover, compared with the magnetite nanoparticles from the γ-radiated soil, which were in a completely random orientation, the nanoparticles in the non-radiated soil had a strongly preferred

orientation, which was documented by the increased intensity of the 220 diffraction line (Fig. S6c†).

For CMC–nZVI, although some aggregation of particles occurred, the morphological shape of individual particles did not change significantly during the incubation period, and most particles remained spherical (Fig. 2b, e, and h). Magnetite occurred mainly in the form of a shell on the nZVI particles. In the SAED patterns and higher magnification images, increases in the thickness of the magnetite shell and the magnetite crystallinity were observed in the aged materials (Fig. 2e and h). Besides, a few larger particles (more than 200 nm) composed of a mixture of nanocrystalline magnetite and amorphous phases were also found in the aged nZVI particles (Fig. S7b and c†).

PAA–nZVI showed the biggest morphological and phase change during the aging. After a 56 day incubation, most of the nZVI was oxidized to magnetite and goethite (Fig. 2f and i). Goethite mainly occurred as particles composed of nanocrystals aligned in a single-crystal manner. Magnetite formed either larger aggregates of nanocrystals (Fig. 2i and S8c†), resembling the original nZVI, or lath-like particles about 50 nm in width composed of nanocrystals (Fig. S8b†). This indicates that PAA coating could accelerate nZVI aging and promote Fe mineral transformation in the soil. In addition, SEM analysis showed that more rod-like minerals (*e.g.* lepidocrocite, goethite *etc.*) occurred in the aging products of PAA–nZVI in the non-radiated soil than in the γ-radiated soil (Fig. S9†), indicating the potential effects of soil microbial community on PAA–nZVI aging.

The CMC and PAA coating influenced nZVI aging differently, as CMC decreased nZVI aging, while PAA increased nZVI oxidation. The reason may lie in the different properties of the PAA and CMC coated nZVI and their ability to resist the effects of cations (such as Mg^{2+}, Ca^{2+}, Zn^{2+}, Fe^{3+} *etc.*) on the stability of nZVI. In the present study, the nZVI particles were exposed to the soil solutions, which usually contained high concentrations of these soluble cations that can destroy the protective PAA-layer surrounding nZVI, due to the ion's effects on the hydration of the carboxylate groups in PAA,[47] resulting in aggregation of the nZVI particles. Besides, these cations also weaken the repulsion of the electric double layer (EDL) and thus reduce the mobility of PAA–nZVI.[55] As PAA–nZVI was more dispersed than bare nZVI due to increased electrostatic, steric and depletion stabilization by PAA, the interaction area between PAA–nZVI particles and soil solutions was larger compared with bare nZVI. The separated PAA–nZVI particles in soils become unstable and easily react with oxidants after the PAA layer is destroyed by cations, causing even more nZVI oxidation and aging than that in the case of bare nZVI. In contrast, for CMC–nZVI, the molecule weight of CMC is much higher than that of PAA and it has more vacant COO^- groups (indicated by Fig. S4†) that could complex with cations such as Ca^{2+} and decrease the compression effects of cations on the EDL, protecting thus the nZVI particles from destruction by cations.[47] Besides, those free COO^- groups in CMC coatings could also prevent available oxidants in the surrounding media and even act as radical scavengers for oxidants[56] and slow down the oxidation of the nZVI particles.

3.3. nZVI aging characterization: spectroscopic study

3.3.1. XRD analysis of nZVI aging. The XRD patterns in Fig. 3 show the mineral phases of fresh and aged nZVI particles. With increasing time, a fraction of nZVI was oxidized mainly into magnetite and goethite, as the intensity of peaks at 2θ = 45° and 65° (represent Fe^0) decreased, while that of peaks at 2θ = 30.1°, 35.2°, 43.8°, and 57.0° (represent magnetite) increased. Besides, at day 56, small peaks appeared at 2θ = 21° and 54.1° (representing goethite). This indicates that nZVI was oxidized to magnetite and goethite, which was consistent with the results of the TEM/SAED analysis. With the time going, the percentage of Fe^0 decreased, while magnetite increased, and at day 56, even half of the nZVI was transformed into magnetite and goethite (Fig. 3a and d).

However, for CMC–nZVI, most of the nZVI remained in the form of Fe^0 even after 56 days in the soils (Fig. 3b and e), although with increasing time, a small peak of magnetite and lepidocrocite appeared. These results indicate that when nZVI was coated with CMC (*ca.* 7 : 1 (w/w)), the nZVI aging decreased, and little of the CMC–nZVI was oxidized, which is different from what Dong *et al.* (2016)[19] found. This may be because the concentration of CMC used in the present study was higher than that used by Dong *et al.* (2016)[19] and more efficient for reducing the interactions of oxygen or water with Fe^0.

Different from bare nZVI and CMC–nZVI, PAA–nZVI aged faster (Fig. 3c and f). The portion of Fe^0 decreased dramatically and nearly dropped to around 30% after 56 days of aging in the non-radiated soils. At the same time, the portion of magnetite increased significantly; up to 40.3% was reached after 56 days' aging in non-radiated soils. Besides, since day 7 of the aging, goethite was formed, which increased significantly afterwards (above 20% at day 56). Besides, a little amount of lepidocrocite (2.5–8.4%) appeared from day 7. The PAA–nZVI in the non-radiated soil had more magnetite and possibly less goethite compared with that in the γ-radiated soil (Fig. 3c and f), showing the possible influence of original soil microbial communities on nZVI aging and transformation.

3.3.2. ATR-FTIR analysis of nZVI aging. Some Fe mineral phases that are disordered or amorphous can hardly be identified by XRD analysis.[57] Therefore, ATR-FTIR was conducted to further confirm nZVI aging products. As shown in Fig. 4a, Fe (oxy)hydroxides including magnetite, goethite, lepidocrocite and hematite had typical peaks at 500–1500 cm^{-1}. Specifically, magnetite and hematite had peaks at around 550 cm^{-1}, which corresponds to the vibration of Fe–O bonds. Goethite had significant peaks at 560, 798 and 891 cm^{-1}, while lepidocrocite had peaks at 741, 1019 and 1145 cm^{-1} and we could thus clearly identify possible Fe (oxy)hydroxides in the nZVI aging products.

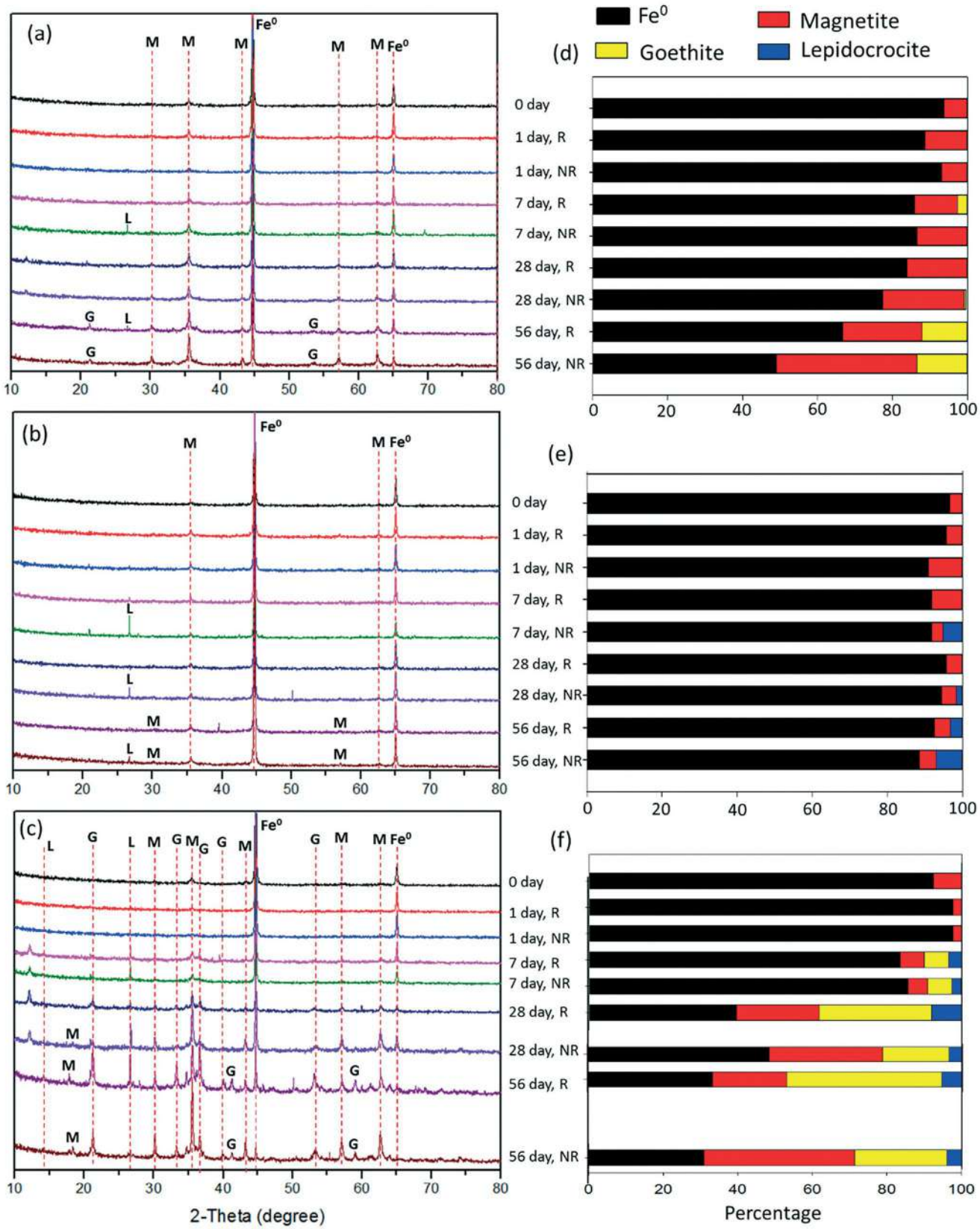

Fig. 3 X-ray diffraction (XRD) patterns of nZVI and their aging products for different periods. (a) Bare nZVI; (b) CMC–nZVI; (c) PAA–nZVI; (d)–(f) show the percentage of different Fe species revealed by quantification of the XRD spectra of the aging products of bare nZVI, CMC–nZVI, and PAA–nZVI, respectively. Note: Fe^0: nZVI; M: magnetite; G: goethite; L: lepidocrocite. R represents γ-radiated soil (altered soil microbial community); NR represents non-radiated soil (with original soil microbial community). nZVI, nano zero-valent iron; CMC, carboxymethyl cellulose; PAA, polyacrylic acid.

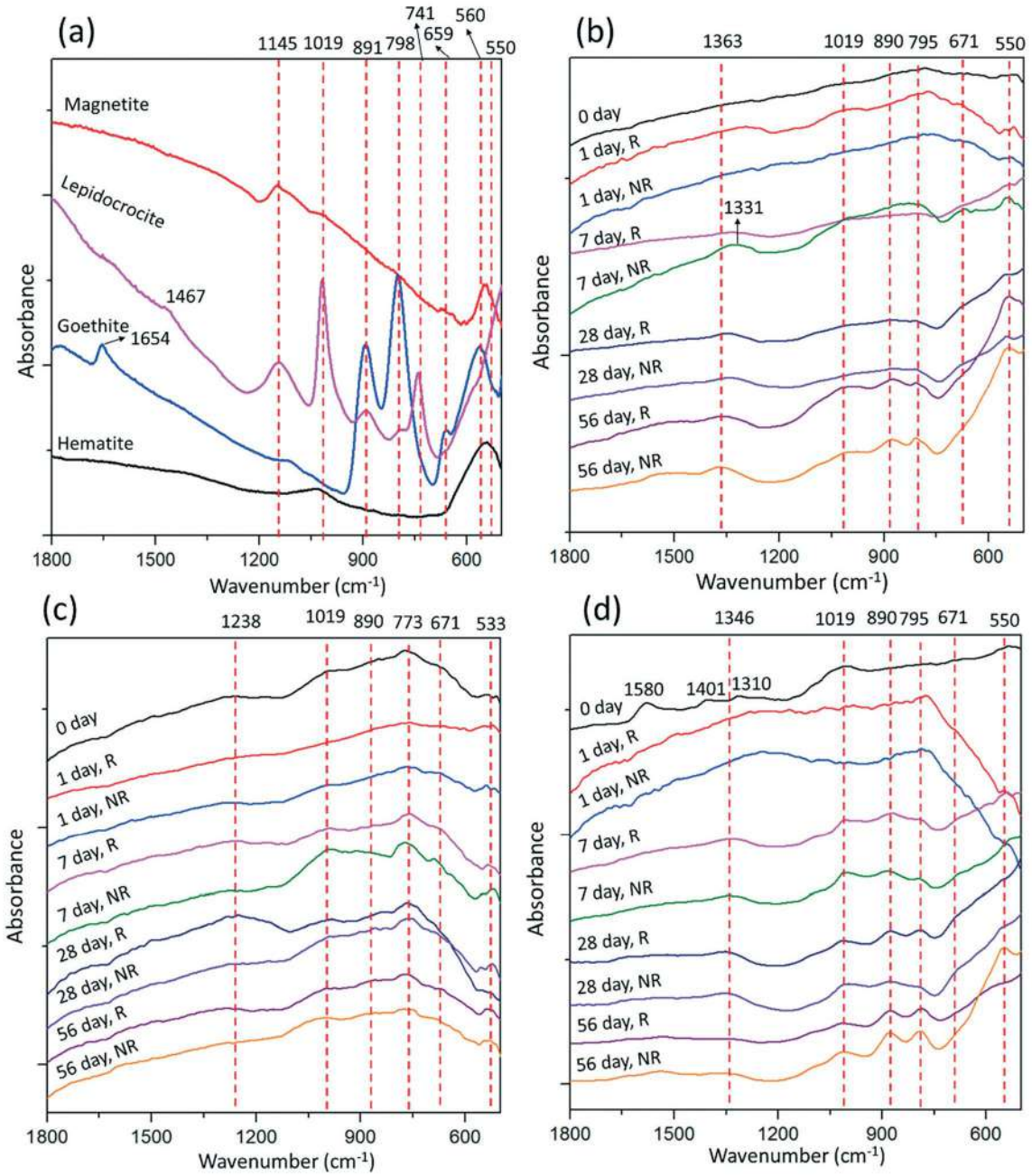

Fig. 4 ATR-FTIR spectra of standard Fe (oxy)hydroxides, nZVI and its aging products at different periods. (a) Standard Fe (oxy)hydroxides; (b) bare nZVI; (c) CMC–nZVI; (d) PAA–nZVI. Note: R represents γ-radiated soil (altered soil microbial community); NR represents non-radiated soil (with original soil microbial community). nZVI, nano zero-valent iron; CMC, carboxymethyl cellulose; PAA, polyacrylic acid.

In bare nZVI, there was a little peak observable at around 550 cm^{-1}, which became clearer after 56 days, indicating the possible existence of magnetite (and/or hematite) (Fig. 4b). Besides, peaks at 795 and 890 cm^{-1} increased from day 56, indicating the possible existence of goethite. When nZVI was coated by CMC, the FTIR spectra did not change significantly at day 56, although there were little peaks at around 533, 671, 773 and 890 cm^{-1}, representing possible magnetite (and/or hematite) (Fig. 4c). In contrast, for PAA–nZVI, peaks at 795, 890 and 1019 (surface –OH groups on lepidocrocite) from day 7 indicated that goethite and lepidocrocite were generated (Fig. 4d). Besides, there were also small peaks at 550 cm^{-1} in fresh PAA–nZVI particles, indicating possibly magnetite. It was interesting to find that at day 56, the PAA–nZVI in non-radiated soils had a peak at 550 cm^{-1}, which was not found in γ-radiated soils, indicating more magnetite was produced in non-radiated soils compared with the γ-radiated soil. This is consistent with the results of XRD analysis, confirming the microbial effects on PAA–nZVI aging.

3.3.3. Raman analysis of nZVI aging. In complementary with the above spectroscopic analysis, Raman analysis was used to further investigate nZVI aging and to identify

possible poorly crystalline minerals.[58] Generally, most of the nZVI aging products had peaks at 217–220, 394–401, 488–494, and 588–602 cm^{-1} (Fig. S10†), which were identified as hematite (possibly also a small amount of magnetite).[59] This is different from the results of the TEM/SAED, XRD and ATR-FTIR analysis, which showed that most of the aging products were magnetite. This may be due to the laser-induced thermal heating of the Fe material, causing transformation of Fe (oxy)hydroxides into hematite.[60] Despite this drawback, Raman analysis provides complementary information. In comparison with bare nZVI, CMC–nZVI aging products had peaks at 250, 348, and 531 cm^{-1} after 7 and 56 days of incubation (Fig. S10†), indicating possibly lepidocrocite.[61] A small amount of lepidocrocite may also exist in PAA–nZVI after 56 days of aging, as a peak was found at 242 cm^{-1} after 56 days of aging in the non-radiated soils (Fig. S10c†). Magnetite was also detected in the Raman spectra at about 660 cm^{-1}, which confirmed the XRD results. It is interesting to note that for CMC–nZVI and PAA–nZVI, the peaks at 242, 348, and 531 cm^{-1} existed in the non-radiated soils rather than in the γ-radiated soils (Fig. S10b and c†), indicating that the original soil microbial community facilitated lepidocrocite formation during CMC–/PAA–nZVI aging.

3.3.4. Possible mechanisms of nZVI aging in the soil ecosystem. From the above spectroscopic study (*i.e.* XRD, ATR-FTIR, Raman spectroscopy), the main corrosion products of nZVI in the present soil system were magnetite and goethite, with a little amount of lepidocrocite, which was partially consistent with previous studies using an aqueous system,[11,19,62] where magnetite (and/or maghemite) and lepidocrocite were the main aging products of nZVI particles. The magnetite (Fe_3O_4) may result from the reaction of Fe^0 (nZVI) with soil pore water. Fe^0 may firstly be oxidized to Fe^{2+}, which then reacts with H_2O and O_2 to form Fe_3O_4(s). The key reaction forms may include (eqn (1)–(3)):

$$Fe^0 + 2H_2O = Fe^{2+} + H_2 + 2OH^- \quad (1)$$

$$2Fe^0 + O_2 + 2H_2O = 2Fe^{2+} + 4OH^- \quad (2)$$

$$6Fe^{2+} + O_2 + 6H_2O = 2Fe_3O_4(s) + 12H^+ \quad (3)$$

A small amount of lepidocrocite (γ-FeOOH) was identified in corrosion products of CMC/PAA coated nZVI after more than 7 days' aging in the soil system (Fig. 3 and 4 and S10†), indicating that more Fe^0, Fe^{2+} or Fe_3O_4 were oxidized and precipitated with time. This is reasonable, as the current microcosm cultivation system was an open system allowing air (containing *ca.* 20% v/v O_2) exchange. The lepidocrocite (γ-FeOOH) may form through the following reactions (eqn (4)–(6)):

$$4Fe^0 + 3O_2 + 2H_2O = 4\gamma\text{-FeOOH} \quad (4)$$

$$4Fe^{2+} + O_2 + 6H_2O = 4\gamma\text{-FeOOH} + 8H^+ \quad (5)$$

$$4Fe_3O_4 + O_2 + 6H_2O = 12\gamma\text{-FeOOH} \quad (6)$$

Besides magnetite and lepidocrocite, goethite was also found to be the aging products of bare nZVI and PAA–nZVI in the present soil ecosystem, which was different from that in an aqueous system.[19,62] This may be due to the complex physico-chemistry of soil pore water (*e.g.* pH, CO_3^{2-}, or Cl^-), which can influence the crystalline structure of Fe (oxy)hydroxides (FeOOH)[63] and favored the formation of goethite (α-FeOOH) rather than lepidocrocite (γ-FeOOH) in the present situation. It is important to point out that the extent of the oxidation of nZVI particles after 56 days' aging in the soils were less than that in previous studies in an aquatic system.[11,19] This may be because the oxygen level and water content in the undisturbed soil system was lower than those in studies in an aquatic environment, and the oxygen level controls nZVI significantly.[64] In addition, the soil physical structure, organic matter, mineralogy and soil microbes may systematically influence nZVI aging.[65]

Similar with TEM-SAED results, the various spectroscopic analyses also confirmed that PAA coating enhanced nZVI oxidation and Fe (oxy)hydroxide formation, while CMC slowed done nZVI aging. As discussed above, this may result from the different capabilities of PAA and CMC to resist the effects of soil cations, which could destroy the protective polymer surrounding nZVI particles due to the ion's effects on the hydration of the carboxylate groups.[47] Both CMC and PAA could enhance colloidal stability and increase the contact of nZVI particles with the soil environment, while at the same time, CMC with a larger molecule weight and more abundant vacant COO^- groups (indicated by Fig. S4†) compared with PAA has stronger protective effects against cations' "attacks".

Through comparison of nZVI aging in γ-radiated and non-radiated soils with different microbial communities, it is possible to uncover the effects of soil microbes on nZVI aging. Specifically, in the present study the γ-radiation treated soil restrained the oxidation of bare nZVI and PAA–nZVI to magnetite and reduced lepidocrocite formation from CMC–nZVI, indicating the possibility of microbial functions on nZVI aging in the soil ecosystem.

3.4. Soil microbial composition in relation to nZVI aging

3.4.1. Soil microbial community structure related to nZVI aging. As revealed by both PLFA and amplicon sequencing analysis, γ-radiation treatment resulted in the development of alternative bacterial and fungal communities in the soil (Fig. 5 and Table S3†), which is consistent with Brown *et al.*[66] The Shannon–Wiener and Simpson Indices of bacterial community diversity (based on Illumina data analysis at the OTU level) in the non-radiated soil samples surrounding the nZVI layer were much higher than those in the γ-radiated soils ($P < 0.05$), showing the complexity and possible stability of the original soil microbial community (Fig. S11†). This is reasonable as 20 kGrey γ-radiation treatment can usually kill most bacteria except those with great resistance to γ-radiation.[28] However, there is no difference in total bacterial biomass in the soils between γ-radiation and non-radiation treatments as

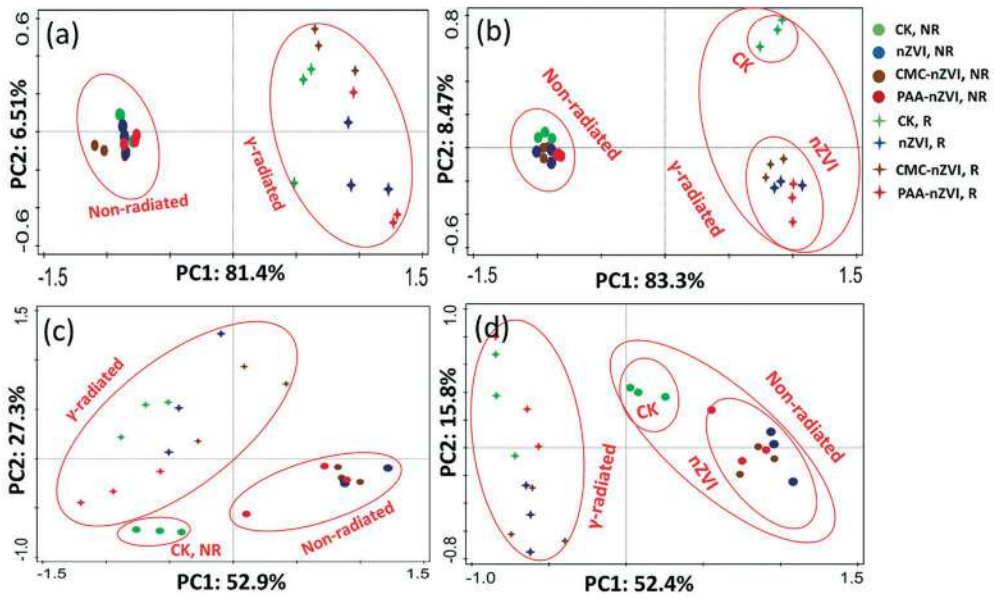

Fig. 5 Multivariate analysis based on bacterial and fungal community information (Illumina data) at the class and genus levels. (a) Principal component analysis (PCA) based on bacterial class level distribution, (b) PCA based on bacterial genus level distribution, (c) PCA based on fungal class level distribution, and (d) PCA based on fungal genus level information. Note: CK, NR represents no nZVI in nylon layers and no soil radiation; CMC–nZVI, NR represents CMC-coated nZVI in nylon layers without soil radiation; nZVI, NR represents bare nZVI in nylon layers without soil radiation; PAA–nZVI, NR represents PAA-coated nZVI in nylon layers without soil radiation; CK, R represents no nZVI in nylon layers with soil γ-radiation; CMC–nZVI, R represents CMC-coated nZVI in nylon layers with soil γ-radiation; nZVI, R represents bare nZVI in nylon layers with soil γ-radiation; PAA–nZVI, R represents PAA-coated nZVI in nylon layers with soil γ-radiation. nZVI, nano zero-valent iron; CMC, carboxymethyl cellulose; PAA, polyacrylic acid.

indicated by PLFA analysis (Table S3†). This may be because some bacteria with high resistance to γ-radiation may develop fast and enrich the total bacterial biomass. For example, the amounts of Gram-positive (G^+) tended to decrease upon γ-radiation, while Gram-negative (G^-) increased upon γ-radiation (Table S3,† $P < 0.05$). Furthermore, PCA at the phylum, class, genus, and OTU levels on the amplicon sequencing results showed that non-radiated and γ-radiated treatments resulted in a substantially different bacterial community composition (Fig. 5 and S12, Table S4;† $P < 0.01$ for both bacteria and fungi at phylum, class, genus and OTU levels based on the three non-parametric multivariate statistical tests, including ANOSIM, Adonis and MRPP). Although there was almost no difference in the fungal diversities between non-radiated and γ-radiated soils (except for PAA–nZVI) (Fig. S11†), the fungal community structure in γ-radiated soils was significantly separated from that in non-radiated soils, as revealed by PCA coupled with ANOSIM analysis (Fig. 5, Table S4†). All of the above indicates that γ-radiation was effective in changing the soil microbial community, and nZVI aging occurred at soils with a different microbial community structure, which may at least partially influence nZVI aging.

One additional concern was that γ-radiation may directly change soil physico-chemical traits, which influenced nZVI aging irrespective of microbial functions. However, this was probably not the case in the present experiment as we found that the γ-radiation generally did not change the physico-chemical characteristics (*e.g.*, no effects on pH, Eh, and DOC, as well as $CaCl_2$-extractable Al, Fe, Mg, K, Zn, and Pb values) initially at day 1, except for slightly increased $CaCl_2$ extractable Mn and EC values (Table S5†). However, after 56 days, there were significant differences in physico-chemistry between γ-radiated and non-radiated soils (Table S6†). This might partially result from the contrasting microbial community (induced by γ-radiation) activities occurring during the 56 days of incubation. As indicated by canonical correspondence analysis (CCA) (Fig. S13†), DOC, pH and $CaCl_2$-extractable Mn interacted intensively with the bacterial community, while $CaCl_2$ extractable Mn, Mg and K dominantly interacted with the fungal community. The changes of these key physico-chemical parameters (*i.e.*, pH and DOC) originating from microbial activities may then influence nZVI aging as well.[67,68] Therefore, the different nZVI aging occuring in γ-radiated soils and non-radiated soils may at least partially be attributed to the different microbial community activities and the induced physico-chemical changes.

In return, nZVI occurrence and aging also influenced the soil microbial community structure. In the γ-radiated soils, the occurrence of nZVI layers caused a substantial shift of the bacterial community at the genus levels (Fig. 5b, analysis of similarity (ANOSIM), $R = 0.343$, $P = 0.03$). Besides, the fungal community structure was influenced significantly by nZVI materials in non-radiated soils at the genus level (Fig. 5d; ANOSIM: $R = 0.909$, $P = 0.002$). The regulation of the soil microbial community by nZVI aging may result from both direct (Fe sources, Fe redox) and indirect (micro-Eh) effects of nZVI.[25] The selected microbes surrounding nZVI may participate in nZVI aging through reducing/oxidizing/complexing

Fe^0 or Fe (oxy)hydroxides, or through influencing physicochemistry (*i.e.*, pH, DOC, EC).

3.4.2. Microbial taxa interactions with nZVI aging

3.4.2.1. Class level. At the class level, the most abundant bacteria is *Betaproteobacteria*, which comprises more than 30% percent in the non-radiated soils, while γ radiation increased its abundance to more than 50% (Fig. 6a). The non-radiated soil contained more *Alphaproteobacteria*, *Actinobacteria*, and *Solibacteres* but less *Gammaproteobacteria* and *Chitinophagia* than the γ-radiated soil did (Fig. 6a). The re-establishment of microbes after γ-radiation may be due to the selection of radiation resistant microbes (based on the sensitivity of the microbes to the γ-radiation) coupled with niche competition between different microbes.[69] Specifically, *Alphaproteobacteria*, *Actinobacteria*, and *Solibacteres* were dominant in the original non-radiated soil, but their abundance decreased after γ-radiation, while those bacteria like *Betaproteobacteria*, *Gammaproteobacteria* and *Chitinophagia* (possibly with high γ-resistance) began to develop and occupied the niche. In addition, nZVI presence increased the abundance of *Gammaproteobacteria* in soils but decreased *Alphaproteobacteria* abundance in the γ-radiated soils, indicating their different tolerance to nZVI particles. Furthermore, *Alphaproteobacteria* and *Actinobacteria* abundance was found to be generally consistent with magnetite abundance (Fig. S14a†), indicating that bacterial species that belong to these two classes may facilitate magnetite formation (probably those magnetotactic bacteria[70,71]). In contrast, *Chitinophagia* and *Gammaproteobacteria* abundance was generally contrary with magnetite abundance, showing that they may probably restrain magnetite formation.

For the fungi, the dominant class in both soil samples was *Eurotiomycetes* (above 70%) belonging to ascomycetes (Fig. 6b). The γ-radiated soil contained more *Dothideomycetes*, but less *Leotiomycetes* and *Tremellomycetes* than the non-radiated soil did, showing that *Dothideomycetes* may be more resistant to γ-radiated radiation. In the non-radiated treatment, nZVI presence increased *Sordariomycetes*, *Leotiomycetes* and *Tremellomycetes* abundance, indicating their high resistance to nZVI particles. Furthermore, the abundance of *Leotiomycetes* and *Tremellomycetes* was consistent with magnetite abundance in the nylon layer (except for CMC–nZVI in non-radiated soil) (Fig. S14b†), showing that their activities may facilitate nZVI oxidation to magnetite.

3.4.2.2. Genus level. At the genus level, about 30% of bacteria in the non-radiated soil samples were below the 95% similarity threshold (data not shown), indicating the complexity of the bacterial community in the indigenous soil microbial pool. Out of the identified bacteria, several genera profited from the γ-radiation and fulfilled niches left empty by other bacteria in the soil surrounding the nZVI layers. These genera comprised *Massilia*, *Shewanella*, *Leifsonia*, *Sediminibacterium*, and *Phenylobacterium* (Fig. 7a). Among these identified bacterial genera, *Shewanella* spp. are heterotrophic facultative anaerobes well known for Fe(III) reduction under anaerobic conditions.[71,72] The nZVI layers increased *Shewanella* spp. abundance in both the γ-radiated and non-radiated soils ($P < 0.05$, Duncan test; Fig. 7a; Table S7†), indicating that the nZVI layer may favor the enrichment of these bacterial species. The induced iron-reducing bacteria by nZVI were also reported previously.[73] This could be explained by an increased Fe(III) content originating from nZVI oxidation together with partial consumption of O_2 near the nZVI layers owing to reactions with Fe^0. Apart from the chemical oxidation of Fe^0 (reaction with O_2 or H_2O), the magnetite formed may also partially result from the functions of *Shewanella* spp., which can facilitate biogenic extracellular magnetite formation,[74] *via* biologically induced

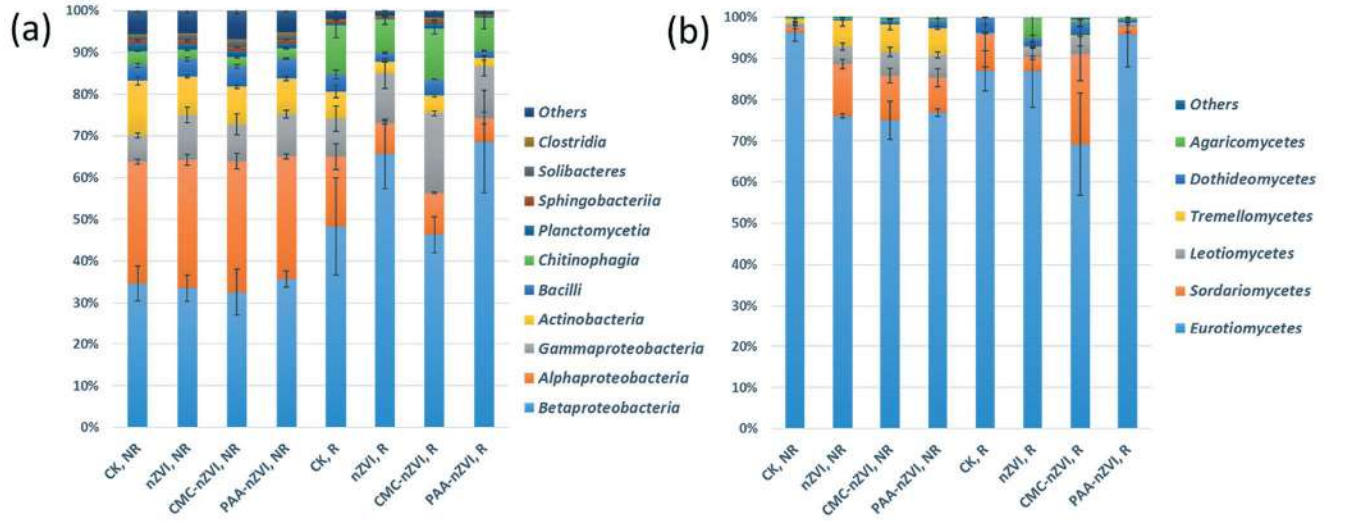

Fig. 6 Bacterial (a) and fungal (b) community composition (Illumina data) at the class level in nZVI-surrounding soils from different treatments. Note: CK, no nZVI in nylon layers; CMC–nZVI, CMC-coated nZVI in nylon layers; nZVI, bare nZVI in nylon layers; PAA–nZVI, PAA-coated nZVI in nylon layers; R represents γ-radiated soil; NR represents non-radiated soil. nZVI, nano zero-valent iron; CMC, carboxymethyl cellulose; PAA, polyacrylic acid.

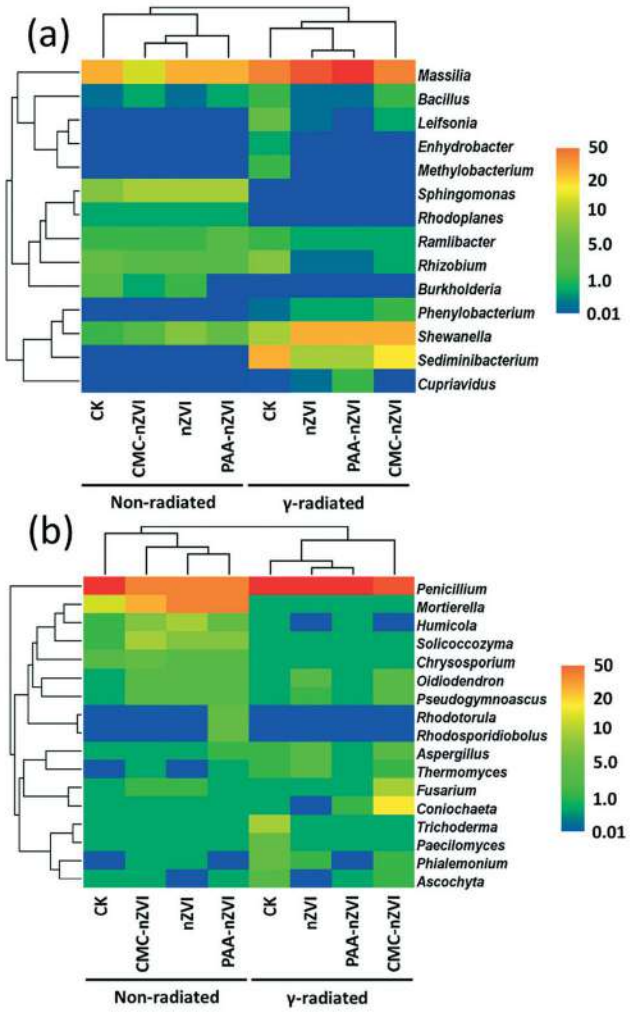

Fig. 7 Relative genus-level abundance of dominant organisms in the bacterial (a) and fungal (b) communities in the 2 mm thick soils intimately surrounding the nZVI layer from different treatments after 56 days of incubation. Notes: CK, no nZVI in nylon layers; CMC–nZVI, CMC-coated nZVI in nylon layers; nZVI, bare nZVI in nylon layers; PAA–nZVI, PAA-coated nZVI in nylon layers. nZVI, nano zero-valent iron; CMC, carboxymethyl cellulose; PAA, polyacrylic acid. γ-Radiation was realized using 20 kGrey.

mineralization or specific biologically controlled mineralization.[75] However, simultaneously, *Shewanella* spp. can also reduce Fe(III) in magnetite and cause dissolution of magnetite,[76] and this seems to be the case in the present study, as the *Shewanella* spp. abundance generally changed contrarily with the magnetite abundance across different treatments (except the situation of the CMC–nZVI layer with non-radiation treatment, Fig. 8a). Although *Bacillus* spp. were not the most dominant, some of this genus have also been reported to have the capacity for Fe(III) reduction.[77,78] The abundance of this genus was significantly elevated in the case of the CMC–nZVI material in both γ-radiated and non-radiated soils ($P < 0.05$, Duncan test; Fig. 7a; Table S7†), indicating that carboxymethyl cellulose could serve as an organic substrate for these bacteria. In addition, the abundance of *Sediminibacterium* spp., a possible iron-oxidizing bacteria,[79,80] increased in the γ-radiated soils ($P < 0.05$, Duncan test). This bacteria may participate in magnetite oxidation and thus reduce magnetite abundance in nZVI layers in the γ-radiated soils, as indicated by XRD and ATR-FTIR analysis, which was also confirmed by the fact that the *Sediminibacterium* spp. abundance generally changed contrarily with magnetite abundance across different treatments (except the situation of the CMC–nZVI layer with non-radiation treatment, Fig. 8a). Several other genera including *Sphingomonas*, *Rhodoplanes*, *Rhizobium*, and *Burkholderia* were detected mostly in the non-radiated soil samples, among which *Rhodoplanes* spp. and *Rhizobium* spp. are reported to be natural fertilizers,[81,82] and their abundance was generally consistent with magnetite abundance across the treatments, indicating that they may facilitate magnetite formation, which should be due to the functions of their exudates such as siderophores.[83]

The fungal genus was also related to nZVI aging. *Penicillium* spp. a common ascomycetes filamentous genus, was the most abundant fungi in both the γ-radiated and non-radiated soils. The genus was especially dominant in the γ-radiated samples (Fig. 7b). However, its abundance was substantially suppressed in the non-radiated samples after exposure to nZVI materials ($P < 0.05$, Duncan test; Fig. 7b, Table S8†), showing its sensitivity to nZVI particles (and/or its aging products). The *Penicillium* spp. abundance was generally contrasting with magnetite abundance (Fig. 8b), indicating that this fungal genus may be sensitive to magnetite or can restrain magnetite formation. The genera *Mortierella* spp., *Solicoccozyma* spp., *Chrysosporium* spp., and *Humicola* spp. were detected almost solely in the non-radiated soil (Fig. 7b), indicating they were typical indigenous fungi in the original soil and sensitive to γ radiation. In particular, the abundances of *Mortierella* sp., *Humicola* sp., *Pseudogymnoascus* spp., and *Oidiodendron* spp. increased with nZVI presence in the non-radiated soils ($P < 0.05$, Duncan test; Fig. 7b; Table S8†), showing their resistance to oxidative stress caused by nZVI or their ability to thrive from the nZVI aging products, *e.g.*, Fe (oxy)hydroxides.[84] Besides, some fungal genera such as *Humicola* sp. may utilize CMC or PAA on the nZVI surface.[85] Interestingly, the abundance of *Mortierella* spp., *Solicoccozyma* spp., *Chrysosporium* spp., and *Humicola* spp. is consistent with magnetite abundance (except for CMC–nZVI with non-radiation treatment) (Fig. 8b), indicating that these indigenous fungal species may facilitate magnetite formation during nZVI aging, which may be due to their exudates (*e.g.* siderophores) that can chelate Fe from solid phases,[86,87] and thus potentially contribute to Fe transformation during nZVI aging in the soils.

3.5. Potential effects of nZVI aging on its functions

The aging of nZVI may influence its functions towards metal(loid) immobilization through changes in surface area, binding sites, reactivity, *etc.*[88] In the present study, the nZVI particles grow owing to aggregation and transformation, as revealed by TEM/SAED and SEM (Fig. 2 and S6–S9†), which may

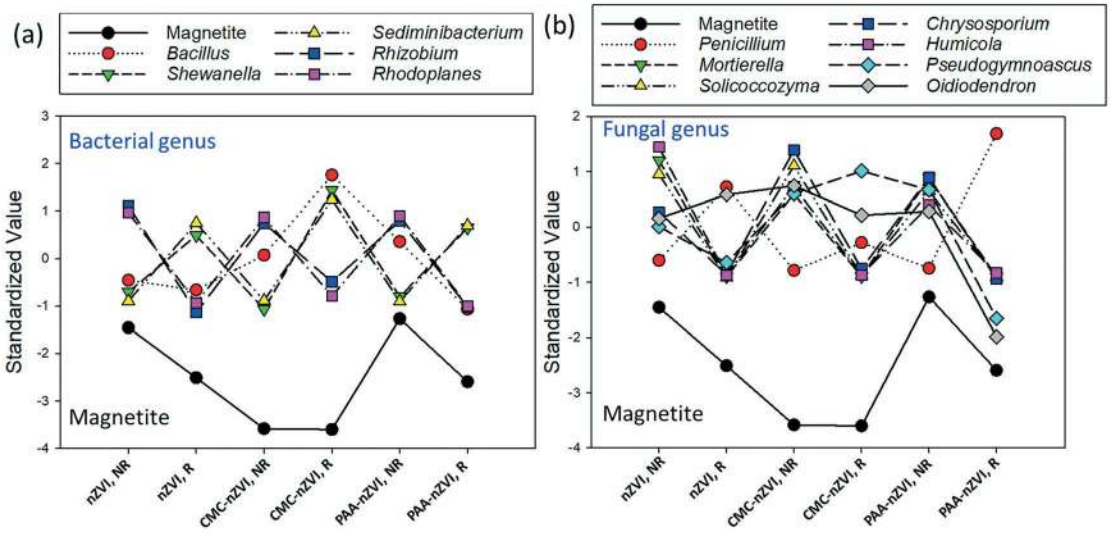

Fig. 8 The changes in key bacterial genus (a) and fungal genus (b) abundance (the mean value of three replicates, based on Illumina data) in the soils surrounding nZVI layers, in comparison with the changes in magnetite abundance (based on the result of quantification analysis of XRD spectra) in the nZVI aging products, from different treatments. The data used for the figure were standardized to make the value of different data types at the same level, and the standardized value of magnetite abundance was set to be 2.5 lower than the standardized microbial abundance value to separate material abundance from microbial abundance. Note: R represents γ-radiated soil; NR represents non-radiated soil. nZVI, nano zero-valent iron; CMC, carboxymethyl cellulose; PAA, polyacrylic acid.

reduce the surface area, thus reducing its capacity for adsorption. Besides, the oxidation of nZVI may decrease its reducibility by some toxic metals such as Cr(VI). However, it is essential to point out that the aging products of nZVI, *e.g.*, Fe (oxy)hydroxides, are also reported to have great potential for removing toxic pollutants.[89–91] In particular, magnetite (and/or goethite), as the main product of nZVI aging under the soil conditions of the present study, can still immobilize metal(loid)s efficiently.[92] Moreover, microbially mediated biogenic Fe (oxy)hydroxides usually had a higher specific surface area and more complex components (such as organic exudates) that reacted more efficiently with soil pollutants than the abiogenic nZVI aging products did.[93,94] In addition, the aging of nZVI may also reduce its toxicity to the microbial (or plant) cells.[95] The present study also revealed that different polymer coatings may influence nZVI aging differently in the soil ecosystem, which should be considered during the application of nZVI in soil remediation. Specifically, CMC coating favors nZVI transport and protects nZVI from quick oxidation and aging, and thus could be potentially used in the remediation of oxidative contaminants, *e.g.*, Cr(VI), which needs Fe^0 as a reducing agent. However, PAA coating favors the transport and quick oxidation of nZVI and accelerates the formation of Fe (oxy)hydroxides, such as magnetite, goethite *etc.*, and thus could be more suitable during the stabilization of metal(loid)s, *i.e.*, As, Cu, Pb, Zn *etc.*, in the soils as these metal(loid)s could be readily adsorbed to Fe (oxy)hydroxides.[89–92]

4. Conclusions

In summary, this study is among the first to reveal the detailed processes of nZVI aging in the soil ecosystem, which were dependent on polymer coatings, and could bilaterally interact with soil microbial communities. In particular, bare nZVI aggregated in the soils and was oxidized predominantly to magnetite. CMC coating decreased nZVI aging, whereas PAA coating increased it and accelerated magnetite, goethite and lepidocrocite formation. The studied soils with different microbial communities (realized by γ-radiation) influenced nZVI aging differently, and original soil microbes favored magnetite and lepidocrocite formation during the aging of nZVI coated with polymers (*i.e.*, PAA, CMC). In return, nZVI presence influenced both bacterial and fungal diversity and composition in its surrounding soils. This study has revealed nZVI aging in the soil ecosystem and its bilateral interaction with the soil microbial community, giving new insights into the understanding of nZVI behavior and impacts in the soil ecosystem. Further study is needed to investigate the mechanisms of nZVI aging in the soil system, as well as key soil microbes–nZVI (and its aging products) interactions and how those interactions affect nZVI functions in contaminated soil remediation. In addition, considering that the aging of nZVI may differ among different soil types with different physicochemical and biological properties, further studies are needed to address nZVI aging in different soil ecosystems.

Conflicts of interest

The authors declare no competing financial interests.

Acknowledgements

This work was financially supported by the Czech Science Foundation (GACR 17-25536Y) and the Czech University of

Life Sciences Prague (project CIGA 20174205). This work was also supported by the Competence Center of the Technology Agency of the Czech Republic (TE01020218) and by the Center for Geosphere Dynamics (UNCE/SCI/006). The use of XRD, SEM, and Raman spectrometry equipment at the Institute of Geology was through an institutional research project (RVO67985831). S. Wu also appreciates the help from the following colleagues: K. Štefečková (kindly provided CMC, NANOFER STAR, and PAA-coated nZVI), P. Šimek and M. Vosátka (soil sterilization), B. Šlapáková (lyophilization), N. Mészárosová (SEM), Z. Chen (UV-vis), F. You and Y. Liu (sequencing analysis). We also thank the associate editor, Prof. Joel Pedersen, and anonymous reviewers for their constructive comments and suggestions which significantly improved the manuscript.

References

1 S. Machado, W. Stawiński, P. Slonina, A. Pinto, J. Grosso, H. Nouws, J. T. Albergaria and C. Delerue-Matos, Application of green zero-valent iron nanoparticles to the remediation of soils contaminated with ibuprofen, *Sci. Total Environ.*, 2013, **461**, 323–329.

2 N. C. Müller and B. Nowack, Nano zero valent iron-The solution for water and soil remediation, *Report of the Observatory NANO*, 2010, pp. 1–34.

3 C. J. Liao, T. L. Chung, W. L. Chen and S. L. Kuo, Treatment of pentachlorophenol-contaminated soil using nano-scale zero-valent iron with hydrogen peroxide, *J. Mol. Catal. A: Chem.*, 2007, **265**, 189–194.

4 X. Zhao, W. Liu, Z. Cai, B. Han, T. Qian and D. Zhao, An overview of preparation and applications of stabilized zero-valent iron nanoparticles for soil and groundwater remediation, *Water Res.*, 2016, **100**, 245–266.

5 M. C. Chang and H. Y. Kang, Remediation of pyrene-contaminated soil by synthesized nanoscale zero-valent iron particles, *J. Environ. Sci. Health, Part A: Toxic/Hazard. Subst. Environ. Eng.*, 2009, **44**, 576–582.

6 R. Singh, V. Misra and R. P. Singh, Synthesis, characterization and role of zero-valent iron nanoparticle in removal of hexavalent chromium from chromium-spiked soil, *J. Nanopart. Res.*, 2011, **13**, 4063–4073.

7 M. Stefaniuk, P. Oleszczuk and Y. S. Ok, Review on nano zerovalent iron (nZVI): From synthesis to environmental applications, *Chem. Eng. J.*, 2016, **287**, 618–632.

8 M. Vítková, S. Rakosova, Z. Michalkova and M. Komarek, Metal(loid)s behaviour in soils amended with nano zero-valent iron as a function of pH and time, *J. Environ. Manage.*, 2017, **186**, 268–276.

9 R. L. Johnson, J. T. Nurmi, G. S. O'Brien Johnson, D. Fan, R. L. O'Brien Johnson, Z. Shi, A. J. Salter-Blanc, P. G. Tratnyek and G. V. Lowry, Field-scale transport and transformation of carboxymethylcellulose-stabilized nano zero-valent iron, *Environ. Sci. Technol.*, 2013, **47**, 1573–1580.

10 L. F. Greenlee, J. D. Torrey, R. L. Amaro and J. M. Shaw, Kinetics of zero valent iron nanoparticle oxidation in oxygenated water, *Environ. Sci. Technol.*, 2012, **46**, 12913–12920.

11 N. Kumar, M. Auffan, J. Gattacceca, J. Rose, L. Olivi, D. Borschneck, P. Kvapil, M. Jublot, D. Kaifas, L. Malleret, P. Doumenq and J. Y. Bottero, Molecular insights of oxidation process of iron nanoparticles: spectroscopic, magnetic, and microscopic evidence, *Environ. Sci. Technol.*, 2014, **48**, 13888–13894.

12 C. Su, R. W. Puls, T. A. Krug, M. T. Watling, S. K. O'Hara, J. W. Quinn and N. E. Ruiz, Travel distance and transformation of injected emulsified zerovalent iron nanoparticles in the subsurface during two and half years, *Water Res.*, 2013, **47**, 4095–4106.

13 T. Phenrat, N. Saleh, K. Sirk, R. D. Tilton and G. V. Lowry, Aggregation and sedimentation of aqueous nanoscale zerovalent iron dispersions, *Environ. Sci. Technol.*, 2007, **41**, 284–290.

14 F. He, M. Zhang, T. Qian and D. Zhao, Transport of carboxymethyl cellulose stabilized iron nanoparticles in porous media: Column experiments and modeling, *J. Colloid Interface Sci.*, 2009, **334**, 96–102.

15 J. Fatisson, S. Ghoshal and N. Tufenkji, Deposition of carboxymethylcellulose-coated zero-valent iron nanoparticles onto silica: roles of solution chemistry and organic molecules, *Langmuir*, 2010, **26**, 12832–12840.

16 T. Raychoudhury, G. Naja and S. Ghoshal, Assessment of transport of two polyelectrolyte-stabilized zero-valent iron nanoparticles in porous media, *J. Contam. Hydrol.*, 2010, **118**, 143–151.

17 A. R. Esfahani, A. F. Firouzi, G. Sayyad, A. Kiasat, L. Alidokht and A. R. Khataee, Pb(II) removal from aqueous solution by polyacrylic acid stabilized zero-valent iron nanoparticles: process optimization using response surface methodology, *Res. Chem. Intermed.*, 2014, **40**, 431–445.

18 Q. Wang, H. Qian, Y. Yang, Z. Zhang, C. Naman and X. Xu, Reduction of hexavalent chromium by carboxymethyl cellulose-stabilized zero-valent iron nanoparticles, *J. Contam. Hydrol.*, 2010, **114**, 35–42.

19 H. Dong, F. Zhao, G. Zeng, L. Tang, C. Fan, L. Zhang, Y. Zeng, Q. He, Y. Xie and Y. Wu, Aging study on carboxymethyl cellulose-coated zero-valent iron nanoparticles in water: chemical transformation and structural evolution, *J. Hazard. Mater.*, 2016, **312**, 234–242.

20 K. C. K. Lai and I. M. C. Lo, Removal of chromium (VI) by acid-washed zero-valent iron under various groundwater geochemistry conditions, *Environ. Sci. Technol.*, 2008, **42**, 1238–1244.

21 E. Lefevre, N. Bossa, M. R. Wiesner and C. K. Gunsch, A review of the environmental implications of in situ remediation by nanoscale zero valent iron (nZVI): Behavior, transport and impacts on microbial communities, *Sci. Total Environ.*, 2016, **565**, 889–901.

22 C. Lee, J. Y. Kim, W. I. Lee, K. L. Nelson, J. Yoon and D. L. Sedlak, Bactericidal effect of zero-valent iron nanoparticles on Escherichia coli, *Environ. Sci. Technol.*, 2008, **42**, 4927–4933.

23 J. Semerád, M. Čvančarová, J. Filip, J. Kašlík, J. Zlotá, J. Soukupová and T. Cajthaml, Novel assay for the toxicity evaluation of nanoscale zero-valent iron and derived nanomaterials based on lipid peroxidation in bacterial species, *Chemosphere*, 2018, **213**, 568–577.
24 S. Wu, M. Vosátka, K. Vogel-Mikus, A. Kavčič, M. Kelemen, L. Šepec, P. Pelicon, R. Skála, A. R. V. Powter and M. Teodoro, Nano zero-valent iron mediated metal (loid) uptake and translocation by arbuscular mycorrhizal symbioses, *Environ. Sci. Technol.*, 2018, **52**(14), 7640–7651.
25 J. Semerád and T. Cajthaml, Ecotoxicity and environmental safety related to nano-scale zerovalent iron remediation applications, *Appl. Microbiol. Biotechnol.*, 2016, **100**, 9809–9819.
26 J. Němeček, O. Lhotský and T. Cajthaml, Nanoscale zero-valent iron application for in situ reduction of hexavalent chromium and its effects on indigenous microorganism populations, *Sci. Total Environ.*, 2014, **485-486**, 739–747.
27 C. Ding, W. Cheng, Y. Sun and X. Wang, Effects of Bacillus subtilis on the reduction of U (VI) by nano-Fe 0, *Geochim. Cosmochim. Acta*, 2015, **165**, 86–107.
28 N. McNamara, H. Black, N. Beresford and N. Parekh, Effects of acute gamma irradiation on chemical, physical and biological properties of soils, *Appl. Soil. Ecol.*, 2003, **24**, 117–132.
29 P. Jiemvarangkul, W.-X. Zhang and H.-L. Lien, Enhanced transport of polyelectrolyte stabilized nanoscale zero-valent iron (nZVI) in porous media, *Chem. Eng. J.*, 2011, **170**, 482–491.
30 H. Christensen, M. Hansen and J. Sørensen, Counting and size classification of active soil bacteria by fluorescence in situ hybridization with an rRNA oligonucleotide probe, *Appl. Soil. Ecol.*, 1999, **65**, 1753–1761.
31 H. Birch, The effect of soil drying on humus decomposition and nitrogen availability, *Plant Soil*, 1958, **10**, 9–31.
32 N. Fierer, J. Schimel and P. Holden, Influence of drying–rewetting frequency on soil bacterial community structure, *Microb. Ecol.*, 2003, **45**, 63–71.
33 L. Žifčáková, T. Větrovský, A. Howe and P. Baldrian, Microbial activity in forest soil reflects the changes in ecosystem properties between summer and winter, *Environ. Microbiol.*, 2016, **18**, 288–301.
34 J. G. Caporaso, C. L. Lauber, W. A. Walters, D. Berg-Lyons, J. Huntley, N. Fierer, S. M. Owens, J. Betley, L. Fraser and M. Bauer, Ultra-high-throughput microbial community analysis on the Illumina HiSeq and MiSeq platforms, *ISME J.*, 2012, **6**, 1621.
35 T. Vetrovský, P. Baldrian, D. Morais and B. Berger, SEED 2: a user-friendly platform for amplicon high-throughput sequencing data analyses, *Bioinformatics*, 2018, **1**, 3.
36 E. Aronesty, Comparison of sequencing utility programs, *Open Bioinf. J.*, 2013, **7**, 1–8.
37 T. Rognes, T. Flouri, B. Nichols, C. Quince and F. Mahé, VSEARCH: a versatile open source tool for metagenomics, *PeerJ*, 2016, **4**, e2584.
38 R. C. Edgar, Search and clustering orders of magnitude faster than BLAST, *Bioinformatics*, 2010, **26**, 2460–2461.
39 S. F. Altschul, T. L. Madden, A. A. Schäffer, J. Zhang, Z. Zhang, W. Miller and D. J. Lipman, Gapped BLAST and PSI-BLAST: a new generation of protein database search programs, *Nucleic Acids Res.*, 1997, **25**, 3389–3402.
40 P. Quevauviller, Operationally defined extraction procedures for soil and sediment analysis I. Standardization, *TrAC, Trends Anal. Chem.*, 1998, **17**, 289–298.
41 P. Legendre and L. Legendre, *Numerical Ecology*, Elsevier, Amsterdam, 1st edn, 1998.
42 R. F. Woolson and W. R. Clarke, *Statistical Methods for the Analysis of Biomedical Data*, John Wiley & Sons, 2nd edn, 2011.
43 K. R. Clarke and R. M. Warwick, *Change in Marine Communities: An Approach to Statistical Analysis and Interpretation*, PRIMER-E Limited, 2nd edn, 2001.
44 K. R. Clarke, Non-parametric multivariate analyses of changes in community structure, *Aust. J. Ecol.*, 1993, **18**, 117–143.
45 J. Oksanen, Multivariate analysis of ecological communities in R: vegan tutorial, *R package version*, 2011, vol. 1, pp. 11–12.
46 F. He, D. Zhao, J. Liu and C. B. Roberts, Stabilization of Fe–Pd nanoparticles with sodium carboxymethyl cellulose for enhanced transport and dechlorination of trichloroethylene in soil and groundwater, *Ind. Eng. Chem. Res.*, 2007, **46**, 29–34.
47 Y. H. Lin, H. H. Tseng, M. Y. Wey and M. D. Lin, Characteristics of two types of stabilized nano zero-valent iron and transport in porous media, *Sci. Total Environ.*, 2010, **408**, 2260–2267.
48 T. Phenrat, H.-J. Kim, F. Fagerlund, T. Illangasekare, R. D. Tilton and G. V. Lowry, Particle size distribution, concentration, and magnetic attraction affect transport of polymer-modified Fe0 nanoparticles in sand columns, *Environ. Sci. Technol.*, 2009, **43**, 5079–5085.
49 N. Saleh, H.-J. Kim, T. Phenrat, K. Matyjaszewski, R. D. Tilton and G. V. Lowry, Ionic strength and composition affect the mobility of surface-modified Fe0 nanoparticles in water-saturated sand columns, *Environ. Sci. Technol.*, 2008, **42**, 3349–3355.
50 C. M. Cirtiu, T. Raychoudhury, S. Ghoshal and A. Moores, Systematic comparison of the size, surface characteristics and colloidal stability of zero valent iron nanoparticles pre- and post-grafted with common polymers, *Colloids Surf., A*, 2011, **390**, 95–104.
51 K. L. Chen, S. E. Mylon and M. Elimelech, Enhanced aggregation of alginate-coated iron oxide (hematite) nanoparticles in the presence of calcium, strontium, and barium cations, *Langmuir*, 2007, **23**, 5920–5928.
52 F. He and D. Zhao, Manipulating the size and dispersibility of zerovalent iron nanoparticles by use of carboxymethyl cellulose stabilizers, *Environ. Sci. Technol.*, 2007, **41**, 6216–6221.
53 T. Phenrat, N. Saleh, K. Sirk, H.-J. Kim, R. D. Tilton and G. V. Lowry, Stabilization of aqueous nanoscale zerovalent iron dispersions by anionic polyelectrolytes: adsorbed

anionic polyelectrolyte layer properties and their effect on aggregation and sedimentation, *J. Nanopart. Res.*, 2008, **10**, 795–814.

54 A. Liu, J. Liu and W.-x. Zhang, Transformation and composition evolution of nanoscale zero valent iron (nZVI) synthesized by borohydride reduction in static water, *Chemosphere*, 2015, **119**, 1068–1074.

55 S. Y. Lin, G. L. Amidon, N. D. Weiner and A. H. Goldberg, Viscoelasticity of anionic polymers and their mucociliary transport on the frog palate, *Pharm. Res.*, 1993, **10**, 411–417.

56 L. Zhou, T. Le Thanh, J. Gong, J.-H. Kim, E.-J. Kim and Y.-S. Chang, Carboxymethyl cellulose coating decreases toxicity and oxidizing capacity of nanoscale zerovalent iron, *Chemosphere*, 2014, **104**, 155–161.

57 M. Kahle, M. Kleber and R. Jahn, Review of XRD-based quantitative analyses of clay minerals in soils: the suitability of mineral intensity factors, *Geoderma*, 2002, **109**, 191–205.

58 Y.-S. Li, J. S. Church and A. L. Woodhead, Infrared and Raman spectroscopic studies on iron oxide magnetic nanoparticles and their surface modifications, *J. Magn. Magn. Mater.*, 2012, **324**, 1543–1550.

59 S. Das and M. J. Hendry, Application of Raman spectroscopy to identify iron minerals commonly found in mine wastes, *Chem. Geol.*, 2011, **290**, 101–108.

60 O. N. Shebanova and P. Lazor, Raman study of magnetite (Fe_3O_4): laser-induced thermal effects and oxidation, *J. Raman Spectrosc.*, 2003, **34**, 845–852.

61 M. Hanesch, Raman spectroscopy of iron oxides and (oxy) hydroxides at low laser power and possible applications in environmental magnetic studies, *Geophys. J. Int.*, 2009, **177**, 941–948.

62 A. Liu, J. Liu, J. Han and W.-X. Zhang, Evolution of nanoscale zero-valent iron (nZVI) in water: Microscopic and spectroscopic evidence on the formation of nano- and micro-structured iron oxides, *J. Hazard. Mater.*, 2017, **322**, 129–135.

63 L. t. Carlson and U. Schwertmann, The effect of CO_2 and oxidation rate on the formation of goethite versus lepidocrocite from an Fe(II) system at pH 6 and 7, *Clay Miner.*, 1990, **25**, 65–71.

64 D. Jiang, X. Hu, R. Wang and D. Yin, Oxidation of nanoscale zero-valent iron under sufficient and limited dissolved oxygen: Influences on aggregation behaviors, *Chemosphere*, 2015, **122**, 8–13.

65 H. Dong, K. Ahmad, G. Zeng, Z. Li, G. Chen, Q. He, Y. Xie, Y. Wu, F. Zhao and Y. Zeng, Influence of fulvic acid on the colloidal stability and reactivity of nanoscale zero-valent iron, *Environ. Pollut.*, 2016, **211**, 363–369.

66 A. R. Brown, C. Boothman, S. M. Pimblott and J. R. Lloyd, The impact of gamma radiation on sediment microbial processes, *Appl. Environ. Microbiol.*, 2015, **81**(12), 4014–4025.

67 H.-J. Kim, T. Phenrat, R. D. Tilton and G. V. Lowry, Effect of kaolinite, silica fines and pH on transport of polymer-modified zero valent iron nano-particles in heterogeneous porous media, *J. Colloid Interface Sci.*, 2012, **370**, 1–10.

68 J. Chen, Z. Xiu, G. V. Lowry and P. J. J. Alvarez, Effect of natural organic matter on toxicity and reactivity of nanoscale zero-valent iron, *Water Res.*, 2011, **45**, 1995–2001.

69 N. P. McNamara, R. I. Griffiths, A. Tabouret, N. A. Beresford, M. J. Bailey and A. S. Whiteley, The sensitivity of a forest soil microbial community to acute gamma-irradiation, *Appl. Soil. Ecol.*, 2007, **37**, 1–9.

70 V. Morillo, F. Abreu, A. C. Araujo, L. G. P. d. Almeida, A. E. Prast, M. Farina, A. T. R. d. Vasconcelos, D. A. Bazylinski and U. Lins, Isolation, cultivation and genomic analysis of magnetosome biomineralization genes of a new genus of South-seeking magnetotactic cocci within the Alphaproteobacteria, *Front. Microbiol.*, 2014, **5**, 72.

71 R. Amann, J. Peplies and D. Schüler, in *Magnetoreception and magnetosomes in bacteria*, Springer, 2006, pp. 25–36.

72 J. K. Fredrickson, M. F. Romine, A. S. Beliaev, J. M. Auchtung, M. E. Driscoll, T. S. Gardner, K. H. Nealson, A. L. Osterman, G. Pinchuk, J. L. Reed, D. A. Rodionov, J. L. M. Rodrigues, D. A. Saffarini, M. H. Serres, A. M. Spormann, I. B. Zhulin and J. M. Tiedje, Towards environmental systems biology of Shewanella, *Nat. Rev. Microbiol.*, 2008, **6**, 592.

73 J. Němeček, P. Pokorný, L. Lacinová, M. Černík, Z. Masopustová, O. Lhotský, A. Filipová and T. Cajthaml, Combined abiotic and biotic in-situ reduction of hexavalent chromium in groundwater using nZVI and why: A remedial pilot test, *J. Hazard. Mater.*, 2015, **300**, 670–679.

74 T. Perez-Gonzalez, C. Jimenez-Lopez, A. L. Neal, F. Rull-Perez, A. Rodriguez-Navarro, A. Fernandez-Vivas and E. Iañez-Pareja, Magnetite biomineralization induced by Shewanella oneidensis, *Geochim. Cosmochim. Acta*, 2010, **74**, 967–979.

75 D. A. Bazylinski, R. B. Frankel and K. O. Konhauser, Modes of biomineralization of magnetite by microbes, *Geomicrobiol. J.*, 2007, **24**, 465–475.

76 H. Dong, J. K. Fredrickson, D. W. Kennedy, J. M. Zachara, R. K. Kukkadapu and T. C. Onstott, Mineral transformations associated with the microbial reduction of magnetite, *Chem. Geol.*, 2000, **169**, 299–318.

77 J. Pollock, K. A. Weber, J. Lack, L. A. Achenbach, M. R. Mormile and J. D. Coates, Alkaline iron(III) reduction by a novel alkaliphilic, halotolerant, Bacillus sp. isolated from salt flat sediments of Soap Lake, *Appl. Microbiol. Biotechnol.*, 2007, **77**, 927–934.

78 S. Kanso, A. C. Greene and B. K. Patel, Bacillus subterraneus sp. nov., an iron- and manganese-reducing bacterium from a deep subsurface Australian thermal aquifer, *Int. J. Syst. Evol. Microbiol.*, 2002, **52**, 869–874.

79 H. Wang, C. Hu, X. Hu, M. Yang and J. Qu, Effects of disinfectant and biofilm on the corrosion of cast iron pipes in a reclaimed water distribution system, *Water Res.*, 2012, **46**, 1070–1078.

80 J. H. Qu and H. L. Yuan, Sediminibacterium salmoneum gen. nov., sp. nov., a member of the phylum Bacteroidetes isolated from sediment of a eutrophic reservoir, *Int. J. Syst. Evol. Microbiol.*, 2008, **58**, 2191–2194.

81 N. Harada, M. Nishiyama, S. Otsuka and S. Matsumoto, Effects of Inoculation of Phototrophic Purple Bacteria on Grain Yield of Rice and Nitrogenase Activity of Paddy Soil in a Pot Experiment, *Soil Sci. Plant Nutr.*, 2005, **51**, 361–367.
82 H. H. Zahran, Rhizobium-legume symbiosis and nitrogen fixation under severe conditions and in an arid climate, *Microbiol. Mol. Biol. Rev.*, 1999, **63**, 968–989.
83 M. L. Guerinot, in *Iron Nutrition and Interactions in Plants: "Proceedings of the Fifth International Symposium on Iron Nutrition and Interactions in Plants"*, ed. Y. Chen and Y. Hadar, Springer, Dordrecht, 1st edn, 1991, pp. 239–249.
84 K. Shi, Z. Gao, L. Lin, W. J. Wang, X. Q. Shi, X. Yu, P. Song, L. J. Ren, H. Huang and X. J. Ji, Manipulating the generation of reactive oxygen species through intermittent hypoxic stress for enhanced accumulation of arachidonic acid-rich lipids, *Chem. Eng. Sci.*, 2018, **186**, 36–43.
85 C. Boisset, C. Fraschini, M. Schulein, B. Henrissat and H. Chanzy, Imaging the enzymatic digestion of bacterial cellulose ribbons reveals the endo character of the cellobiohydrolase Cel6A from Humicola insolens and its mode of synergy with cellobiohydrolase Cel7A, *Appl. Environ. Microbiol.*, 2000, **66**, 1444–1452.
86 A. Thieken and G. Winkelmann, Rhizoferrin: a complexone type siderophore of the Mucorales and entomophthorales (Zygomycetes), *FEMS Microbiol. Lett.*, 1992, **73**, 37–41.
87 R. Schuler and K. Haselwandter, Hydroxamate siderophore production by ericoid mycorrhizal fungi, *J. Plant Nutr.*, 1988, **11**, 907–913.
88 Y. Sun, C. Lei, E. Khan, S. S. Chen, D. C. W. Tsang, Y. S. Ok, D. Lin, Y. Feng and X. D. Li, Aging effects on chemical transformation and metal(loid) removal by entrapped nanoscale zero-valent iron for hydraulic fracturing wastewater treatment, *Sci. Total Environ.*, 2018, **615**, 498–507.
89 M. Komarek, A. Vanek and V. Ettler, Chemical stabilization of metals and arsenic in contaminated soils using oxides–a review, *Environ. Pollut.*, 2013, **172**, 9–22.
90 M. Komarek, C. M. Koretsky, K. J. Stephen, D. S. Alessi and V. Chrastny, Competitive Adsorption of Cd(II), Cr(VI), and Pb(II) onto Nanomaghemite: A Spectroscopic and Modeling Approach, *Environ. Sci. Technol.*, 2015, **49**, 12851–12859.
91 M. Komárek, J. Antelo, M. Králová, V. Veselská, S. Číhalová, V. Chrastný, V. Ettler, J. Filip, Q. Yu, J. B. Fein and C. M. Koretsky, Revisiting models of Cd, Cu, Pb and Zn adsorption onto Fe(III) oxides, *Chem. Geol.*, 2018, **493**, 189–198.
92 H. Karami, Heavy metal removal from water by magnetite nanorods, *Chem. Eng. J.*, 2013, **219**, 209–216.
93 D. Fortin and S. Langley, Formation and occurrence of biogenic iron-rich minerals, *Earth-Sci. Rev.*, 2005, **72**, 1–19.
94 L. Castro, M. L. Blázquez, F. González, J. A. Muñoz and A. Ballester, Biogenic iron compounds for hazardous metal remediation, *Solid State Phenom.*, 2017, **262**, 551–554.
95 T. Phenrat, T. C. Long, G. V. Lowry and B. Veronesi, Partial oxidation ("aging") and surface modification decrease the toxicity of nanosized zerovalent iron, *Environ. Sci. Technol.*, 2009, **43**, 195–200.

Chapter 20

Nano-Bioremediation: Nanoscale Zero-Valent Iron for Inorganic and Organic Contamination

Jaroslav Semerad*, Martin Pivokonsky and Tomas Cajthaml

Abstract The present chapter is describing two pilot-scale experiments and showing the potential of the combined technology (i.e., nanoremediation and bioremediation) for in situ heavy metal removal and dechlorination of chlorinated solvents. Successful applications of the nano-bioremediation approach at two different sites in the Czech Republic contaminated with hexavalent chromium are summarized and evaluated in this chapter. High effectivity of nZVI and the further microbial bioaugmentation step by whey addition resulted in reduction and geofixation of hexavalent chromium in both localities. In addition, a high removal of chlorinated ethenes was observed in the locality 2 after the whey application. The successive abiotic and biotic processes involving the chemical reduction and further microbial bioreduction of chromium and dechlorination of chlorinated ethenes were evaluated by monitoring of physicochemical and biological parameters. The results of both applications of the combined remediation technology clearly prove feasibility and high efficiency of this approach for chromium and chlorinated ethenes removal.

Keywords Nano-bioremediation · Bioreduction · Geofixation · Ecotoxicity · Hexavalent chromium

20.1 INTRODUCTION—TWO FIELD STUDIES

Since zero-valent iron nanoparticles have been invented, the number of published laboratory studies has reached several hundreds. The outcomes of these studies have proved the effectiveness of the above-mentioned nanoparticles and their composites for degradation and elimination of organic and inorganic contamination. In the light of this knowledge, the number of successful full-scale applications has been increasing for the past 15 years and the degradation effectivity of nZVI has also been confirmed by in situ applications (Mueller et al. 2012). Recent studies from the contaminated sites where nZVI was applied also reported its

J. Semerad (*) · T. Cajthaml
Institute of Microbiology, Czech Academy of Sciences, v.v.i., Vídeňská 1083, 142 20 Prague 4, Czech Republic
e-mail: jaroslav.semerad@biomed.cas.cz

J. Semerad · T. Cajthaml
Institute for Environmental Studies, Faculty of Science, Charles University, Benátská 2, 128 01 Prague 2, Czech Republic

M. Pivokonsky
Institute of Hydrodynamics of the Czech Academy of Sciences, Pod Patankou 30/5, 166 12 Prague 6, Czech Republic

stimulation effect on selected microbial species and its potential for the combination of nanoremediation and bioremediation (Němeček et al. 2014, 2015, 2016). This chapter is summarizing two pilot-scale experiments done in the Czech Republic during which nZVI and whey as a microbial substrate were successfully applied for geofixation of Cr(VI) and dechlorination of chlorinated ethenes.

20.2 LOCALITY 1

20.2.1 Sampling and Site Monitoring

The first test site is situated at the Kortan site in the north of the Czech Republic where a leather processing plant was set up in the past. Up to the 1990s, the factory used potassium dichromate for leather tanning whence the contamination with Cr(VI) comes. The current levels of Cr(VI) in groundwater are close to 3 mg/L. The aquifer is surrounded by a mixture of Quaternary sands and gravels with clayey admixture. The saturated zone of the aquifer is approximately 5 m thick; the groundwater table fluctuates at 4.5–5.5 m below the surface of the ground and the flow velocity staggers from 0.2 to 2 m/day. Finally, the groundwater discharges to a nearby river located approximately 500 m from the site. The physicochemical parameters of the groundwater reach values of pH 5.4, total organic carbon < 1.5 mg/L, the total dissolved solids < 0.3 g/L, and a high oxidation-reduction potential (450 to 550 mV).

The site monitoring was carried out by 19 sampling rounds during both phases, whereas groundwater samples of each round were collected from seven different wells. Before the pilot test, nine wells were drilled: three nZVI injection wells (PV-209, PV-213, and PV-215), three downgradient (PV-214, PV-216, PV-217) and one upgradient monitoring well (PV-212), which served as a reference. Besides the seven main wells, another two downgradient monitoring wells (PV-201 and PV-210) were sampled for additional analysis. The positions of the monitoring and the injection wells are displayed in Fig. 20.1.

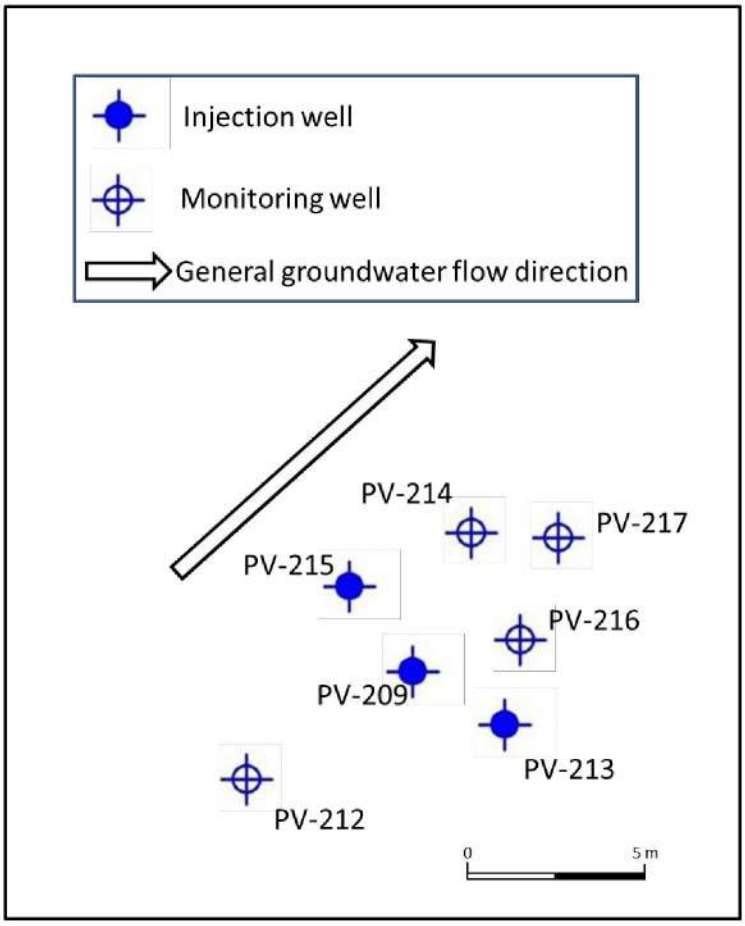

Fig. 20.1 Positions of monitoring and injection wells in locality 1 (adapted from Němeček et al. 2014)

20.2.2 Pilot Application of nZVI and Subsequential Whey Injection

The pilot test at the Kortan site consisted of two phases—abiotic and biotic. In summer 2012, during the first (abiotic) phase of the pilot test, 120 kg of nZVI (NANOFER 25, NANO IRON, s.r.o., Czech Republic) in tap water (2 g/L) was applied into three injection wells (PV-209, PV-213, PV-215). The injection wells were situated in one line with a spacing of 2.8 m to form the barrier configuration. Nine months after the injection of nZVI, the biotic phase was set up. During the biotic phase, to support indigenous bacteria, 5 m^3 of cheese whey was injected into the wells as the microbial substrate. The substrate was mixed with groundwater in a volumetric ratio of 1:50 abstracted from the downgradient wells and then injected back into the upgradient injection wells. Afterward this circulation carried on for 50 days. At the end of the circulation process, the natural groundwater flow was restored. The whole pilot test consisting of both the abiotic and the biotic phase lasted approximately 21 months.

20.2.3 Evolution of Physicochemical Parameters and Concentration of Contaminants

The measurements of physicochemical parameters such as pH and oxidation-reduction potential (ORP) were carried out directly on the site electrochemically. Other inorganic parameters were determined after several preparation steps in a laboratory. Additionally, the evolution in the Cr(VI) concentration dissolved in groundwater is displayed in Fig. 20.2.

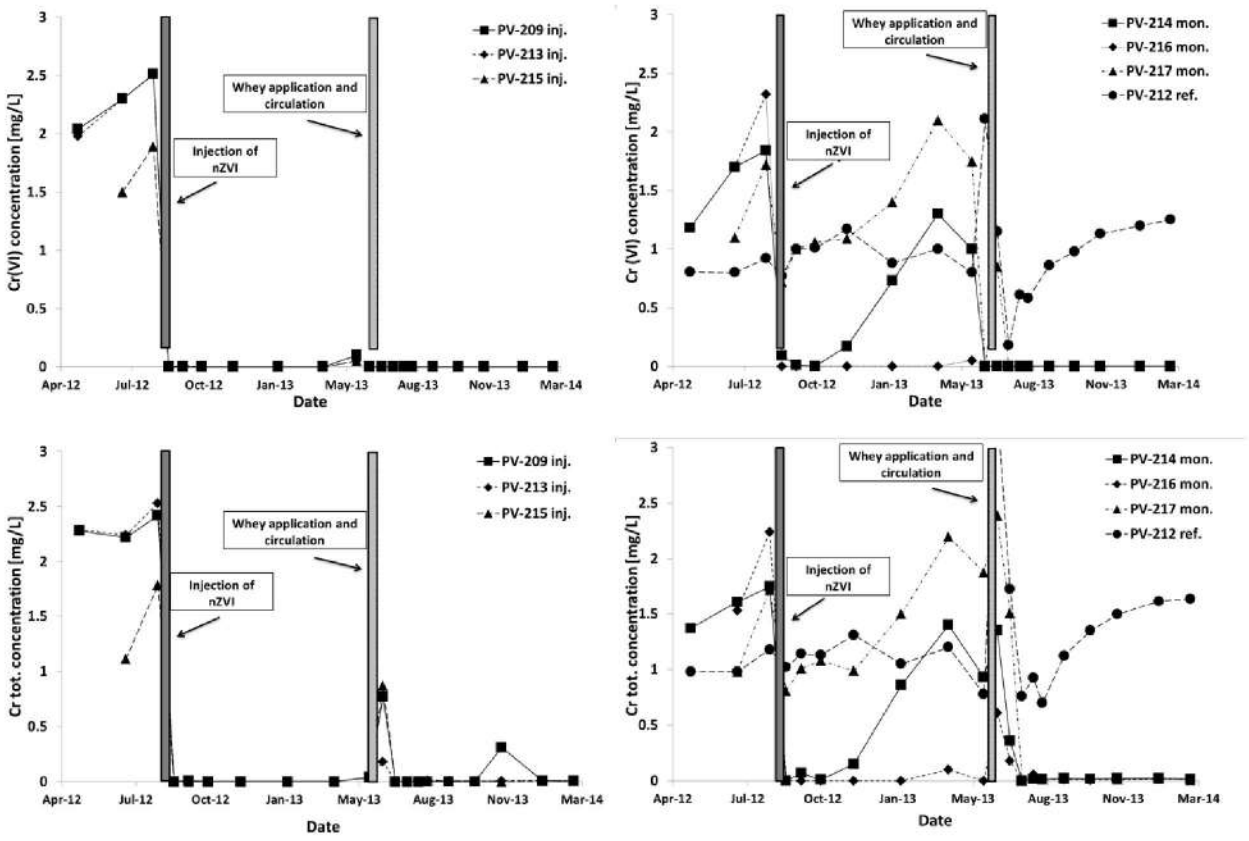

Fig. 20.2 The evolution of chromium contamination (Cr(VI) and Cr(total)) in groundwater during whole pilot-scale test (adapted from Němeček et al. 2015)

From the results of the thorough site monitoring, it is clear that the immediate decrease of ORP was closely connected with the nZVI application. The fast decrease of ORP (down to –484 mV within one day in injection wells and –330 mV in monitoring wells) and the reduction of dissolved Cr(VI) concentrations to the detection limits in all injection wells and the two nearest monitoring wells (PV-214 and PV-216) were observed. Additionally, in the distance of 7 m from the nZVI barrier (PV-217), the effect of the nZVI injection was less pronounced. The decrease in the concentrations of Cr(VI) was attributed to the reduction of Cr(VI) to Cr(III) by nZVI followed by the geofixation of reduced Cr(III) into the soil in the system of insoluble Fe(III)-Cr(III)-oxyhydroxides. Therefore an additional step was required, so the abiotic phase was followed by the biotic phase. After the abiotic phase, which was started by the injection of nZVI and lasted nine months, whey was applied according to the

previously described circulation system in order to support the resident microbial species. The application of the organic substrate resulted in a gradual and substantial grow of bacteria followed by a further repeated decrease in the Cr(VI) concentrations in all the injection and the monitoring wells, see Fig. 20.2.

20.2.4 Microbial and Ecotoxicological Assessment of Both Pilot Test Phases

In both studies, Němeček et al. 2014 and 2015, the authors also provided detailed microbial and ecotoxicological assessment of the whole 21-month period of the pilot test duration. Using standard approaches such as microbial cultivation tests and inhibition of bioluminescence of *Vibrio fischeri*, the authors assessed the possible ecotoxicological impact of nZVI. The impact on autochthonous microbial population was also monitored by phospholipid fatty acid analysis (PLFA) and 16S rRNA 454 pyrosequencing. Overall, the authors did not observe any negative effect on the microbial population in the groundwater after the nZVI application and even growth stimulation of Gram-positive bacteria was observed in the soil samples using PLFA.

Notwithstanding the acute toxicity of nZVI detected during the in vitro tests (Semerád et al. 2018), the lack of negative or less pronounced toxic effect during in situ application corresponds with the findings of several other authors (Semerád and Cajthaml 2016). Bacterial stimulation was probably caused by the elimination of highly toxic Cr(VI) from the aquifer and thus by the decrease of overall toxicity during the first abiotic phase. Additionally, in the second phase, after nine months from nZVI application the microbial growth was stimulated by the addition of cheese whey and the increase of anaerobic bacteria contributed to the biotic reduction of residual Cr(VI). The direct or indirect effect of biotic reduction was clearly long-term and persisted even after ten months from the whey injection even when the substrate was completely depleted.

20.3 LOCALITY 2

20.3.1 Sampling and Site Monitoring

The second locality is polluted by Cr(VI) and chlorinated ethenes originating from historical degreasing and chromium coating activities. The initial levels of contamination in the groundwater reached values from 4.4 to 57 mg/L for Cr(VI) and from 400 to 6,526 μg/L for the sum of chlorinated ethenes at the beginning of the pilot test. Similarly to locality 1, the aquifer is situated in Quaternary sands and gravels with silty admixture and is covered by a layer of clay and clayey loam with a thickness of 5 m. The saturated zone of the aquifer is approximately 4 m thick and the hydraulic conductivity of the aquifer is 7.6×10^{-4} m/s. The groundwater discharges into the neighboring river at the distance of 430 m from the contaminated site. Physicochemical parameters of the groundwater reached values of pH 6.9–7.0, total organic carbon < 1.0 to 5.4 mg/L, the total dissolved solids from 0.9 to 1.2 g/L, and

oxidation-reduction potential ranging from +130 to –490 mV. Samples of the groundwater were collected during the whole pilot application from seven different monitoring wells representing two downgradient lines (first line: MV-2, MV-3, MV-4 and the second line: MV-5, HV-2, HS-1, HS-2) and one upgradient well, which served as a control to provide background values (MV-1). In addition, well HV-8 contaminated only by chlorinated ethenes and located cross-gradient from the contamination source was sampled. The detailed distribution of wells in locality 2 is presented in Fig. 20.3.

Groundwater samples were collected from the monitoring wells and used for further analyses of various physical, chemical, and inorganic parameters, including microbial populations using PLFA. In addition, two types of passive samplers were emplaced in each monitoring well for more detailed evaluation of microbial populations and for solid phase analyses (oxidation state of Cr via X-ray photoelectron spectroscopy). The last type of sample was the sediment from five different monitoring wells (HV-8, MV-1, MV-3, MV-4, and MV-5), which was collected at the end of the pilot test and used for microbial community analysis.

20.3.2 Application of Combined Nano-Biotechnology

The pilot test in locality 2 included abiotic and biotic phases similarly to the test in locality 1 (Němeček et al. 2016). The abiotic phases consisted of two applications of nZVI at four months interval and lasted six months and a half. nZVI (NANO IRON, s.r.o., Czech Republic) was injected in a water suspension using direct push technology. During the first injection, surface-passivated nZVI (NANOFER STAR) was injected in a concentration of 1 g/L. For the second injection, the author used the same nZVI as in locality 1, i.e., NANOFER 25S in a concentration of 2 g/L. The injection boreholes were located perpendicularly to the groundwater flow, see Fig. 20.3.

The abiotic phase was followed by a biotic phase, which started approximately two months and a half after the second injection of nZVI. Cheese whey was used as the substrate owing to its successful application in locality 1 in order to support microbial populations. Whey was applied using a circulation system; the substrate was mixed with groundwater from downgradient monitoring wells (HS-1 and HS-2) and then injected back to the injection wells (IN-1 A and IN-2 A) at a rate of 0.5–0.7 L/s. During the biotic phase, 8.3 m^3 of whey was applied in total in a dosing ratio of 1/50 (substrate/groundwater). After the application period (five weeks) the circulation of groundwater continued for nine days and therefore the natural groundwater flow was reestablished and the locality was monitored for another five months.

20.3.3 Monitoring of Physicochemical Parameters and Levels of Contamination

Similarly to the pilot test in locality 1, the drop in the oxidation-reduction (to –400 mV) potential was observed after the first injection of nZVI. A less significant decrease in E_h was also observed after the second nZVI injection and the substrate application. Finally, the

oxidation-reduction potential was stabilized at 50 mV and 100 mV in the first and second monitoring line, respectively. The drop of the E_h supported by the analysis of inorganics documents the course of reducing conditions in the monitoring wells during the whole remediation experiment including the biotic phase.

The first injection of nZVI resulted in a decrease of the Cr(VI) concentration (below the detection limits) in the first monitoring line, but the concentrations started to rebound within several weeks. After the second injection, the level of chromium contamination reached only 10–15% of the initial concentrations. The reductive effect of nZVI in the second monitoring line was less pronounced. However, the final Cr(VI) removal was achieved by the second phase. After addition of the microbial substrate, the concentration of Cr(VI) decreased below the analytical limits of detection in a very short time and lasted for the whole monitoring period, even after 188 days from the whey application, shown in Fig. 20.3. In addition, the laboratory studies showed that the concentration of total chromium in the soil samples corresponded to the initial concentration of Cr(VI), which documents fixation of Cr(III) in the soil matrix.

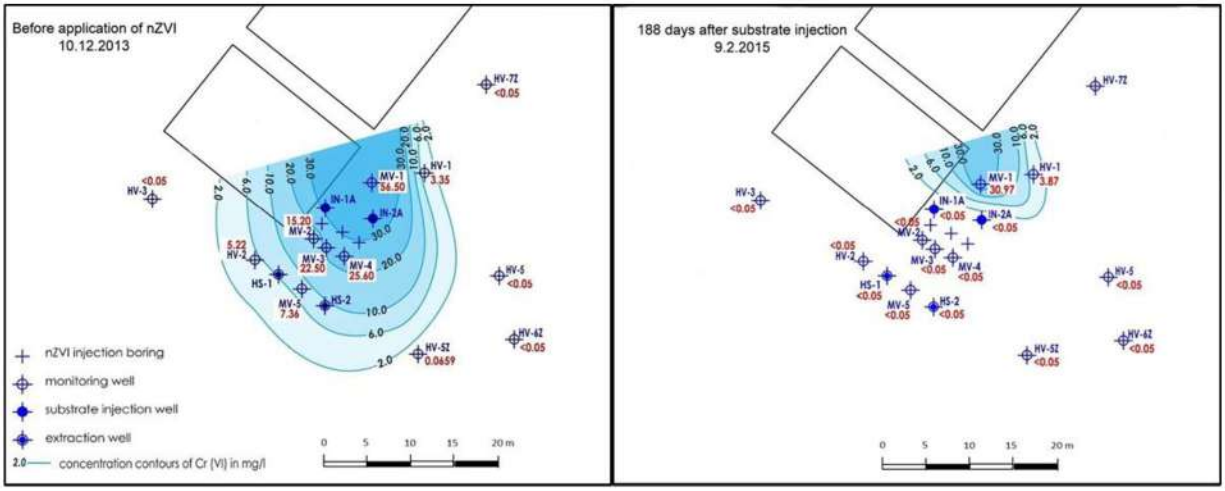

Fig. 20.3 Distribution of injection and monitoring wells and 2D model of Cr(VI) contamination of groundwater before and after the pilot test in locality 2 (adapted from Němeček et al. 2016)

Transformation of chlorinated ethenes by nZVI even after the second injection was not observed in the monitoring wells. The authors attributed the limited degradation efficiency during the first phase to the competition with Cr(VI), which is a thermodynamically more favored reducible compound. However, the addition of the organic substrate resulted in a rapid decrease of parent trichloroethene (TCE) below the limit of detection together with a temporal increase and a further decrease of its transformation products—less chlorinated and dechlorinated ethenes. The concentration of parent TCE remained below the detection limit for the rest of the monitoring period (six months) in the first monitoring line. In the second

monitoring line, 36–97% removal of chlorinated ethenes was achieved at the end of the pilot test.

20.3.4 Microbes and Their Role in the Whole Nano-Bioremediation Process

The results of the microbial analysis done by the authors indicate that the degradation of the pollutants to a level below the toxicity threshold created preferable environmental conditions for autochthonous microflora in the site. On the basis of the results of qPCR and PLFA, the injection of the substrate resulted in an increase of microbial biomass including microbial degraders. Despite the same results obtained from both types of the analyses, the massive increase (approximately 10× estimated by PLFA) in the biomass was only temporal. After depletion of the substrate, the biomass expeditiously decreased within two months from the whey application (see Fig. 20.4). Additionally, a stable reducing condition persisted even after the complete consumption of the substrate and the simultaneous decrease in microbial biomass. The possible explanation proposed by the authors is that the persistent reducing conditions were partially caused by regenerated iron formed by microbial reduction of Fe(III) to Fe(II) during the application of whey and the increase in biomass. A solid-state analysis of sample MV-4 (passive samplers) by ^{57}Fe Mössbauer spectroscopy supported this hypothesis. At the end of the experiment, the results showed that 21% of present Fe is in oxidation state Fe(II).

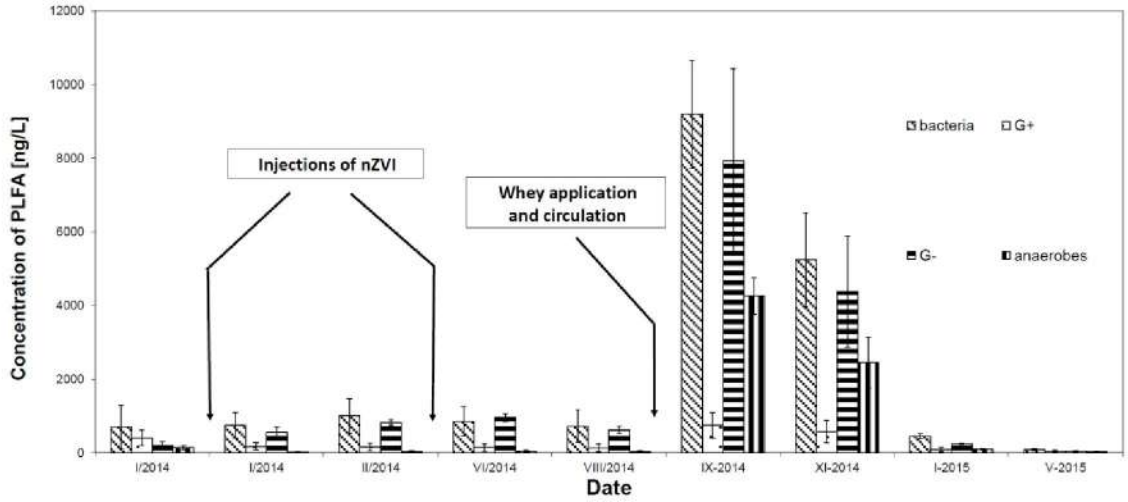

Fig. 20.4 The estimation of biomass via PLFA (adapted from Němeček et al. 2016)

Moreover, microbial community analysis of sediment samples at the end of the pilot test proved the occurrence of reducing bacterial genera, such as *Geobacter* and *Rhodoferax*, which are able to reduce iron and sulfur during catabolic processes. These reduced forms could have served as reducing agents in Cr(VI) fixation even after the substrate depletion. The Illumina sequencing data also showed the presence of halorespiring bacteria, which were possibly involved in degradation of chlorinated ethenes. In addition, some of the found phylotypes

could (besides chloroethene respiration) have reduced also the metals (Fe(III) and Cr(VI)). Another interesting genus found in the sediment samples was *Dehalococcoides*, which is a typical representative of chlororespiring bacteria. After the whey circulation period, an increase in *vcr*A gene copies was recorded, which greatly corresponded to an increase in the detected degradation products of chlorinated ethenes and to a decreasing chlorine number.

20.4 CONCLUSION

The results of the two presented pilot tests clearly demonstrate the potential of nZVI for nano-bioremediation application of sites with Cr(VI) contamination via geofixation of the metal into the soil. The decrease in contamination after the nZVI application and the closely connected improvement of the living conditions for microbial species (e.g., lower toxicity, ORP) facilitated the implementation of the next bioremediation step. The subsequent injection of the inexpensive organic substrate caused an increase in the microbial biomass, which was consequently able to continue with reduction of chromium or transformation of TCE even after complete oxidation of nZVI. Both studies document the feasibility and high efficiency of the combination of nanotechnology and biotechnology in remediation of chromium-contaminated sites with a clearly long-term effect.

REFERENCES

Mueller NC, Braun J, Bruns J, Černík M, Rissing P, Rickerby D, Nowack B (2012) Application of nanoscale zero valent iron (NZVI) for groundwater remediation in Europe. Environ Sci Pollut Res 19(2):550–558. doi:10.1007/s11356-011-0576-3

Němeček J, Lhotský O, Cajthaml T (2014) Nanoscale zero-valent iron application for in situ reduction of hexavalent chromium and its effects on indigenous microorganism populations. Sci Total Environ 485–486:739–747. doi:10.1016/j.scitotenv.2013.11.105

Němeček J, Pokorný P, Lacinová L, Černík M, Masopustová Z, Lhotský O, Filipová A, Cajthaml T (2015) Combined abiotic and biotic in-situ reduction of hexavalent chromium in groundwater using nZVI and whey: A remedial pilot test. J Hazard Mater 300:670–679. doi:10.1016/j.jhazmat.2015.07.056

Němeček J, Pokorný P, Lhotský O, Knytl V, Najmanová P, Steinová J, Černík M, Filipová A, Filip J, Cajthaml T (2016) Combined nano-biotechnology for in-situ remediation of mixed contamination of groundwater by hexavalent chromium and chlorinated solvents. Sci Total Environ 563–564:822–834. doi:10.1016/j.scitotenv.2016.01.019

Semerád J, Cajthaml T (2016) Ecotoxicity and environmental safety related to nano-scale zerovalent iron remediation applications. Appl Microbiol Biotechnol 100(23):9809–9819. doi:10.1007/s00253-016-7901-1

Semerád J, Čvančarová M, Filip J, Kašlík J, Zlotá J, Soukupová J, Cajthaml T (2018) Novel assay for the toxicity evaluation of nanoscale zero-valent iron and derived nanomaterials based on lipid peroxidation in bacterial species. Chemosphere 213:568–577. doi:10.1016/j.chemosphere.2018.09.029